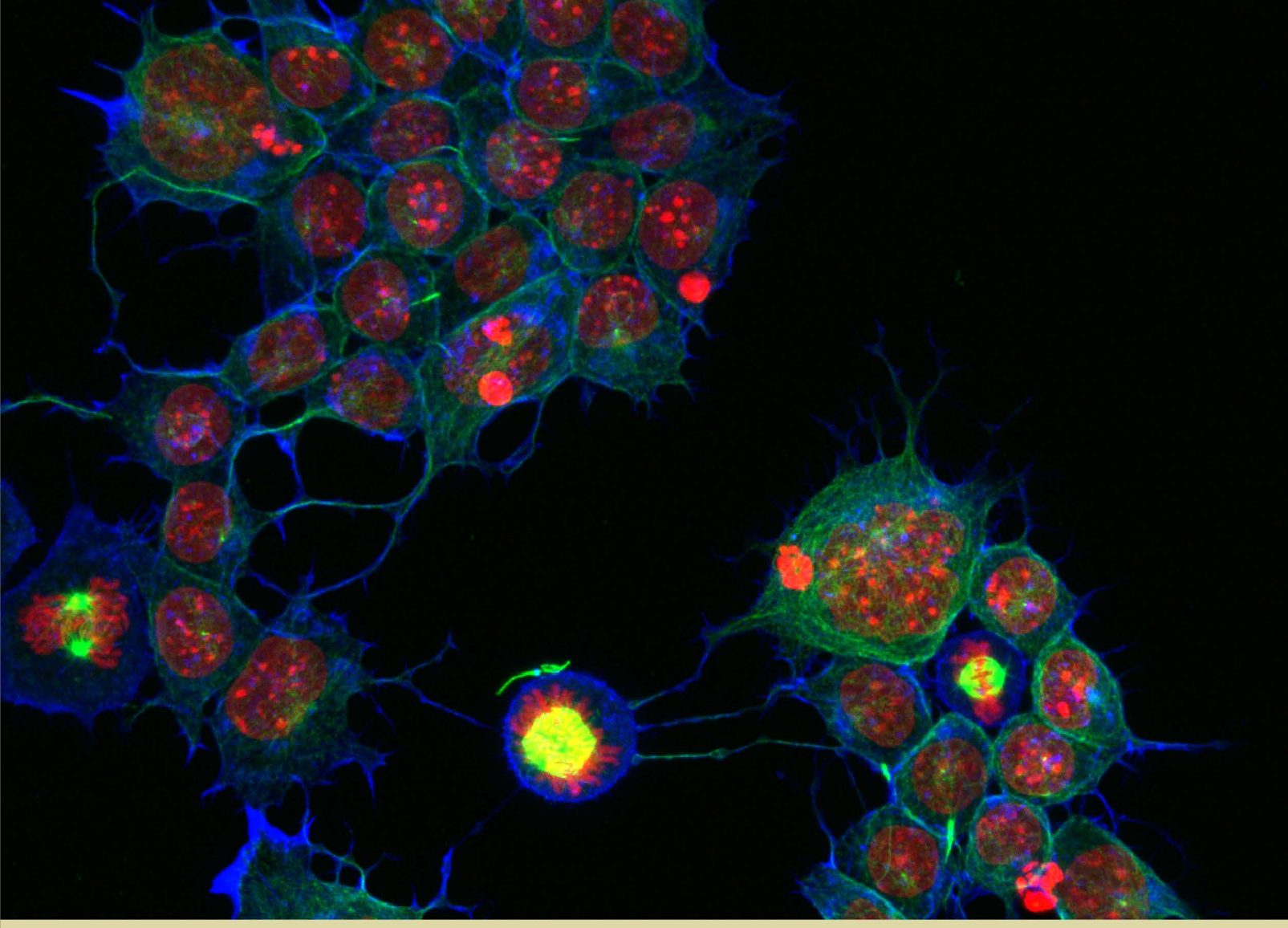

Tânia Marisa Melim Perestrelo

FRAMING PLURIPOTENCY: FROM GENE TO IMAGE

Tese de Doutoramento em Biologia Experimental e Biomedicina, ramo de Biologia Molecular, Celular e do Desenvolvimento, orientada pelo Professor Doutor João Ramalho-Santos, apresentada ao Instituto de Investigação Interdisciplinar da Universidade de Coimbra.

Maio 2017

· U C ·

Universidade de Coimbra

UNIVERSIDADE DE COIMBRA

Framing Pluripotency: From Gene to Image

by

Tânia Marisa Melim Perestrelo

Thesis submitted to the Institute for Interdisciplinary Research of the University of Coimbra in conformity with the requirements for the degree of Doctor of Philosophy in the area of Experimental Biology and Biomedicine, specialization in Molecular, Cellular and Developmental Biology.

May 2017

The work here presented was conducted on the Biology of Reproduction and Stem Cell Group at the Center for Neuroscience and Cell Biology (CNC) of University of Coimbra, and on Dr. Wirtz lab, at Johns Hopkins University. This work was under the scientific supervision of Dr. João Ramalho Santos.

The study presented in this dissertation was supported by an individual fellowship from the Portuguese Foundation for Science and Technology (FCT) attributed to Tânia Perestrelo (SFRH/BD/51684/2011) by the Doctoral Programme in Experimental Biology and Biomedicine (PDBEB). This work was also supported by FCT under the strategic project (UID/NEU/04539/2013) and by FEDER/COMPETE 2020 under the research project (POCI-01-0145-FEDER-007440).

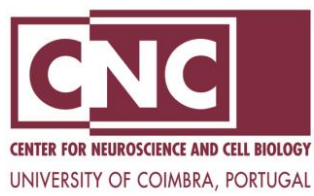

"Deus escreve certo por linhas tortas…"

Autor desconhecido

Dedico esta tese a todos os que se cruzaram comigo ao longo destes seis anos
e que a cada obstáculo, me deram força e me fizeram acreditar que eu era capaz.
Vocês sabem quem são…

I would like to dedicate this thesis to all of you that cross my path during these six years,
shared my tears and concerns, and gave me the support and strength to achieve this goal.
You know who you are…

Acknowledgments

Gostaria de começar por agradecer aos meus pais pelo apoio incondicional a cada aventura que me proponho. Um muito obrigado por todas as palavras amigas, conselhos e, pela vossa luta constante para que eu possa seguir os meus sonhos!

Gostaria de agradecer ao professor João Ramalho, por ter aceite ser meu orientador e ter-me dado a liberdade de desenhar e tentar concretizar o "meu" projeto. Obrigada por me dar liberdade de errar e, quando as coisas correram menos bem, apoiar-me a continuar em frente e ensinar-me a olhar para os resultados e ver o que "eles dizem". Obrigada pela continua aprendizagem, hei de lhe dever isso para sempre! Obrigada por acreditar em mim!

I would like to thank Dr. Wirtz, who gave me the opportunity to work in his lab. You adopt me as a true member of Wirtz Lab and I am really grateful for that! Your enthusiasm for science is contagious! Thank you for being at my desk for hours to brainstorm and guide me among these years. More importantly, thank you for believing in me!

I would also like to thank all the present and past members of Wirtz Lab for your support! It was a privilege to work with all of you. To Pei-Hsun and Daniele, a special thank you for all your support and mentoring, your help was precious! Angela, thank you so much to take care of me when I arrived! Wei, "oh well…", thank you for teaching me the "real science world" and for all the coffee! Jude, thank you for being our "Teddy bear" in lab, and my fellow on the long nights in lab! Leonor, thank you for the support and to be also my fellow of the long nights! To the "Portuguese crew", Inês, Duarte and Alex, thank you for the amazing six months! Alex, thank you for working with me, it was a great experience. Nico, thank you for the support, the brain storms, to be the crazy Latino physicist desk neighbor and friend! Thank you to the Postdocs, Meng, Lijuan and Yu-Tai who teach me so much! You guys are amazing! I would also like to thank Hasini and Jake for all your help from ordering a thousand things to dealing with crazy microscopes! Ivie, thank you for your support on dealing with the pain of no-results! Anjil, thank you for all your help! I would also like to thank Allison and Zev for being always supportive whenever I needed. To the undergrads that help me among these years in the

Wirtz lab: Mosisa, Nikki, Megan and Chris, thank you, I learned a lot with each of you! Nevertheless, a special thanks to Chris, to choose me as a lab mentor and for helping me to succeed! To Jeron and Sarah, thank you for receiving me so well, you guys made me feel at home; and off course, special thank you to Jeron for all the tips and brainstorming about rheology and image analysis!

I would also like to express my gratitude to all the INBT staff, with a special thank you to Ellie, Tracy, Gregg and Camille!

To the amazing people that I met in Baltimore, with a special and enormous thank you to Abhiram, Aditi, Alyssa (thank you so much for proofreading my thesis!!), Lola and Amin! There is no way to put in few words how amazing was to have you around! You are my Baltimore family!

Gostaria também de agradecer aos meus companheiros de jornada no BEB! O primeiro ano de doutoramento foi e será para sempre inesquecível graças a vocês! Desde as divagações sobre coisas e cenas, ao meu tico e teco estarem a morrer, várias serão as memórias que ficarão para sempre e me farão sempre lembrar que o doutoramento é de facto feito de altos e baixos e, que vocês proporcionaram um primeiro ano cheio de sorrisos, boa disposição e crença que com espírito crítico a "coisa" vai lá! Obrigada António, Patrícia, Mariline, Guedes, Sara, Nina, Dó, Sopi, André, Ribas e Marcelo!

Aos meus colegas de laboratório em Coimbra, um muito obrigada! Paula, Renata, Marta, Andreia e Sandra obrigada por toda a ajuda e boa disposição e, claro está, um agradecimento muito especial ao Marcelo, Sandro, Ana Sofia e Inês pelas várias horas de "brainstorming" por Skype.

Aos pais do Mário, ao Luís e à minha restante família e família do Mário, obrigada pelo apoio!

E, claro está, a todos os meus amigos do "Monte" (da Caparica), de Coimbra e da Madeira, obrigada por acreditarem em mim! Um obrigada especial ao André, Sopi, Joana Pedro, Filipa, Rui e Marino que, de maneiras únicas, me fizeram acreditar que isto era atingível!

E, como os últimos são "sempre" os primeiros… Um muito obrigada à minha irmã, Catarina, pelo apoio incondicional. Obrigada por batalhares que também tens razão, e acreditares que eu vou ser capaz. Obrigada pelas palavras de confiança!

E, por fim, um agradecimento muito especial ao Mário. Obrigada pelo sorriso sempre presente e pelas palavras sempre encorajadoras. Obrigada por sempre acreditares em mim, por me apoiares quando decidi partir à aventura e, pela força que sempre me deste, estando eu longe ou perto. Sem ti

não teria conseguido! Obrigada por me fazeres acreditar que eu era capaz.... sim, tinhas razão! Por fim, obrigada por esperares…

Table of Contents

List of abbreviations

2i medium	Serum-free Media with CHIR99021, PD0325901 and LIF
3BrP	3-Bromopyruvate
3D	Three Dimensions
AA	Antimycin A
alternative 2i	Serum-free Media with GP77675 and PD0325901
Amot	Angiomotin
AP	Alkaline Phosphatase
aPKC	Atypical Protein Kinase C
APS	Ammonium Persulfate
APTES	Aminopropyltriethoxysilane
ATP	Adenosine Triphosphate
AVE	Anterior Visceral Endoderm
BMP	Bone Morphogenic Protein
BSA	Bovine Serum Albumin
CHIR99021	Gsk3 Inhibitor
DCA	Dichloroacetate
DNMTs	DNA Methyltransferases
Drp1	Dynamin-Related Protein 1
DVE	Distal Visceral Endoderm
Ebs	Embryoid Bodies
ECM	Extracellular Matrix
EMT	Epithelial-Mesenchymal Transition
EPI	Epiblast
EpiSC	Epiblast-Derived Stem Cells
ERK	Extracellular Receptor Kinase
ESC	Embryonic Stem Cells
ETC	Electron Transport Chain
$FADH_2$	Flavin Adenine Dinucleotide
FGFr2	FGF Receptor 2
Gal	Galactose
GP77675	Src Inhibitor
Gsk3	Glycogen Synthase Kinase-3
GTP	Guanosine Triphosphate
HATs	Histone Acetyltransferases
HDACs	Histone Deacetylases
hESC	Human Embryonic Stem Cells
Hif1α	Hypoxia-inducible Factor 1 α
HMTs	Histone Methyltransferases
ICM	Inner Cell Mass
IMM	Inner Mitochondrial Membrane
iPSC	Induced Pluripotent Stem Cells
JAK	Janus Kinase
KEGG	Kyoto Encyclopedia of Genes and Genomes
LDHA	Lactate Dehydrogenase A

LIF	Leukemia Inhibitory Factor
LIFr	LIF Receptor
LINC	Linker of Nucleoskeleton and Cytoskeleton
MAPK	Mitogen-Activated Protein Kinase
mEpiSC	Mouse Epiblast-derived stem cells
mESC	Mouse Embryonic Stem Cells
MFN	Mitofusin
mtDNA	Mitochondrial DNA
Mx	Myxothiazol
N2B27	Neuronal Differentiation Medium
NADH	Nicotinamide Adenine Dinucleotide
NHS	Acrylic Acid *N*-hydroxysuccinimide ester
O.N.	Overnight
OCR	Oxygen Consumption Rate
OMM	Outer Mitochondrial Membrane
OXPHOS	Oxidative Phosphorylation
PBS	Phosphate-Buffered Saline
PD0325901	MEK Inhibitor
PDH	Pyruvate Dehydrogenase Complex
PDK1	Pyruvate Dehydrogenase Kinase 1
PDMS	Polydimethylsiloxane
PI3K	Phosphatidylinositol 3-Kinase
Pluripotency Medium	ESC Cultured in Serum with LIF
PrE	Primitive Endoderm
ROS	Reactive Oxygen Species
RT	Room Temperature
ShcA	Src-Src Homology/Collagen A
so	Soft substrate
st	Stiff substrate
T	T Brachyury
TCPS	Tissue Culture Polystyrene
TE	Trophectoderm
TEMED	N,N,N′,N′-Tetramethylethylenediamine
UCP2	Uncoupling Protein 2

Abstract

Self-renewal and pluripotency are the two major hallmarks of embryonic stem cells (ESC). Since ESC were first isolated in culture, one of the big challenges has been the maintenance of their pluripotency *in vitro*. ESC cultures require specific factors, which are responsible for the activation of pluripotency pathways and inhibition of differentiation pathways. A plethora of biochemical and mechanical modulators have been shown to individually affect the pluripotency state. However, how these different modulators work together to determine the pluripotency/differentiation state of ESC remains to be established.

The work developed in this thesis aimed at uncoupling the biochemical and mechanical modulators effect in ESC fate. To understand how different modulators regulate pluripotency, the ESC gene expression was evaluated upon the effect of different biochemical modulators – leukemia inhibitory factor (LIF) and mitochondria respiratory chain modulators – and mechanical modulators – substrate stiffness. First, multiple combinations of the different stimuli were performed. Then, the effect of each modulator in ESC gene expression and the inter-relationship between paired modulators was determined.

As expected, when two modulators were combined, ESC gene expression changed. Nevertheless, the magnitude of LIF effect (- LIF *vs.* + LIF) was dependent on mitochondria respiratory chain inhibitor Antimycin A (AA). However, it was independent of the indirect activation of oxidative phosphorylation through galactose. Interestingly, the magnitude of mitochondria respiratory chain modulators effect was dependent on the presence of LIF. Unexpectedly, the magnitude of stiffness effect (stiff substrates *vs.* soft substrates) in gene expression was not dependent on any biochemical pluripotent modulator tested. These results suggest that stiffness and biochemical modulators regulate ESC pluripotency through non-interfering pathways, where stiffness is a key modulator in the regulation of ESC fate.

Challenged by the common heterogeneity of ESC culture, the increase of image-based-assays to evaluate pluripotency, and the lack of image analysis approaches available to automatically quantify pluripotency, we developed an open-source software, Pluri-IQ, to quantify ESC pluripotency in culture.

Pluri-IQ was designed to automatic segment ESC colonies in both phase-contrast and fluorescence images, with high precision. With a low user input required, Pluri-IQ was able to quantify the percentage of pluripotent, mixed and differentiated colonies after alkaline-phosphatase, or pluripotent antibodies staining assays. Moreover, it was capable to analyze single or multiple low magnification images, with an accuracy around 90%.

In summary, the results presented in this thesis identify the stiffness as a key role in ESC fate, working independently of biochemical pluripotent cues. In addition, a new free-software for ESC image quantification was developed, which has the potential to be routinely used, increasing unbiased data acquisition and reproducibility.

Keywords: Embryonic Stem Cells (ESC), pluripotency, LIF, mitochondria, substrate stiffness, Pluri-IQ, quantification of pluripotency

Resumo

As células estaminais embrionárias (ESC) apresentam como principais características a capacidade de autorrenovação e pluripotência. Refira-se que a manutenção da pluripotência destas células *in vitro* constitui um dos principais desafios desde que as ESC foram pela primeira vez isoladas em cultura. As ESC em cultura necessitam de fatores específicos responsáveis quer pela ativação de vias de sinalização de pluripotência quer pela inibição de vias de diferenciação. Numerosos moduladores bioquímicos e mecânicos foram já implicados no controlo do estado de pluripotência das células, mas o grau de influência mútua entre tais moduladores, responsável pela referida capacidade de pluripotência / diferenciação das ESC, continua por demonstrar.

O trabalho desenvolvido nesta tese teve como objetivo desacoplar o efeito de moduladores bioquímicos e mecânicos na regulação das ESC. De modo a avaliar a influência que os diversos moduladores possuem na expressão genética das ESC, testaram-se os efeitos de diferentes moduladores bioquímicos – efeito de LIF (do inglês *leukemia inhibitory factor*) e moduladores da cadeia respiratória mitocondrial – e mecânicos – rigidez do substrato. Para tal, começou-se por realizar múltiplas combinações com os diferentes estímulos. Por fim, o efeito de cada modulador na expressão genética das ESC e a inter-relação entre combinações de moduladores foi determinado.

Como esperado, a expressão genética das ESC foi alterada quando os moduladores foram combinados. A magnitude do efeito do LIF (- LIF *vs.* + LIF) mostrou-se dependente do inibidores da cadeia respiratória mitocondrial Antimicina A (AA), mas independente da ativação indireta da fosforilação oxidativa através do uso de galactose. No entanto, a magnitude do efeito dos moduladores da cadeia respiratória mitocondrial mostrou-se dependente da presença de LIF. Inesperadamente, a magnitude do efeito da rigidez do substrato (substratos

rígidos *vs.* substratos menos rígidos) na expressão genética das ESC não se mostrou dependente de qualquer modulador bioquímico testado. Estes resultados sugerem que a rigidez do substrato e os vários moduladores bioquímicos regulam a pluripotência das ESC através de vias de sinalização independentes sendo que a rigidez do substrato se assume como um modulador chave na regulação das ESC.

Em resposta à normal heterogeneidade das ESC em cultura assim como ao aumento dos ensaios de pluripotência baseados em imagem e escassez de procedimentos para a quantificação automática da pluripotência associados aos mesmos, a presente tese descreve igualmente o desenvolvimento de um software de código aberto, designado por Pluri-IQ, para quantificar a pluripotência das ESC em cultura.

O software Pluri-IQ segmenta automaticamente colónias de ESC com elevada precisão, sendo capaz de utilizar imagens de contraste de fase ou de fluorescência para tal. Pluri-IQ minimiza a necessidade de intervenção humana no seu funcionamento, conseguindo quantificar a percentagem de colónias pluripotentes, mistas e diferenciadas após ensaios de fosfatase alcalina ou de imunocitoquímica com anticorpos específicos para pluripotência. Destaca-se ainda a sua capacidade de análise de uma imagem única ou de imagens múltiplas combinadas, de microscopia de baixa ampliação, com uma exatidão de cerca de 90 %.

Em suma, os resultados apresentados nesta tese permitiram identificar a rigidez do substrato como um modulador chave na regulação das ESC, sendo o seu efeito independente de estímulos bioquímicos de pluripotência. Por outro lado, o desenvolvimento de um software de código aberto para quantificação de pluripotência em imagens de ESC, reúne as características necessárias para a sua utilização como uma ferramenta de análise rotineira capaz de aumentar a imparcialidade e a reprodutibilidade de dados obtidos neste tipo de estudos.

Palavras-chave: Células Estaminais Embrionárias (ESC), pluripotência, LIF, mitocôndria, rigidez do substrato, Pluri-IQ, quantificação de pluripotência.

Chapter 1

General Introduction[1]

[1] This chapter is part of a review paper: Tânia Perestrelo, et al; *in preparation*

Mammalian development is a tightly regulated process. The control of gene expression by multiple factors is essential in all embryonic stages in order to achieve the correct development. In this chapter, we will describe how embryonic development occurs *in vivo*, how *in vitro* derived embryonic stem cells (ESC) can mimic some aspects of early differentiation, and which pathways of metabolism and mechanical forces, are responsible for the regulation of pluripotency, embryonic development and ESC maintenance.

1.1. Embryonic Development

Embryogenesis is a complex, dynamic and precise process. It begins with the fertilization of the oocyte with a sperm cell, which gives rise to a totipotent cell, the zygote (Figure 1.1). This cell has the potential to produce all embryonic and extraembryonic lineages. The zygote undergoes a series of cleavages, resulting in the formation of cells called blastomeres, and at the 8-cell stage blastomeres get compacted against each other and the morula stage embryo is formed [1]. At this stage, the first cell fate decision occurs: embryonic cells divide into trophectoderm (TE), which forms the fetal portion of the placenta; or the inner cell mass (ICM) also known as pluriblast, that contributes to the embryonic cell lineages, and is thus composed of pluripotent cells [1]. Shortly after ICM and TE specification, and prior to implantation, the blastocyst stage embryo is formed. At this stage, the second fate decision occurs. ICM cells differentiate into primitive endoderm (PrE, also known as hypoblast), and epiblast (EPI, also known as primitive ectoderm), which is the precursor cell lineage of the future fetus [2]. After implantation, and upon gastrulation and primitive streak region specification, mesoderm, definitive endoderm and ectoderm specification occurs (Figure 1.1) [3].

In order to recapitulate pluripotency, commitment and differentiation, different cell populations have been isolated *in vitro*: mouse ESC (mESC), human ESC (hESC), epiblast-derived stem cells (EpiSC) and induced pluripotent stem cells (iPSC) (Figure 1.1). mESC were first isolated from the ICM of mouse preimplantation blastocyst, in 1981, by two independent groups [4,5] and became the model for studies of pluripotency and differentiation due to their pluripotency and self-renewal capability. The ability to culture mESC lead to the increase interest and attempts to isolate hESC, and in 1998, for the

first time, hESC were successfully isolated from preimplantation blastocysts, donated from *in vitro* fertility treatments [6]. These cells also fulfill the pluripotency criteria, as they are able to differentiate *in vitro* as well as *in vivo* into the three embryonic lineages. Nevertheless, hESC medium specifications as well as their morphological characteristic are different from mESC.

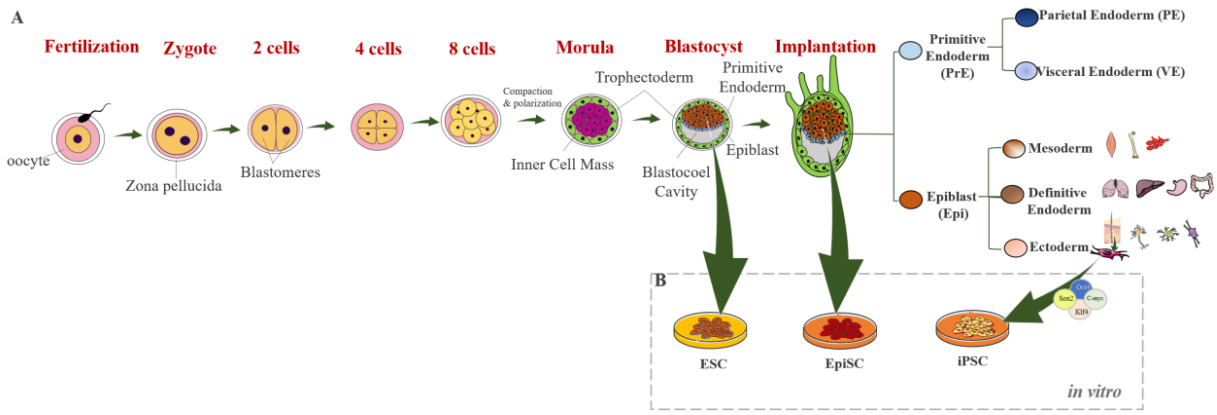

Figure 1.1 - Embryonic development in mammals and in vitro derived cells: from preimplantation to gastrulation.

(A) Schematic representation of cell fate decisions that lead to the formation of the three embryonic germ layers and the extraembryonic lineages. After fertilization, the zygote is formed. The zygote gives rise to two-cells, four-cells and then eight-cells that are morphologically distinct from each other. At this point, the cells undergo compaction, polarization and asymmetric cell division, giving rise to a compact morula, and the first cell-fate decision occurs: TE (green) and ICM (purple) are formed. At 32-cell stage, the blastocoel cavity starts to form inside the embryo, giving rise to the blastocyst, where the second cell-fate decision occurs: ICM gives rise to the EPI (orange), and the PrE (blue). PrE is positioned facing the blastocoel cavity, while EPI is positioned between the PrE and the TE. At this stage, the blastocyst is ready to be activated and to implant. After implantation, PrE will give rise to PE and VE and EPI will give rise to mesoderm, definitive endoderm and ectoderm. **(B)** Different pluripotent cell populations have been isolated and propagated in *in vitro* conditions. ESC are derived from the ICM of the pre-implanted blastocyst whereas EpiSC are derived from the post-implantation EPI. iPSC are derived from somatic cells molecularly reprogrammed *in vitro* by forced exogenous expression of a combination of key pluripotent transcription factors such as Oct4, Klf4, Sox2 and c-myc. Abbreviations: ICM: inner cell mass; iPSC: induced pluripotent stem cells; EPI: epiblast; ESC: embryonic stem cells; EpiSC: epiblast-derived stem cells; PE: parietal endoderm; PrE: primitive endoderm; TE: trophectoderm; VE: visceral endoderm.

Pluripotent cells can also be derived from the post-implantation EPI, between E5.5 and E8 from mouse and rat embryos (Figure 1.1) [7]. EpiSC have been proposed to be the *in vitro* pluripotent counterpart of the post-implantation EPI, as the maintenance of EpiSC pluripotency *in vitro* is

dependent of the same pathways required to maintain pluripotency of the post-implantation EPI *in vivo* [7,8].

The barrier to generate pluripotent cells derived from differentiated cells was broken in 2006, when iPSC were established for the first time [9]. iPSC are somatic cells molecularly reprogrammed *in vitro* by forced exogenous expression of a combination of key pluripotent transcription factors (Figure 1.1). Although these cells do not have an embryonic origin, they acquire ESC characteristics, such as morphology and ability to differentiate into the three embryonic lineages *in vitro* as well as *in vivo* [9,10].

1.1.1. Mouse embryonic development: from Zygote to blastocyst

After the fertilization, a totipotent cell, the zygote, is formed. The zygote goes through a series of cleavages, where each blastomere is spherical and morphologically distinct until the third cleavage, where the 8-cell embryo experiences compaction (Figure 1.1). Blastomeres flatten against each other, their cell-cell contact is maximized, and they cannot be distinguished morphologically anymore [11]. At this stage, symmetric and asymmetric division occurs, which results in polar (outside cells) and apolar cells (inside cells), which ends with the formation of the first two distinct cell lineages, where polar cells are known to give rise to TE and apolar cells to ICM (Figure 1.1).

The Hippo signaling pathway has been shown to be decisive for TE / ICM lineage specification (Figure 1.2). While Hippo inhibition induces TE lineage, its activation promotes ICM [12]. Through a positive feedback mechanism, Oct4 maintains its high expression and represses *Cdx2* and *Eomes* expression in inside cells, giving rise to ICM cells [13]. Therefore, by the 32-cell stage, Cdx2 is restricted to the outer cells whereas Oct4, Sox2 and Nanog form a specific network of pluripotent genes that are limited to the ICM [14–16].

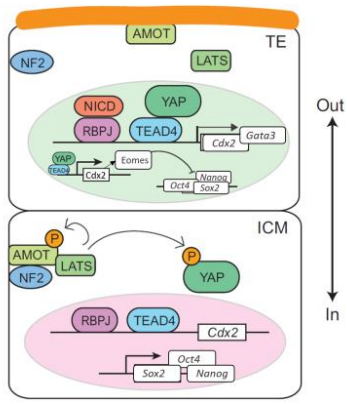

Figure 1.2 – TE and ICM specification: regulation cascade mediated by the Hippo pathway in the mouse embryo.

In outer cells the Hippo pathway is inactive. Amot is sequestered to the apical domain of the cell. Consequently, YAP is able to accumulate in the nucleus where it activates Tead4. Tead4-YAP complex activates the specific transcription factors of TE lineage including Cdx2 and Gata3. Cdx2, is in turn, responsible for the activation of *Eomes* and repression of *Oct4* and *Nanog* expression and consequently segregation of these two last transcription factors to the ICM only. In the inner cells, Amot is restricted to the adhesion junctions, where it sequesters YAP in the cytoplasm or induces its phosphorylation by Lats1/2, ending up with YAP degradation and Tead4 inactivation, while *Oct4*, *Sox2* and *Nanog* maintain their expression. Abbreviations: ICM: inner cell mass; TE: Trophectoderm. *Adapted from*: Chazaud *et al.* (2016) [1].

After ICM and TE specification, the blastocyst is formed. The inner cells get positioned to one pole of the embryo, adjacent to the TE, while a blastocyst cavity is created (Figure 1.1). At this point, the second fate decision occurs: ICM cells differentiate into PrE and EPI. The transcription factors Nanog and Gata6 expressed in ICM cells become asynchronously expressed during E3.0 to E3.75, in a "salt and pepper" distribution, until E4.0 approximately, where Nanog and Gata6 are restricted to EPI and PrE lineage, respectively [17,18]. The mechanism behind Nanog and Gata6 restriction has been recently uncovered, with Fgf signaling crucial for PE commitment (Figure 1.3). After specification, EPI and PrE cells change their random position, where PrE cells migrate towards the cavity and form a polarized single layer, while EPI cells migrate away of the cavity (Figure 1.1). How this migration occurs is still not totally understood but recent studies have shown that not only polarization, but also adhesion molecules, actin polymerization and programmed cell death of incorrectly positioned cells, can have an important role in this mechanism [1].

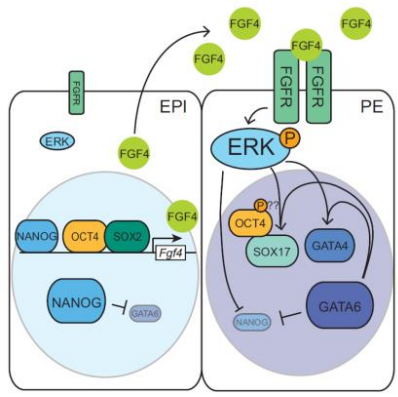

Figure 1.3 – EPI and TE formation mediated by Fgf4 signaling pathway in the mouse embryo.
Nanog represses *Gata6* expression and in collaboration with Oct4, and Sox2 increases the expression levels of *Fgf4*. Fgf4 is secreted and binds to Fgfr2 of adjacent cells, which activates the Fgf signaling pathway and consequently increases the levels of Gata6. Gata6 is then responsible for activation of other PrE specific genes, such as *Sox17* and *Gata4* and inhibition of *Nanog*. Abbreviations: EPI: Epiblast; PE: Primitive Endoderm; Fgfr: Fgf receptor. *Adapted from*: Chazaud *et al.* (2016) [1].

1.1.2. Mouse embryonic development: Implantation

After the specification of TE, EPI and PrE cell lineages, the blastocyst is ready to be activated in order to successfully implant into the uterus (Figure 1.1). Concomitantly, the uterus has to be receptive to the embryo. This mutual activation is triggered by estrogen and progesterone and determines the "window" of implantation [19,20]. Changes in cell cycle, cell signaling and energy metabolic pathways on the blastocyst make it competent [21]. In the uterus, estrogen and progesterone activate molecular pathways that are crucial for uterus receptiveness [22]. Leukemia inhibitory factor (LIF) is a member of the interleukine-6 family and is one of the cytokines crucial for uterine preparation for implantation in rodents [23].

The process of implantation can be classified into three phases: apposition, attachment and penetration. During apposition, the uterine lumen becomes reduced and the luminal epithelium becomes close to the external surface of the TE. The presence of adhesion molecules as well as cytokines, growth factors and their receptors in TE, and luminal epithelium interface mediates the attachment of the competent blastocyst to the receptive uterus. The increase of endometrial vascular permeability due to prostaglandins, and the direct contact between the mural TE (TE cells that surround the blastocyst

cavity) and luminal epithelium, leads to mural TE cells migration and invasion into the endometrial stroma, which leads to blastocyst implantation [22].

1.1.3. Mouse embryonic development: From egg cylinder formation to gastrulation

During implantation in the mouse, there is a burst of cell proliferation, and, oppositely to what happens during preimplantation, the embryo changes its shape, elongating along the proximal-distal axis to form the egg cylinder stage (Figure 1.4). The PrE differentiates into two cell types: the parietal endoderm, which lines up with the mural TE, and the visceral endoderm, which wraps the EPI and the extraembryonic ectoderm. The cells that constitute the EPI change their shape and polarize, reorganizing themselves into a rosette-like structure due to production of extracellular matrix signals from the TE and the PrE [24]. The TE that surrounds the EPI proliferates and differentiates into extraembryonic ectoderm and ectoplacental cone. The extraembryonic ectoderm maintains a subpopulation of self-renewing TE cells that is dependent of Fgf and Nodal, produced from the neighbor cells, the EPI (Figure 1.4 a) [25,26]. In the extraembryonic ectoderm, Fgf signaling pathway promotes the expression of *Cdx2,* which upregulates *Bmp4* expression. The crosstalk occurs as Bmp4 produced by extraembryonic ectoderm acts as a paracrine factor, essential for correct EPI development after implantation [27]. Nodal signaling produced by the EPI also promotes the specialization, at the distal tip of the egg cylinder, of the distal visceral endoderm (DVE) (Figure 1.4 b). Nodal signaling induces *Cer1* and *Lefty1* expression in the DVE, which are antagonists of Nodal signaling. As a consequence, Nodal is attenuated in the adjacent EPI cells, leading to the formation of a proximal-distal gradient of Nodal signaling in the EPI [28]. After specification, visceral endoderm cells migrate until they reach the border of the extraembryonic ectoderm, where they move laterally, overlying the EPI and forming the anterior visceral endoderm (AVE) [29]. AVE also expresses *Lefty1* and *Cer1* and establishes an anterior – posterior axis gradient of Nodal signal. This Nodal gradient promoted by AVE in addition with Wnt3 produced in the embryonic region and BMP4 produced in the extraembryonic ectoderm are responsible for the formation of the primitive streak in the posterior region of the embryo and the onset of gastrulation [30,31].

In the primitive streak region, EPI undergo epithelial-mesenchymal transition (EMT) and migrate away from the primitive streak to the anterior region where they form two embryonic germ layers, mesoderm (the middle sheet) and definitive endoderm (the outside tissue layer). Mesoderm gives rise to blood, muscle, bone, cartilage and connective tissues, while definitive endoderm forms the lung, liver, pancreas, gut tube and the intestinal tract. EPI cells that fail to migrate to the primitive streak region originate the ectoderm, a germ layer that forms the neural tissues, neural crest and skin [31].

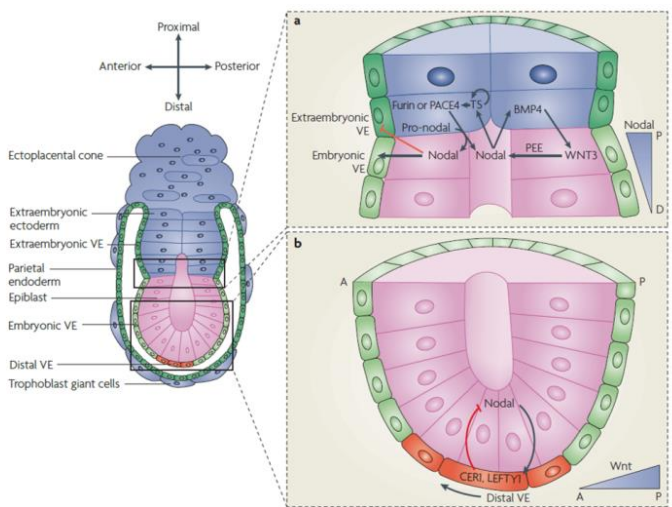

Figure 1.4 – Schematic representation of the mouse embryo pre-gastrulation.

(a) The proximal-distal axis is delineated due to a Nodal signaling gradient. Precursor Nodal is secreted from EPI whereas extraembryonic ectoderm secretes convertases furin and PACE4, which cleaves the Nodal prodomain. Nodal upregulates BMP4 in the extraembryonic ectoderm as well as increases Wnt3 pathway in EPI. **(b)** Specification of distal visceral endoderm. At the distal point, visceral endoderm cells become specialized and initiate the expression of *Cer1* and *Lefty1* responsible for the inhibition of Nodal and its gradient formation in the EPI. Abbreviations: VE: visceral endoderm. *Adapted from* Arnold *et al.* (2009) [32].

1.1.4. Pluripotency *in vitro*: mouse and human ESC, EpiSC, and iPSC

The need for a better understanding of early mammalian development led scientists to look for *in vitro* models, able to recapitulate cell pluripotency, commitment and differentiation. To fulfill the criteria of pluripotent stemness, cells need to be pluripotent, i.e., they have to be able to differentiate *in vitro* as well as *in vivo*, giving rise to all three embryonic lineages and germ cells, as well as to be able

of self-renewal: proliferate indefinitely in culture, while maintaining pluripotency [33,34]. To evaluate functional assessment of pluripotency, different assays have been developed.

In vitro, pluripotent cells have to be able to form embryoid bodies (EB). To test for EB formation, cells are grown as suspension aggregates in order to induce differentiation, and the differentiated cells have to comprise the three embryonic lineages. Both mESC, mEpiSC and hESC are capable of forming EB [7,8,34,35].

To assess the developmental potential i*n vivo,* different assays can be used based on the ESC origin. Teratomas are the gold standard to evaluate pluripotency *in vivo* in both hESC and mEpiSC [36]. Teratoma assay assess the ability of cells to spontaneously differentiate into tissues from the three germ layers when injected into immunocompromised mice. Embryo chimera assay is another test utilized to evaluate pluripotency. In this assay, cells are injected into the embryo, at the blastocyst stage, and the ability of the injected cells to re-enter the development process, giving rise to embryonic tissues, and germ line, along with the host cells, is assessed [36]. While mESC are capable to generate embryo chimeras, mEpiSC are not [7,8]. This is associated with the developmental stage difference between mEpiSC and mESC.

1.1.4.1. Mouse ESC

The discovery, in the 1950's, of teratocarcinomas, tumors containing multiple adult tissue types, and the knowhow obtained from the isolation of embryonal carcinoma cell lines derived from these tumors, were crucial for the development of culture conditions to successfully isolate and culture *in vitro* mESC, in 1981 [4,5,37]. mESC fulfill the criteria of pluripotency and seem to represent the immortalization of the ICM, with the cell lines derived from the preimplantation blastocyst considered to be in the naïve state of pluripotency, i.e., less committed.

The use of serum in combination with a feeder layer of mitotically inactivated mouse fibroblasts was the key to successfully isolate and maintain mESC in culture. However, the culture formulation was not totally controlled with the use of serum and mouse fibroblasts as feeders. Moreover, mESC

were only successfully derived from 129 strain mice. Therefore, the deconvolution of the molecules involved in the maintenance of mESC pluripotency in culture became crucial.

In 1988, LIF was identified as the protein secreted from the feeder cells responsible for mESC maintenance in culture [38,39], and, for the first time, in 1990, mESC were derived and cultured for a long-term in serum without feeders [40,41]. LIF is responsible for downstream transduction signals that, in mESC, promote self-renewal, pluripotency but also differentiation (Figure 1.5). Therefore, mESC fate is a balance between differentiation-inhibition and differentiation-induction signals, where the formers seem to compensate the latter one in culture, but still results in a heterogeneous mixture of cells with different transcription profiles.

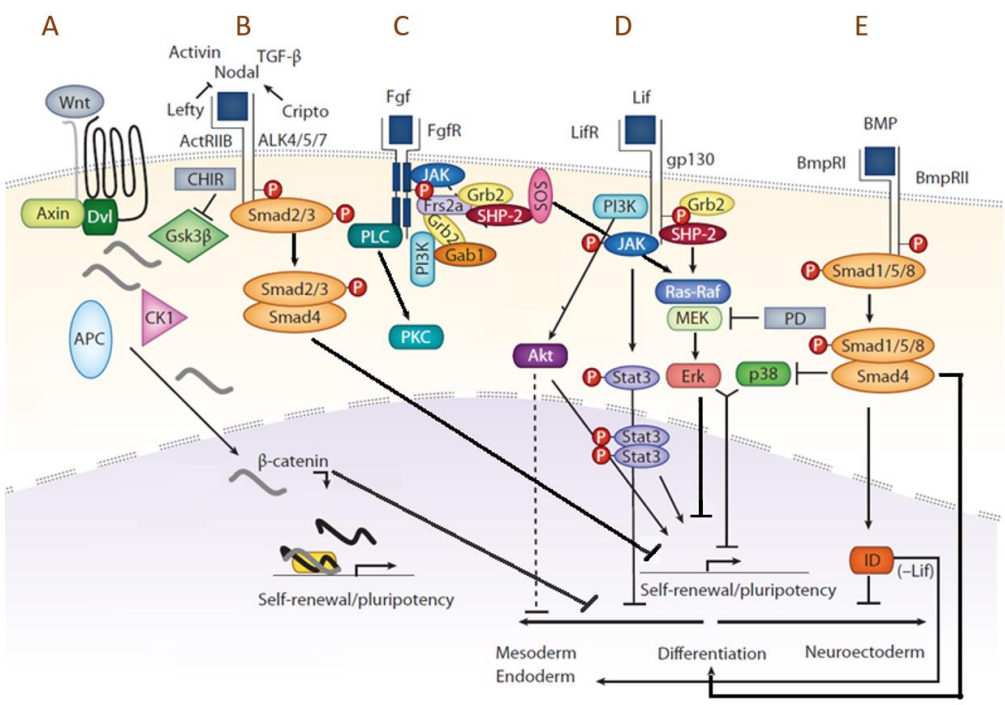

Figure 1.5 – Signaling pathways involved in mESC self-renewal and differentiation.

(A) Wnt canonical pathway activation leads to the translocation of β-catenin to the nucleus, where it inhibits mESC differentiation, while promoting mESC self-renewal and pluripotency. **(B)** Nodal and Activin are able to bind to the same receptors. Their activation leads to Smad signaling activation, which culminates in the inhibition of pluripotent genes. **(C)** FGF binds to its receptor, Fgfr, which results in Fgfr autophosphorylation. Fgfr phosphorylation leads to the recruitment of diverse proteins, with mitogen-activated protein kinase/ extracellular receptor Kinase (MAPK/ERK) pathway becoming activated. **(D)** LIF starts its signaling pathway by binding to its signaling receptor, LIFr, present in the cytoplasmic membrane. The binding of LIF to LIFr recruits gp130, another signaling receptor, and both form a heterodimer responsible for the activation of the receptor-associated

Janus Kinase (JAK). STAT3 is then recruited to the LIF receptor complex, and phosphorylated by JAK, which activates the JAK/STAT pathway. Two phosphorylated STAT3 dimerize, and the dimers are translocated to the nucleus, where they regulate the transcription genes crucial for maintenance of pluripotency. The LIF receptor complex also promotes ESC self-renewal and pluripotency through activation of phosphatidylinositol 3-kinase (PI3K) pathway. However, LIF signaling pathway also leads to the activation of MAPK/ERK pathway, known to induce mESC differentiation. **(E)** BMP binds to transmembrane BMP receptors, which promote the translocation of activated SMAD complex to the nucleus, where they inhibit genes responsible for neuronal differentiation. Moreover, BMP signaling pathway is able to inhibit MAPK/ERK pathway. *Adapted from:* Dejosez *et al.*, (2012) [42].

The maintenance of ESC in culture, however, requires the combination of LIF and serum in the medium, since serum withdrawal in media with LIF, still leads to ESC differentiation. Taking into account that ESC differentiates mostly towards to the neuronal lineage upon serum withdrawal [43], bone morphogenetic protein (BMP), an anti-neurogenic factor, was discovered to successfully replace serum in the medium (Figure 1.5) [44]. Nevertheless, only the combination of BMP and LIF, promote ESC self-renewal and maintenance of pluripotency [44,45]. In spite of efforts to produce a defined culture medium to maintain pluripotency, the ability to derive ESC from the preimplantation blastocyst, in LIF and BMP, continue to be restricted to embryos of some mouse strains.

The signaling pathways responsible for the maintenance of pluripotency during embryonic development have been actively compared with the pathways capable of maintaining pluripotency *in vitro*. Similar to the ICM in the mouse embryo, cultured mESC secrete Fgf and have the Fgfr in their membrane (Figure 1.5). Binding of Fgf to Fgfr activates mitogen-activated protein kinase/ extracellular receptor Kinase (MAPK/ERK) pathway, which leads to mESC differentiation [46]. Moreover, Wnt3 induces nuclear translocation of active β-catenin, which, oppositely to Fgf4, is responsible for preventing mESC differentiation (Figure 1.5) [47,48]. Therefore, a serum-free medium with the MEK inhibitor PD0325901, in combination with the inhibitor of the glycogen synthase kinase-3 (Gsk3), CHIR99021, which stabilizes β-catenin, was discovered to be capable to promote mESC self-renewal and pluripotency in serum-free medium [49]. The combination of these two inhibitors and LIF in serum free medium, was named 2i medium. Interestingly, 2i medium promotes a more homogeneous mESC culture when compared to mESC cultured in the presence of serum. Therefore, the *in vitro* manipulation

of these pathways allowed ESC to be finally derived with high efficiency not only from embryos of other strains of mice but also from rats [50–52]. In addition, mESC can be successfully maintained *in vitro* when derived between E3.5 and E4.5 blastocyst stages; however, their transcription profile cluster similar to the E4.5 naïve EPI *in vivo* [53], suggesting that these conditions promote the naïve state of ESC *in vitro*.

1.1.4.2. Mouse EpiSC

Pluripotent cells can also be derived from the post-implantation epiblast. These cells, named EpiSC, were successfully derived for the first time in 2007, from the EPI of the mouse egg cylinder in medium containing Fgf2 and Activin A [7,8]. More recently, mEpiSC have been derived in an alternative growth condition, a combination of GSK3 inhibitor together with IWR1, a stabilizer of Axin2, that leads to the stabilization of β-catenin in the cytoplasm and together promote mEpiSC self-renewal [54].

mEpiSC express the pluripotent markers Oct4, Nanog and also early post-implantation EPI markers, such as Fgf5 and T-brachyury [7,8]. Moreover, mEpiSC are able to differentiate into the three embryonic lineages *in vitro* and form teratomas *in vivo* [7,8]. Despite these cells fulfilling the pluripotency criteria *in vitro*, they are not able to generate chimeras *in vivo*, when injected into the preimplantation blastocyst [7,8]. Nevertheless, similarly to the post-implantation EPI, mEpiSC are capable to contribute to the embryonic development when grafted to the EPI of embryos at the post-implantation stage *ex vivo* [55]. These characteristics have been attributed to the mEpiSC embryonic tissue of origin, and the signaling pathways responsible for maintenance of their pluripotent status, which seem to promote a developmental asynchrony between mEpiSC and the preimplantation blastocyst. Therefore, mEpiSC are referred to be in a primed pluripotency state.

1.1.4.3. Human ESC

hESC have also been successfully isolated from the preimplantation blastocysts and fulfill the pluripotency criteria. However, hESC have been described to be more similar to mEpiSC than to mESC. In order for hESC to maintain pluripotency they have to be cultured in Fgf2, TGFβ1 and Activin A

containing medium. In addition, hESC grow in flat and compact colonies morphologically identical to mEpiSC and not to mESC, which grow in rounded colonies [8]. Moreover, contrary to mESC, which have two active X chromosomes, female hESC have already one inactive X chromosome, like mEpiSC; and similar to mEpiSC, hESC are not responsive to LIF nor have the ability to self-renew in 2i medium. However, hESC seem to be less primed than mEpiSC. Recently, naïve hESC have been established in culture using different medium combinations [56]. Nevertheless, these naïve hESC require more characterization in order to better understand if these are truly naïve pluripotent cells and if they actually correspond to a real embryo stage *in vivo*.

1.1.4.4. iPSC

iPSC are somatic cells molecularly reprogrammed by forced exogenous expression of a combination of key transcription factors, such as Klf4, Oct4, Sox2 and c-Myc, which acquire ESC characteristics. Since 2006 (in mouse), iPSC have been generated with different combinations of transcription factors and with different delivery techniques in order to improve iPSC reprogramming efficiency [57]. Nowadays, iPSC can be originated from different somatic cells and from different species, including human [57,58]. Therefore, iPSC are seen not only as an *in vitro* model to understand pluripotency and reprogramming signaling pathways, but also as a unique tool to derive cells to study diseases, with a potential application in cell therapy. In general terms miPSC are similar to mESC and hiPSC to hESC.

1.1.5. The pluripotent state: key transcription factors in mouse ESC

The maintenance of each developmental state is achieved through a balance of different networks of transcription factors (Figure 1.6).

1.1.5.1. Core transcriptional factors

Oct4, Sox2 and Nanog are the master regulators in the pluripotency core of transcription factors. They are expressed *in vivo* in the pluripotent section of the mouse embryo, from pre- to post-implantation stage, where they are crucial for the correct embryonic development. Similar to what takes

place *in vivo*, Oct4, Sox2 and Nanog regulate each other's expression, and are expressed at the same time in both mESC and mEpiSC. Consequently, Oct4, Sox2 and Nanog are essential for maintenance of pluripotency but not specific to naïve or primed states *in vitro*.

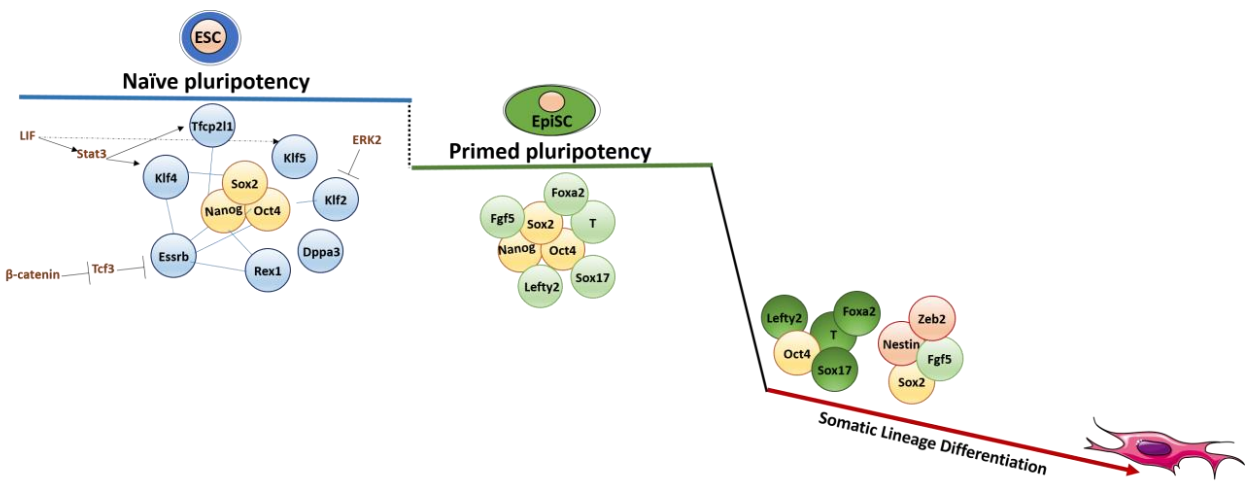

Figure 1.6 – Role of transcription factors in mouse ESC pluripotency.

The main transcription factors involved in mESC naïve and primed pluripotency, as well as in lineage specification (mesendoderm and ectoderm) are represented. The core pluripotency transcription factors (Oct4, Sox2 and Nanog) are represented in yellow. When together, Oct4, Sox2 and Nanog maintain ESC in a pluripotent state. In blue are represented the transcription factors specific of the naïve state of pluripotency, with the outer circle boxes representing some of the pathways that activate these genes. Primed specific transcription factors are represented in green. Upon differentiation, specific transcription genes are maintained in each lineage: mesendoderm (Oct4, Sox17, Lefty2. Foxa2, T (T-brachyury)) and ectoderm (Sox2, Fgf5, Nestin and Zeb2).

1.1.5.1.1. Oct4

Oct4 was the first transcription factor identified as a key regulator of pluripotency [59]. Oct4 is a member of the family of POU transcription factors. It is expressed during the early mouse embryonic development until gastrulation, where its expression becomes restricted to the primordial germ cells [59]. Mouse embryos lacking the *Oct4* gene develop until the blastocyst stage, but fail to specify the first cell commitment, i.e., cells get their ICM localization, but instead of maintaining pluripotency, they also differentiate into TE [60]. *In vitro*, mESC also express *Oct4* and upon induction of differentiation, *Oct4* expression is lost [61]. Nevertheless, recent studies show that *Oct4* overexpression induces differentiation

[62], while reduced levels of *Oct4* impair differentiation [63]. Therefore, Oct4 seems to play a dual role, and, as a consequence, the regulation of its expression, *in vivo* and *in vitro*, must be tightly controlled.

1.1.5.1.2. Sox2

Sox2 is another transcription factor crucial for the maintenance of pluripotency. *In vivo*, *Sox2* is highly expressed not only in the mouse ICM, pre- and post-implantation EPI, but also in the TE and later on by neuroectodermal cells [15]. *In vitro*, Sox2 positively regulates *Oct4* transcription and, upon Sox2 inactivation, mESC differentiate towards TE [64]. *Sox2* overexpression leads to a predisposition of mESC to neuroectoderm differentiation [65], which suggests that Sox2 levels must be also constrained in order to efficiently promote self-renewal. Importantly, Sox2 is also able to interact with Oct4, and both bind to the DNA at Oct/Sox motifs, synergistically regulating transcription of themselves as well as other genes, such as *Fgf4* and *Nanog* [66–69].

1.1.5.1.3. Nanog

Nanog is another key regulator of pluripotency. Its expression is crucial for the second cell fate in the mouse embryo: acquisition of PrE or EPI specification. In Nanog null embryos ICM only generates PrE, while *in vitro*, Nanog null mESC can sustain self-renewal but are highly prone to differentiation [16,70]. However, contrary to Sox2 and Oct4, *Nanog* overexpression promotes mESC self-renewal even in the absence of LIF. Nonetheless, endogenous Nanog levels are not sufficient to sustain self-renewal in the absence of LIF [14].

1.1.5.2. The Naïve pluripotent state

The naïve pluripotent state is maintained as a result of a tight and unique network of transcription factors that promote self-renewal and inhibit differentiation pathways, while preserving pluripotency pathways. This state is regulated not only by Oct4, Sox2 and Nanog, but also by specific naïve transcription factors, such as Esrrb, Klf4, Klf2, klf5, Rex1, Stat3, Tfcp2l1 and Dppa3 (Figure 1.6).

1.1.5.2.1. Esrrb

Esrrb is an important mediator of self-renewal in mESC. Esrrb is a transcription factor that binds to promoters of key pluripotent genes such as *Oct4*, *Nanog* and *Rex1*, and regulates their expression [71,72]. Esrrb is a direct target of Nanog and, in Nanog null mESC, Esrrb is able to maintain self-renewal independently of LIF signaling [73]. In addition, Esrrb is a direct target of Tcf3 repressor, and it is the main effector of mESC self-renewal upon GSK3 inhibition [48]. Esrrb deletion promotes a reduction of mESC ability to self-renew and, mESC cultured in the absence of LIF differentiate [74]. However, in the presence of LIF, mESC can still be propagated, which suggests that Esrrb acts in a parallel pathway to LIF/Stat3 to maintain mESC self-renewal [48,73]. Recently, Esrrb has also been shown to be a mitotic bookmarking factor. Esrrb is able to remain retained to key regulatory regions of chromosomes during all phases of mitosis, which results in the upregulation of self-renewal genes such as *Klf4* upon re-entry in interphase [75].

1.1.5.2.2. Klf

Klf2, Klf4 and Klf5 are members of the kruppel-like factor family, responsible for the regulation of transcription in biological processes, such as development and differentiation. The triple knockdown of Klf2, Klf4 and klf5 leads to loss of self-renewal and mESC differentiation [76]. While Klf4 works as a mediator of LIF signaling, it is a direct target of Stat3, regulates *Sox2* expression, and its overexpression is able to confer partial independence of LIF [77], Klf5 is not a direct target of LIF/Stat3 pathway; however, its expression is regulated by this pathway [78]. On the other hand, Klf2 is not responsive to LIF [78]. Instead, Klf2 is the protein that mediates pluripotency in Mek inhibition 2i medium [79]. Erk2 has recently been shown to phosphorylate Klf2, leading to its proteasome degradation. Therefore, Mek inhibition stabilizes Klf2, which leads to the activation of self-renewal genes [79].

1.1.5.2.3. Tfcp2l1

Tfcp2l1 is also a Stat3 target and plays a central role in self-renewal [80,81]. Tfcp2l1 fully recapitulates LIF self-renewal effect and its downregulation leads to ESC differentiation even in the presence of LIF [80]. In addition, Tfcp2l1 expression also increases in ESC cultured in the presence of

MEK or Gsk3 inhibitors. Tfcp2l1 regulates self-renewal by inducing the expression of transcription factors such as *Nanog* [81].

1.1.5.2.4. Rex1

Rex1, also known as Zfp42, is expressed specifically in the mouse preimplantation blastocyst and in mESC, but not in the mouse post-implantation blastocyst neither in mEpiSC [82,83]. Therefore, it is commonly used as a landmark of the naïve state. Rex1 is a direct target of Nanog, but unlike Nanog, Rex1 is not necessary for pluripotency maintenance *in vitro*, although ESC are more prone to differentiate. Rex1 is not necessary *in vivo* either, as Rex1 knockout mice are viable and fertile [83–85].

1.1.5.2.5. Dppa3

Similar to Rex1, Dppa3, also known as stella or Pgc7, is heterogeneously expressed in mESC but is not expressed in mEpiSC, which makes it also a good marker of naïve mESC [86]. *In vivo*, Dppa3 is expressed until preimplantation, and subsequently re-expressed after specification of primordial germ cells [87].

1.1.5.3. The Primed Pluripotent State

Unlike mESC, mEpiSC are already primed to differentiate. As described above, mEpiSC still express the core pluripotency factors *Oct4*, *Sox2* and *Nanog*, but they also express early post-implantation EPI markers such as Fgf5, as well as lineage-specific markers, such as *Lefty*, *Foxa2* and *T-brachyury* (Figure 1.6). Interestingly, during mESC differentiation, cells recapitulate a gene expression profile similar to mouse post-implantation EPI cells, where they lose the expression of naïve pluripotency genes, and express post-implantation markers, interconverting into mEpiSC [88,89].

1.1.5.3.1. Fgf5

In vivo, *Fgf5* is expressed in the mouse post-implantation EPI, and ceases its expression upon gastrulation [90]. Interestingly, Rex1 and Fgf5 are mutually exclusive, with the latter working as a good marker of the primed pluripotency state [82]. *In vitro*, Klf2, Klf4 and Klf5 transcription factors are able to bind to *Fgf5* promoter and, Klf2, Klf4 and Klf5 triple knockdown, induces *Fgf5* expression [76]. On the

contrary, Otx2 regulates the binding of transcription factors, such as Oct4, to *Fgf5* enhancer and promotes *Fgf5* expression [91].

1.1.5.3.2. T-brachyury

T-brachyury is an early marker of the primitive streak *in vivo*, crucial for early mouse development and, when co-localized with Oct4, implies that those cells are in the primed pluripotent state. During gastrulation, two populations are formed, T-brachyury positive and negative cells. While T-brachyury negative cells tend to differentiate to the ectodermal lineage, T-brachyury positive cells tend to differentiate to mesoderm or definitive endoderm lineages [92]. Therefore, T-brachyury is crucial for the mesendodermal commitment. T-brachyury promotes the expression of *Foxa2* and *Sox17*. While Foxa2 promotes a positive feedback in the expression of *T-brachyury*, giving rise to mesoderm, Sox17 represses *T-brachyury* expression, giving rise to endoderm [93].

1.1.5.3.3. Lefty2

As described before, Nodal signaling is crucial for mouse embryonic development. Nodal-null mutants fail to form the primitive streak and, do not express *T-brachyury* [94]. Nodal promotes *Lefty2* expression, which it is required for the formation of the mesoderm along the proximal-distal region of the streak [95]. However, Lefty2 promotes a negative feedback in *Nodal* expression, restringing Nodal signaling. This negative feedback is crucial for the primitive streak normal formation and the correct development of the embryo [95]. *In vitro*, *Lefty2* is already expressed in mESC, however, its expression increases upon differentiation. Lefty2 knockdown impairs differentiation and maintains self-renewal [96].

1.1.5.3.4. Zeb2

Zeb2, also known as Sip1 or Zfhx1b, is a transcription factor that is crucial for the exit of the primed state and induction of differentiation (Figure 1.6). In Zeb2 knockout cells, the majority of mESC remain uncommitted upon induction of differentiation [97]. In addition, Zeb2 has been shown to be crucial to the acquisition of the neuroectoderm specification during differentiation [98]. *Zeb2* expression inhibits Activin/Nodal signaling, mesendoderm genes such as *T-brachyury*, and upregulates neuroectodermal genes [98].

1.1.5.3.5. Nestin

Nestin is a marker of neural progenitor cells. *In vivo*, *Nestin* is expressed in the neural ectoderm at E7.0 [99]. *In vitro*, Fgf4 signaling through ERK1/2 is required to initiate neural commitment, since it promotes upregulation of primary neural markers, such as *Nestin* and *Sox1*, on Fgf5 positive cells (Figure 1.6) [46,100].

It is important to note that the ability of artificially maintaining pluripotency *in vitro* may also lead to a better understanding of the signaling mechanisms responsible for the correct development of the embryo *in vivo*. The combination of tight and unique networks of transcription factors are key for maintenance of the different pluripotent states, and for the correct induction of differentiation or reprogramming.

1.2. Metabolism: an important player in stem cell fate

Metabolism is a combination of anabolic and catabolic mechanisms that occur inside a cell. While anabolic pathways are responsible for the production of macromolecules, such as nucleotides, amino acids and lipids, and require energy from adenosine triphosphate (ATP) or nicotinamide adenine dinucleotide (NADH), catabolic pathways break down molecules into smaller units, in order to produce energy or building blocks. The metabolic requirements of a cell are known to be dependent of cell state energetic demand.

Cells can rely on two different ways to produce energy: the glycolysis pathway or the oxidative phosphorylation (OXPHOS) pathway (Figure 1.7). Glycolysis occurs in the cytoplasm of the cell. This pathway is responsible for the breakdown of one molecule of glucose into two molecules of pyruvate, and the production of two net molecules of ATP and two net molecules of NADH [101] (Figure 1.7). Pyruvate, the end product of glycolysis, can then go one of two ways: in anaerobic conditions, pyruvate is reduced to lactate, which is excreted to the extracellular space; while in aerobic conditions, pyruvate is oxidatively decarboxylated to acetyl-CoA by the pyruvate dehydrogenase complex (PDH), in the mitochondrial matrix, with production of one NADH molecule. Acetyl-CoA is then the fuel of the

Krebs cycle, which occurs inside the mitochondria (Figure 1.7). In the Krebs cycle, three molecules of NADH, one moiety of flavin adenine dinucleotide ($FADH_2$), and one molecule of guanosine triphosphate (GTP) are produced from each acetyl-CoA that gets into the Krebs cycle [101]. At the end, from each glucose molecule, four molecules of ATP, ten molecules of NADH and two reduced $FADH_2$ (part of the enzyme succinate dehydrogenase) are generated. In the inner mitochondrial membrane, the mitochondrial respiratory chain, formed by five multi-subunit protein complexes, is responsible for OXPHOS (Figure 1.7). The NADH and $FADH_2$ produced thus far are oxidized, and the electrons derived are transported through the electron transport chain (ETC), where they mediate the combination of hydrogen ions with molecular oxygen in complex IV, which culminates in the production of water molecules. The movement of electrons on complexes I, III and IV are also coupled with the pumping of protons from the mitochondrial matrix into the mitochondria intermembrane space. In the intermembrane space, the electrochemical gradient created is responsible for driving the synthesis of ATP from ADP and inorganic phosphate, as protons flow back into the matrix via the ATP synthase (sometimes labeled Complex V), which generates in average 34 additional ATP molecules per molecule of glucose [101]. Therefore, mitochondria are known as the powerhouse of the cell. In addition to its role in energy production, the Glycolysis and Krebs cycle provide intermediates for other molecular pathways (Figure 1.7). In order to match their current energetic and precursors requirements, cells have the plasticity to shift between metabolic pathways. Nonetheless, most differentiated cells rely on the OXPHOS to achieve their energetic demands.

1.2.1. Glycolysis and OXPHOS in embryonic development

During embryonic development, the metabolic pathways are tightly regulated to accomplish demands for both energy and precursor molecules, essential for cellular replication and specialization. It all starts before fertilization, during oogenesis, where the boost of mitochondria biogenesis results in a two to three orders of magnitude increase of mitochondrial content [102]. Since mitochondria do not replicate during cleavage, the increase in mitochondrial content before fertilization is crucial to ensure sufficient mitochondrial numbers, to meet the energetic and precursors demands in all cells of the

embryo. In the early embryonic stages, mitochondria are very small, with a globular shape and poorly developed cristae; nevertheless, they are still active. After fertilization, the embryo relies on the OXPHOS metabolism [103,104]. After several divisions, the mitochondria content in each cell declines, and, in the morula state, there is an increase of glucose transporters in each cell, which gradually shifts the OXPHOS metabolism to a glycolytic metabolism [101,104]. After implantation, glycolysis is the major metabolic pathway in the EPI, where all glucose is metabolized to lactate, due to the hypoxic uterine wall environment. Only after the blood flow is established in the embryo, OXPHOS metabolism is re-established and mitochondria biogenesis and maturation occur again in all cells of the embryo [105].

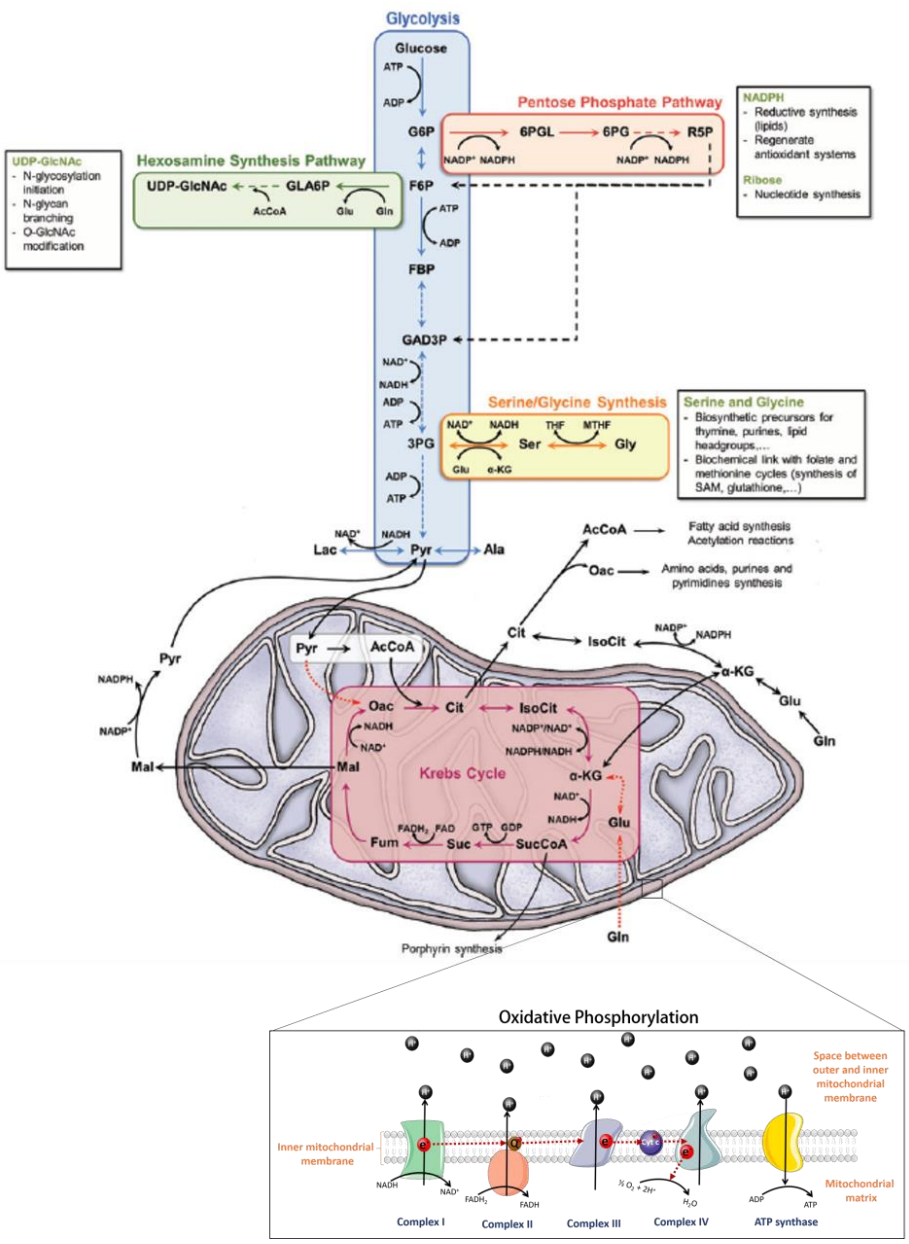

Figure 1.7 – Glycolysis, glycolysis interconnected pathways and oxidative phosphorylation.

Glycolysis is responsible for the breakdown of glucose into pyruvate and the production of metabolites and intermediates to other pathways, such as pentose phosphate pathway and Krebs cycle. Oxidative phosphorylation is responsible for the oxidation of NADH and $FADH_2$, and synthesis of ATP. *Adapted from* Pereira *et al.* (2014)[101].

1.2.2. Glycolysis and OXPHOS in mESC, mEpiSC and differentiated cells

In vitro, mESC and mEpiSC seem to recapitulate the metabolic program of the pre- and post-implantation EPI, respectively. Similarly to the preimplantation EPI cells, naïve mESC have small and spherical mitochondria, with immature cristae and reduced mitochondrial DNA (mtDNA) copy number. Nevertheless, these cells have a bivalent metabolism, and are able to switch between glycolysis and OXPHOS [106]. Importantly, mitochondria function is dependent not only of their own genome, mtDNA, but also from nuclear DNA. Stat3, a downstream effector of LIF pathway, was recently shown to be able to bind mtDNA and increase the expression of mitochondrial transcripts, enhancing OXPHOS metabolism [107]. These results suggest a synergetic role between mitochondria respiratory chain and nuclear transcription of pluripotent genes mediated by Stat3.

Similar to the post-implantation EPI, mEpiSC have a more mature mitochondria network, but still, less mature than those of differentiated cells. mEpiSC are more glycolytic and, consequently, their basal and reserve levels of respiration are much lower, when compared to naïve mESC [106]. These features have been related to the low expression of multiple nuclear encoded proteins of the respiratory chain complexes, namely cytochrome c oxidase, from complex IV and NADH dehydrogenase, complex I [106,108]. In addition, hypoxia-inducible factor 1 α (Hif1α) levels are increased in mEpiSC, when compared to mESC [106]. Hif1α is a transcription factor that works as an oxygen sensor inside the cell. Low levels of oxygen promote the expression of Hif1α, which is responsible for the gene expression control of essential genes that promote the glycolysis pathway, such as lactate dehydrogenase A (LDHA), responsible for the conversion of pyruvate to lactate; and pyruvate dehydrogenase kinase 1 (PDK1), responsible for the phosphorylation of PDH and, consequently, its inactivation [109]. Interestingly, ectopic expression of Hif1α, or reduced oxygen concentrations, promotes the transition of mESC from the naïve to the primed state [106,110]. In addition, dichloroacetate (DCA), an inhibitor of PDK1 and, therefore, an activator of PDH complex, promotes mESC differentiation, suggesting PDK

as a metabolic gatekeeper of pluripotency [111]. Moreover, 3-bromopyruvate (3BrP), an inhibitor of hexokinase II and GAPDH, which are crucial enzymes in the glycolysis pathway, leads to a metabolic switch and loss of pluripotency, even in the presence of pluripotent conditions in the medium [112]. According to this idea that reduction of OXPHOS in the primed state is essential for maintenance of pluripotency, antimycin A (AA), an inhibitor of complex III of the ETC, is able to maintain pluripotency in hESC and inhibit differentiation of mESC [113–116].

Upon induction of differentiation, cells change their glycolytic status to an OXPHOS status. In these cells, there is an increase of mtDNA replication, mitochondrial biogenesis, an upregulation of ETC subunits, and finally, mitochondria morphology changes from round to elongated mitochondria network occupying all cytoplasm [117–119].

The mitochondria number and morphology is dependent of fission and fusion processes, which are carefully balanced in the cell. Mitochondria fission is mediated by two proteins: dynamin-related protein 1 (Drp1) and hFis1. During fission, the cytosolic dynamin Drp1 translocates from the cytosol to the fission site where it interacts with hFis1, a protein uniformly localized to the outer mitochondrial membrane (OMM). This interaction leads to the mitochondrial division, a mechanism dependent on GTPase activity [120]. On the other hand, mitochondrial fusion is dependent on mitofusion (MFN) 1 and 2, GTPases localized in the OMM and OPA1, a GTPase localized in the inner mitochondrial membrane (IMM). MFN 1 and 2 are responsible for the initiation of mitochondria interaction with each other and for the outer membrane fusion, while OPA1 is responsible for the induction of the inner membrane fusion [120]. The ratio between mitochondria fission and fusion is accurately controlled in the cell, since the balance of mitochondrial dynamics is required to maintain a functional mitochondrial population.

1.2.3. Metabolism, epigenetics and reprogramming

Besides its role in energy production, metabolism has also been implicated in the generation of cellular building blocks and regulators of epigenetics. Glycolysis and Krebs cycle provide precursors for nucleotides, non-essential amino acids and lipids, used to produce macromolecules essential for cell division, as well as intermediates employed in enzymatic reactions, such as acetylation and methylation

(Figure 1.7) [121,122]. Acetyl-CoA, for example, contributes not only to the Krebs cycle but also to the synthesis of lipids and acetylation of amino acid residues, such as lysine, on histone and non-histone proteins [123,124], while α-ketoglutarate contributes to demethylation of DNA and histones [125]. Histone acetylation and demethylation, as well as DNA demethylation, are crucial epigenetic features on embryonic stem cell fate.

The acetylation/deacetylation of histones regulate global chromatin architecture, and consequently, the control of gene transcription and stem cell fate. There are two main protein families involved in the control of this process, histone acetyltransferases (HATs) and histone deacetylases (HDAC). Acetylation of histones is associated with open chromatin structures, and play a critical role in the maintenance of stem cell pluripotency [126]. Acetate levels regulate histone acetylation levels. Glucose-derived citrate is converted to Acetyl-CoA through an adenosine triphosphate-citrate lyase [123]. Equivalently, inhibition of glycolytic enzymes decreases histone acetylation, connecting glycolytic production of Acetyl-CoA with histone acetylation and the maintenance of the pluripotent state [124]. On the other hand, HDAC promotes histone deacetylation, which is one of the primary features upon embryonic stem cell differentiation [124,127]. HDAC are divided in two main groups: "classical" HDAC, which are Zn^{2+} dependent, and sirtuins, which are dependent of the NAD^+ pool. While the former remove acetyl groups from histones and convert them to acetate, the latter convert NAD^+ and the acetyl group into nicotinamide and 2'-O-Acetyl-ADP-Ribose [128]. Shifts from anaerobic (glycolysis) to aerobic (OXPHOS) metabolism and vice-versa are linked to changes in the NAD^+/NADH ratio. Consequently, sirtuins are considered cell metabolic sensors [128].

Methylation is another epigenetic marker that plays a crucial role in the maintenance of stem cell pluripotency. Methylation/demethylation promotes a modulation of chromatin structure and this process is tightly interconnected with the metabolic status of the cell [129]. DNA and histone methylation is a process regulated by DNA methyltransferases (DNMTs) and histone methyltransferases (HMTs), respectively. In ESC, the lack of DNMTs, for example, promotes maintenance of pluripotency and self-renewal, while these cells fail to differentiate [130,131]. Histones demethylases can be lysine-specific demethylases, which target Histone3-Lysine4 residues and Histone3-Lysine9 residues and require FAD to catalyze this process or, lysine and arginine demethylases, which require α-ketoglutarate to promote

demethylation. In ESC, an elevated α-ketoglutarate succinate ratio, maintained by glucose or glutamine metabolism, promotes pluripotency through histone demethylation [125].

Metabolism and the cell state are also interconnected during reprogramming [132]. Upon induction of pluripotency, cells have to remodel their chromatin in order to re-activate pluripotent associated genes, while silencing differentiated genes. Reprogramming factors, with the exception of Oct4, can be replaced by stimulating glycolytic genes expression through the activation of key metabolic enzymes [133]. In addition, the increase of PDK and hexokinase II or the inhibition of ETC through AA or rotenone increases reprogramming efficiency [134,135]. Interestingly, recent studies suggest that during iPSC formation the glycolytic shift occurs before expression of pluripotency genes, suggesting metabolism as a key player in cell fate [136,137].

In summary, metabolism is a regulator of stem cell fate due to its role not only in energy production but also in the production of important precursors, which are crucial for chromatin remodeling and gene transcription regulation, as well as key building blocks for anabolic pathways, essential for proliferation and cell division.

1.3. Mechanical cues: the forgotten key in stem cell fate

Mechanical cues have recently been recognized as important regulators of cell fate. Changes in extracellular matrix (ECM) mechanics, substrate stiffness, topography, and physical forces such as shear stress, tension, and compression, are examples of mechanical cues that influence cell fate. It is now accepted that mechanical cues work together with biochemical cues in the regulation of embryogenesis and organogenesis, while cell mechanical properties are associated to a read-out of physiological functions or pathological features.

1.3.1. Mechanotransduction

Inside the cell, mechanical stimuli are converted into biochemical signals, in a process called mechanotransduction. This process enables cell adaptation to the surrounding environment, and can be divided into three stages: mechanotransmission, mechanosensing and mechanoresponse [138].

Mechanotransmission is the transmission of mechanical forces, through protein-protein interaction, between the ECM and the cell (Figure 1.8) or between neighboring cells (Figure 1.9).

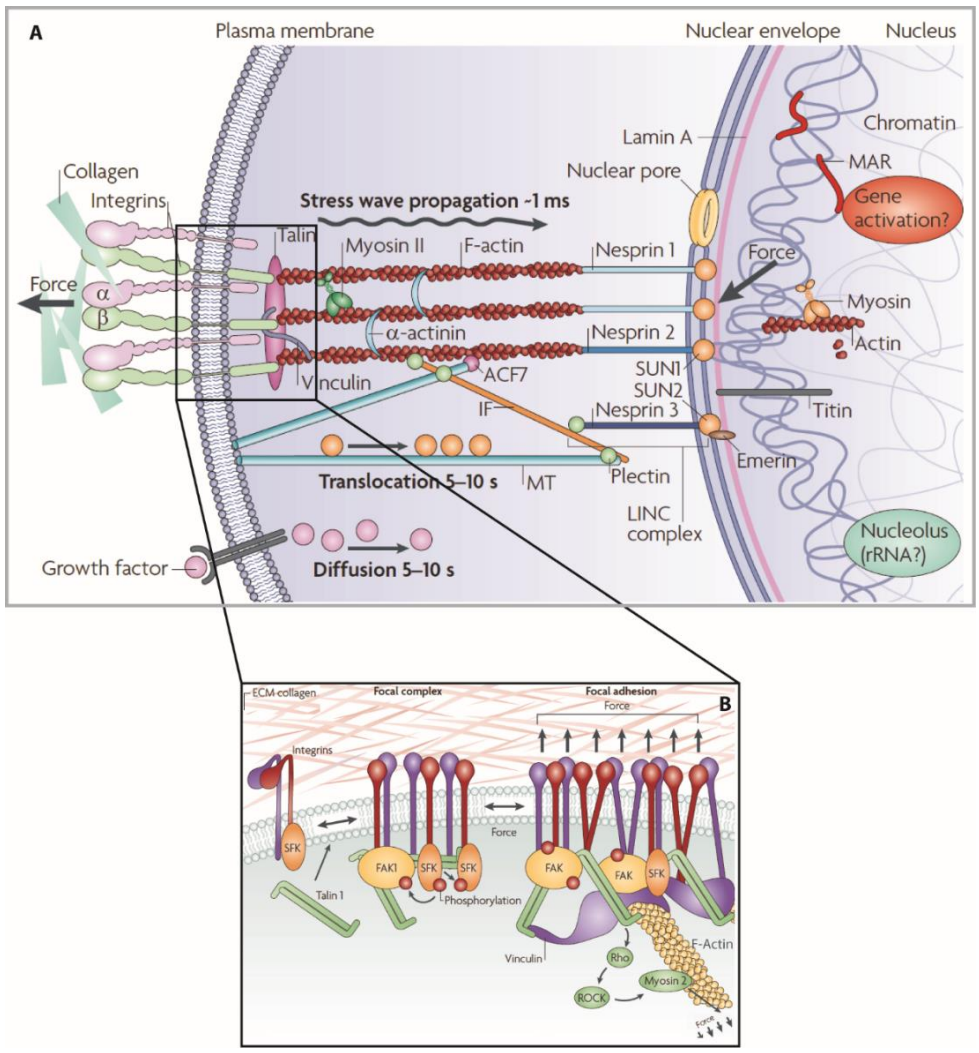

Figure 1.8 – The transmission of mechanical forces between ECM and a cell.

(A) Mechanical forces are transmitted through multiple force-sensitive proteins. Cells sense the substrate through ECM – integrin interactions. Inside the cell, interactions between focal adhesions (talin and vinculin) and integrins lead to the transmission of force to F-actin, which is connected to intermediate filaments and to microtubules. Nesprin connects F-actin to the inner nuclear membrane, promoting the transmission of force to the nucleus. **(B)** Signaling cascade activated by integrin activation, leads also to the biochemical signaling cascade initiation by FAK and SFK, and the force transduction by vinculin and talin, resulting in actomyosin contractility and actin remodeling. Abbreviations: ECM – Extracellular Matrix; FAK – focal adhesion kinase; SFK – Src family kinase. *Adapted from* Wang *et al.* (2009) and Butcher *et al.* (2009) [139,140].

Transmembrane integrins are the bridge between the cell and the ECM and work as both force transmitters and mechanosensors (Figure 1.8). The mechanical linkage between the ECM and the actin cytoskeleton is mediated by focal adhesion complexes [141]. Inside the cell, structural scaffolds bind to the cytoplasmic domain of integrins and continue the transduction pathway mechanically, with the transduction of the force to the actin cytoskeleton, with regulation of actomyosin structure, and transmission of force until the nucleus through the LINC (linker of nucleoskeleton and cytoskeleton) complex (Figure 1.8) [138,142]. These forces can be transmitted for long distances and faster than the biochemical signal since the propagation of the mechanical force is dependent of the resistance of the protein-protein interactions.

Cells can also receive mechanical signals through their neighbor cells via cell-cell adhesions (Figure 1.9) [143]. Cadherins are the transmembrane proteins responsible for the transmission of the force between adjacent cells, and similar to integrins, they act as both force transmitters and mechanosensors [143]. Cadherin's cytoplasmic domain recruits catenins, which have associated cytoskeleton-binding proteins, whereas the cadherin extracellular domain forms intercellular bonds with cadherin of neighbor cells (Figure 1.9).

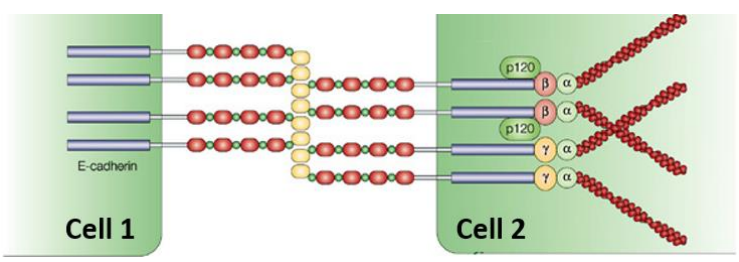

Figure 1.9 – The transmission of mechanical forces between adjacent cells.
Cadherins are responsible for the force transmission between adjacent cells. Inside the cell, cadherins recruit catenins, which have associated cytoskeleton binding proteins responsible for the signaling transmission. Abbreviations: α: α-catenin, β: β-catenin; γ: γ-catenin; p120: p120-catenin. *Adapted from:* Cavallaro *et al.* (2004)[144].

Mechanosensing is the ability to convert the mechanical force into a biochemical output through conformational changes of focal adhesions. Inside the cell, there are also signaling scaffolds

that bind to the cytoplasmic domain of integrins and continue the transduction pathway biochemically (Figure 1.8 and Figure 1.10) [138,145]. Finally, the mechanoresponse, as implied by the name, is the downstream effect of the applied force, which in the short term promotes the modulation of cell-ECM binding of focal adhesions stability and of cytoskeleton strength; and in a long term induces the activation of signaling pathways and changes of gene expression [138,145].

1.3.2. Mechanical cues in embryonic development

Recently, different laboratories have taken mechanical characteristics into consideration and developed different methods to analyze oocyte and zygote quality. In the fertilization process, the sperm cell first penetrates the zona pellucida (a specialized extracellular matrix, constituted of a network of glycoproteins, that surrounds the oocyte and protects it) [146,147]. Upon fertilization, there is a trigger of biochemical signals that induce a three-dimensional architecture change of the zona pellucida, which is known as zona reaction or "hardening" [147]. Mechanically, different studies have been conducted in order to analyze zona pellucida elasticity prior to and after fertilization. One of the first studies was reported in 1988, where with a capillary suction apparatus the authors measured the stiffness of zona pellucida of the embryo and showed that it gets 1.8 times stiffer when compared to the zona pellucida of the oocyte [148]. Since then, the techniques to evaluate stiffness have improved and other studies have been reported. Nevertheless, all of them show that zona pellucida becomes stiffer after fertilization, when compared to prior fertilization [149–151]. All these studies suggest a link between oocyte mechanics and its viability, but only recently were the mechanical properties of the oocyte after fertilization associated with viable and non-viable embryos [152,153]. Yanez and colleagues reported that human and mouse zygote viscoelasticity parameters, measured 24h after fertilization, can predict blastocyst formation [152]. These parameters were correlated with zona pellucida "hardening" or immature/mature oocytes before fertilization as RNA-seq data of zygotes, with a mechanical read out of non-viable, show misexpression of genes involved in regulation of transcription, DNA repair as well as cell cycle, among others. Therefore, these studies suggest that mechanical properties of zona pellucida can function, in an early stage, as a predictable factor of embryonic development.

The mechanical properties of embryonic cells are also crucial for their precise development and recent knowledge of the mechanical properties during different cell stages of the embryo have brought to light the role of mechanosensing in cell fate decision. For example, the evaluation of surface tension in the 8-cell stage blastomeres, through micropipette aspiration technique, demonstrated that surface tension, promoted by actomyosin contractility, is essential to induce blastomere compaction [154]. For a long time, blastomere compaction has been related with the increase of adhesion molecules such as E-cadherin [155], but the molecular pathways that regulate this event are poorly understood. Recently, E-cadherin was shown to be present in filopodia-like protrusions that occur at the 8-cell stage, which have been proposed to be responsible for maintaining tension in order to control cell shape and promote compaction [156]. Although in this study the mechanical forces to promote compaction are proposed to be generated from E-cadherin-dependent filopodia, an independent study proposes that compaction is generated by actiomyosin cortex tension, where E-cadherin prevents the increase of contractility at cell-cell contacts [154].

During blastomere compaction, an apico-basal cell polarity in each blastomere is established and blastomeres undergo two rounds of symmetric or asymmetric division [157]. In the first case, both daughter cells inherit the apical domain resulting in two polar cells, both maintaining their outer position, whereas the second case, only one daughter inherits the apical domain, resulting in one polar (outside cell) and one apolar cell (inside cell). However, how a blastomere adopts an internal or external position within the embryo has been topic of debate, with cell polarity, cell position and contractility models described as independent regulators of TE/ICM fate [158,159]. Recently, mechanosensing was shown to be crucial for the correct position of cells during TE/ICM specification, acting as the bridge between polarity, position and cell fate [160]. This model suggests that upon asymmetric division, the two daughter cells acquire different levels of contractility; apolar blastomeres have low levels of aPKC and increased levels of cortical myosin, which increases cell contractility and regulates YAP localization in the cytoplasm, opposite to polar blastomeres [160].

In addition to the mechanical properties of the embryo, the uterus has been suggested as an external mechanical force involved in the anterior-posterior axis formation of the embryo, critical for post-implantation development [161,162]. With the use of microfabricated cavities to recapitulate the

external constraints promoted by the uterus during implantation, Hiramatsu and colleagues reported that egg-cylinder shape acquisition and DVE specification is dependent of the external spatial restriction, with the width and stiffness of the cavity vital players in the correct DVE development and anterior-posterior axis acquisition [161]. However, doubts about this model have emerged due to the ability to induce the DVE in embryos cultured in a hanging drop method or in a dish without a physical constraint [24,163]. Nevertheless, mechanical forces are increasingly recognized as key regulators in gastrulation and organs formation, where cells undergo changes in their motility and shape, which are either affected by mechanical forces, or generate mechanical forces that are crucial for the correct embryo development [145,164–166].

1.3.3. Substrates

To culture ESC, tissue culture polystyrene (TCPS) and glass bottom dishes are commonly used. However, when stiffness is taken into account, these dishes are orders of magnitude greater than the preimplantation embryo or the uterine epithelium [150,167,168]. Therefore, ESC are normally cultured in super stiff substrates.

Synthetic polymers or biologically derived materials are commonly used to obtain different stiffness or topographies substrates [169]. The most frequent synthetic polymers utilized are polyacrylamide gels and polydimethylsiloxane (PDMS). Polyacrylamide gels can form hydrogels with elastic moduli ranging between 0.2 kPa and 700 kPa, while PDMS stiffness can range from 0.1 kPa to 2.3 MPa [170]. Hydrogels with different stiffness can also be formed from biological materials such as collagen, which is widely used for cell encapsulation [169]. Regardless of the material chosen to evaluate substrate stiffness effect, different stiffness are achieved by modifying the crosslinking density or polymer concentration [169].

1.3.4. Stiffness in ESC fate

ESC fate *in vitro* has also been shown to be regulated through biophysical cues in addition to biochemical cues. Generally, ESC are cultured in TCPS, and their fate is regulated only through

biochemical factors. However, reports have shown that ESC sense mechanical properties: when mESC and hESC are cultured on different stiffness ranges, their fate changes according to the stiffness that cells are on. This effect was firstly reported in mesenchymal stem cells, where the commitment to a cell lineage is dependent of the similarity of the substrate elasticity to the tissue *in vivo* [167] (Figure 1.10). Soft substrates (approximately 1 kPa) have been reported to mimic the preimplantation embryo, the uterine epitelium and the brain, while intermediate substrates (approximately 10 kPa) mimic the muscle and stiffer substrates (approximately 100 kPa) mimic the bone [150,167,168]. mESC cultured on very soft substrates (0.2 kPa, 0.6 kPa and 2kPa polyacrylamide gels) maintain pluripotency for many passages, even in the absence of LIF [171,172]. On these conditions, mESC cultures are homogeneous, with round and compact colonies and these cells are able to develop teratomas [171]. The increase of substrate stiffness promotes an increase of mESC colonies basal traction, affects cell spreading but not cell attachment [171,173].

Upon induction of spontaneous mESC differentiation, substrate stiffness also plays an important role. mESC cultured in the absence of LIF on 7.5 kPa tend to differentiate into mesoendoderm [172]. Embryoid bodies derived from mESC have an increase in cardiomyogenic differentiation when cultured on substrates with an elasticity of approximately 6 kPa [174]. Nevertheless, the use of a high range of substrate stiffness (0.041 to 2.7 MPa) to culture mESC in the absence of LIF leads to a positive correlation between genes expressed in the primitive streak during gastrulation and substrate stiffness [173]. *T-brachyury, Eomes, Foxa2* and *N-cadherin* increase their expression as stiffness increases, with this effect independent of cell density [173]. In addition, in the presence of osteogenic supplements, stiffer substrates promote an increase of osteogenic differentiation, when compared to mESC cultured on soft substrates [173]. Similar results have been reported in hESC triggered to differentiate, where cells were cultured in three dimensional (3D) scaffolds with different stiffness in order to model the germ layer specification upon gastrulation. The culture of hESC in 1.5 to 6 MPa scaffolds induces a transition from primitive streak expression to mesoderm lineage, while intermediate elastic modulus scaffolds (0.1 to 1 MPa) induce endoderm specific gene expression and soft scaffolds (lower than 0.1 MPa) increased the expression of ectodermal specific genes [175]. In addition, hESC cultured in two dimensions (2D) on soft substrates (0.1 kPa and 0.7 kPa) form neural ectoderm more efficiently that hESC cultured on stiffer

substrates (75 kPa) but, contrary to mESC, hESC do not maintain their pluripotency in soft substrates in the absence of biochemical pluripotent cues [176]. Interestingly, mESC cultured on 2 kPa polyacrylamide gels in the presence of 2i medium, but in the absence of LIF, have higher expression of ectoderm lineage markers, indicating that these cells differentiate even in the presence of specific inhibitors. However, the presence of a Src inhibitor (GP77675), in combination with GSK3 in serum free medium, designated as "alternative 2i medium", was able to inhibit mESC differentiation, with maintenance of mESC self-renewal and pluripotency, with these cells able to form teratomas and produce chimeric mice [172]. Therefore, Src is proposed to be the initial mechanotransduction signal that induces differentiation when mESC are cultured on substrates with specific elasticities. This mechanism was shown to involve the Src-Src homology/collagen A (ShcA) MAPK pathway [172]. In addition, cell stiffness also dictates the cell sensitivity to respond to mechanical stimuli. Soft cells, such as mESC, upon the induction of a local, small cyclic stress are more prone to spread and to lose *Oct4* expression than stiffer cells, with Src, myosin II contractility and cdc42 involved in the induction of this focal adhesion cell spreading [177].

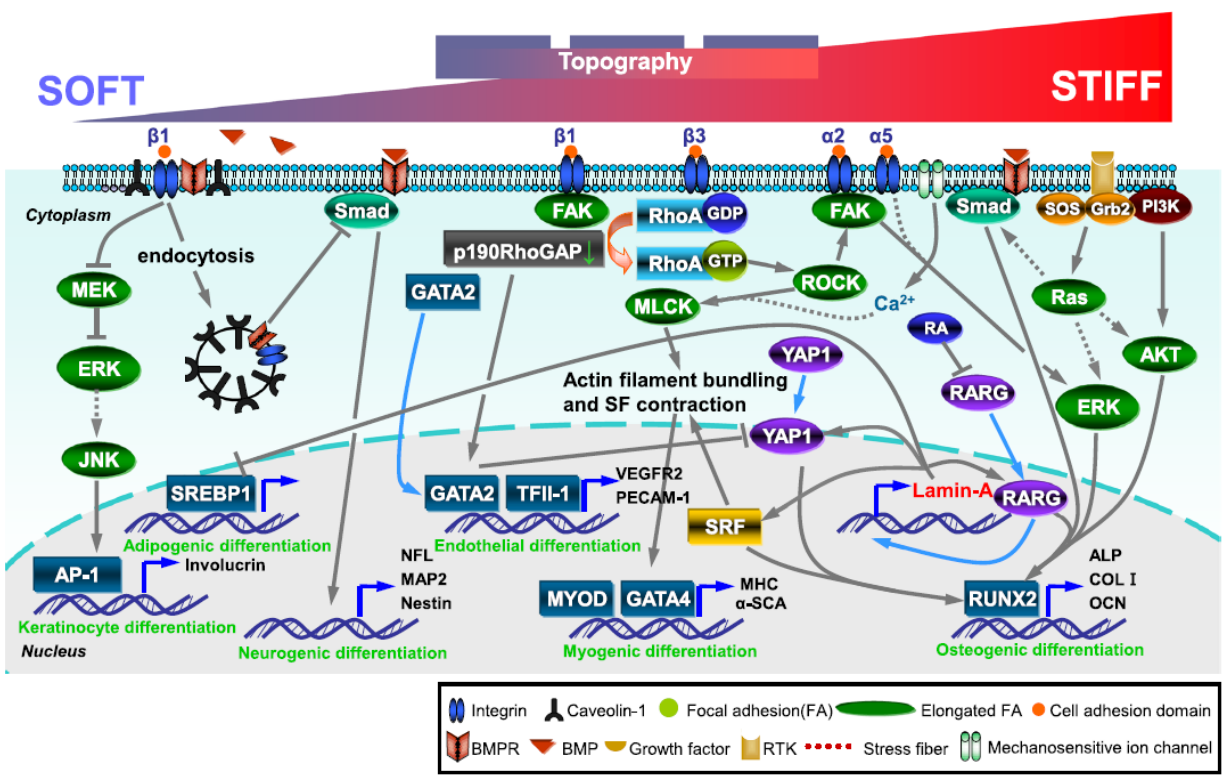

Figure 1.10 – Stiffness induces different biochemical transduction pathways in mesenchymal stem cells.

Different signaling transduction pathways are activated taking into account the stiffness of the substrate, which culminates in different cell lineage specifications. Soft substrates induce the endocytosis of β-1 integrin, which decreases BMP/Smad signaling. This BMP/Smad signaling decrease promotes neurogenic differentiation. Medium stiffness activates β-1 integrin, which results in a reduction of p190RhoGAP and translocation of GATA2 to the nucleus, leading to endothelial differentiation. On stiff substrates, α2-integrin-ROCK-FAK-ERK1/2 increases the activity of RUNX2, which results in osteoblast differentiation. Dashed lines represent unknown or putative signaling. *Adapted from* Hongwei *et al.* (2015) [178].

1.3.5. Stiffness and substrate topography in cell reprogramming

Besides the ability to influence ESC fate, biophysical cues can also influence cellular reprogramming. Substrate stiffness has recently been shown to facilitate cellular reprogramming [179,180]. Soft substrates, such as 0.1 kPa polyacrylamide gels, increase the reprogramming efficacy of fibroblasts through the facilitation of mesenchymal to epithelial transition, which is one of the crucial steps for the success of reprogramming [179]. In addition, substrate topography is able to facilitate cellular reprogramming. Small microgrooves (10 μm width) or aligned nanofibers significantly improve reprogramming efficiency. They induce cytoskeleton reorganization and are responsible for the decrease in HDAC activity and increase of a subunit of H3 methyltransferase (WD repeat domain 5), and consequently, increase of histone H3 acetylation and methylation [181]. iPSC formed by the combination of gene transfer and soft substrates or specific substrate topography are able to generate teratomas *in vivo* and embryoid bodies *in vitro* [179,181]. These results suggest that gene transfer and biophysical cues synergistically stimulate pluripotent gene expression, and the combination of both factors should be taken into account in order to increase reprogramming efficacy.

In summary, mechanical forces have an important role in pluripotency, with mechanotransduction playing an important role not only in the maintenance but also in the induction of pluripotency or differentiation.

Chapter 2

Objectives

Biochemical and mechanical stimuli influence cell fate. Although it is acknowledged that these different stimuli regulate ESC, the inter-relationship between the different modulators in ESC fate is not well understood. In addition, even though multiple stimuli have been described to maintain ESC in a pluripotent state, ESC *in vitro* are still, most of the times, heterogeneous, with a mix of pluripotent, mixed and differentiated colonies. Therefore, this work had as main goals:

1) Evaluate ESC gene expression upon combination of biochemical modulators with different substrate stiffness;
2) Decouple the LIF effect, AA effect, galactose effect and stiffness effect;
3) Understand the relationship between different biochemical modulators and stiffness in ESC gene expression;
4) Develop an open source software to quantify ESC pluripotency levels in low magnification images in order to facilitate unbiased pluripotency quantification under different circumstances.

Chapter 3

Stem cell fate regulation: the role of extracellular stimuli[2]

[2] Tânia Perestrelo, Daniele Gilkes, Teresa Luperchio, Jevon Cutler, Marcelo Correia, Christopher Le, Ana S. Rodrigues, Yu-Tai Chang, Sandro L. Pereira, Maria I. Sousa, Karen Reddy, João Ramalho-Santos, Pei-Hsun Wu, and Denis Wirtz (*in preparation)*

Abstract

Work over the last three decades has identified a plethora of biochemical and physical modulators that individually affect the pluripotency state of embryonic stem cells (ESC) *in vivo* and in *vitro*. These modulators work in concert, but decoupling their phenotypic effects is an unmet challenge. In this work, we present a general machine-learning system-based analysis to identify functional interrelationships among different mouse ESC modulators when applied conjointly using ESC gene expression patterns as readouts. Our results show that the magnitude of changes in gene expression in response to LIF is dependent on the presence of mitochondria oxidative phosphorylation inhibitor Antimycin A (AA), but not on matrix stiffness. Surprisingly, our analysis also demonstrates that the effect of stiffness on ESC fate is independent of LIF, AA and GSK3β and Mek1/2 inhibitors (i.e. 2i). This new approach allows to decouple, compare and rank-order disparate biochemical and biophysical modulators of ESC pluripotency and differentiation.

3.1. Introduction

Due to their pluripotency and self-renewal capability, embryonic stem cells (ESC) are an important and commonly used research model of development of organs, tissues, and whole organisms. The maintenance of ESC pluripotency in culture has been a topic of major interest since the first isolation of ESC. A plethora of modulators that maintain ESC pluripotency have been identified and characterized. The first such modulator to be discovered was the leukemia inhibitory factor (LIF) [38,39]. LIF induces downstream transduction signals through the JAK/STAT and PI3K pathways, which result in ESC self-renewal and maintenance of pluripotency in culture [41,42]. More recently, the MEK inhibitor PD0325901 in combination with the inhibitor of the glycogen synthase kinase-3 (GSk3) CHIR99021 and LIF have been shown to inhibit differentiation and promote self-renewal and pluripotency in serum free-medium, also called 2i medium [49]. Moreover, chemical modulation of glycolysis and oxidative phosphorylation (OXPHOS) has been described to control ESC fate [111–116].

In addition to biochemical cues, matrix stiffness – a physical cue – has been shown to regulate ESC fate *in vitro*. This effect was first reported in mesenchymal stem cells (MSC) [167], but is also true for ESC [171,172]. ESC cultured in the absence of LIF on mechanically soft substrates (typically a gel of controlled low stiffness covered with ECM molecules) are able to maintain pluripotency through many passages, and form embryoid bodies and teratomas [171–173]. In contrast, an increase in mechanical stiffness can readily induce ESC differentiation [171–173].

The fate of ESC *in vitro* is commonly measured by the expression of multiple transcripts specific of different cell stages. With the exception of ESC cultured in suspension, cells *in vitro* are typically in contact with a stiff substrate (glass or plastic). Consequently, the vast majority of experiments performed in stem-cell studies conjugate pluripotent modulators in the medium, such as LIF or 2i, with mechanical stiffness. Therefore, stem cell fate is defined by an interplay of multiple stimuli, where the inputs/outputs of each contributor are difficult to determine.

A systems-level understanding of how these different modulators may work together to determine the pluripotency/differentiation state of stem cells remains to be established. To understand how biochemical and physical regulators modulate stemness at a systems level, the effects of various

combinations of different extracellular stimuli need to be quantitatively examined. Moreover, a high-throughput and quantitative method is essential to further develop such approach to efficiently and precisely derive the basic principles that regulate stem fate in various biological contexts. RNA-Seq is a high-throughput sequencing method and it has been in vogue due to its ability to quantify expression genome-wide of many conditions [182]. However, RNAseq remains expensive and its analysis complex [183,184]. Here we develop machine-learning approaches based on a limited set of assessed genes by qPCR, which allows for the quantitative comparison, rank-ordering, and decoupling of different modulators of ESC fate.

3.2. Experimental Procedure

3.2.1. Cell culture

Mouse embryonic stem cells (E14Tg2a.4, derived from 129P2/OlaHsd, RRID:MMRRC_015890-UCD, and WT R1, kindly provided by Dr. Michael McBurney and Xiaohong He (University of Ottawa and Ottawa Hospital Research Institute, Ontario, Canada [185]) were maintained and propagated in feeder-free conditions and, unless otherwise stated, in medium containing KnockOut-DMEM (Thermo Fisher Scientific) supplemented with 15% Fetal Bovine Serum, ESC-qualified, USDA-approved regions (Thermo Fisher Scientific), 2 mM L-Glutamine (Thermo Fisher Scientific), 1% non-essential amino acids (Sigma-Aldrich), 100 U/mL penicillin/streptomycin (Thermo Fisher Scientific), 0.1 mM 2-Mercapthoethanol (Thermo Fisher Scientific) and 1000 U/mL of ESGRO Leukemia inhibitory factor (LIF) (Merck Millipore). Mouse embryonic stem cells were also maintained and propagated in serum-free medium, indicated as 2i medium throughout, which consisted in 1:1 mix of DMEM/F12 (Thermo Fisher Scientific) and Neurobasal medium (Thermo Fisher Scientific), N2 (Clontech) and B27 (Thermo Fisher Scientific) supplements, 100 U/mL penicillin/streptomycin, 0.1 mM 2-Mercapthoethanol, 2 mM L-Glutamine and 1000x dilution of the supplements LIF and MEK/GSK3 inhibitors (Millipore).

Cells were maintained at 37 ºC in a humidified incubator with 5 % CO_2. Cell medium was changed daily, and cells were split every three days. For the different experiments, cells were dissociated in accutase (Life Technologies) after washing with phosphate-buffered saline (PBS, Sigma-Aldrich), centrifuged at 300 xg for 5 min and plated in the different substrates for four days. ESC were plated at 4000 cells/cm^2, except ESC cultured in medium with galactose, which were plated at 8000 cells/cm^2.

3.2.2. Substrate preparation

Polyacrylamide gels were attached to glass coverslips as previously described [186,187]. Briefly, amino-silanated coverslips were firstly prepared: glass coverslips (Fisher Scientific) were coated with 0.1 N NaOH solution for 3 min, dried and then coated with aminopropyltriethoxysilane (APTES,

Sigma-Aldrich) for 3 min, rinsed with DI H_2O, and coated afterwards with 0.5 % glutaraldehyde (Sigma-Aldrich) solution for 30 min, washed extensively in DI H_2O and finally air dried. Then, compliant hydrogels with an elastic Young's modulus of either 0.5 kPa or 35 kPa were prepared. In order to achieve an elastic Young's modulus of 0.5 kPa, 6 % of a 40% (w/v) acrylamide stock solution and 0.12 % of a 2% (w/v) bis-acrylamide stock solution (BioRad) were combined with 1:1 saturated solution of acrylic acid *N*-hydroxysuccinimide ester (NHS, Sigma-Aldrich), 1:100 of a 10% ammonium persulfate (APS) solution (Sigma-Aldrich) and 1:1000 of N,N,N′,N′-Tetramethylethylenediamine (TEMED, Sigma-Aldrich). A 35 kPa elastic Young's modulus was achieved by combining 20% of a 40% (w/v) acrylamide stock solution and 0.6 % of a 2% (w/v) bis-acrylamide stock solution with 1:1 NHS saturated solution and finally adding 1:100 of a 10% APS solution and 1:1000 of TEMED. Amino-silanated coverslips were placed on top of each polyacrylamide gel and incubated at room temperature (RT) until acrylamide polymerized. After polymerization, the hydrogel (polymerized acrylamide on top of the glass) was placed into well plate with PBS for a quick wash. Hydrogels were then covered with 2mL of rat tail type I collagen (BD Biosciences, Ca) solution (200 µg/mL in 50 mM Hepes, pH 7.3), and incubated at 4 ºC, overnight (O.N). Unreacted NHS was then blocked with 1 mg/mL heat-inactivated fatty-acid free bovine serum albumin (Thermo Fisher Scientific) in serum free media for 1h. Finally, hydrogels were rinsed three times with PBS and cell culture medium was added at least 1h prior cell plating.

To evaluate the behavior of ESC cultured on normal culture conditions, glass coverslips (stiffness in the order of GPa) were coated with 2mL of rat tail type I collagen solution (200 µg/mL in 50 mM Hepes, pH 7.3), and incubated at 4 ºC, O.N. Glass coverslips were then rinsed and cell culture medium was added at least 1h prior cell plating.

3.2.3. Immunofluorescence microscopy

ESC were fixed with 4 % paraformaldehyde (Electron Microscopy Sciences) for 15 min at RT, permeabilized with 0.1 % Triton X-100 (Sigma) in PBS for 10 min, and blocked for non-sepecific binding with 1% (w/v) bovine serum albumin (BSA, Sigma-Aldrich) in PBS for 1 h at RT. Primary

antibodies: rabbit anti-OCT-4 (#2840, Cell Signaling Technology) at 1:100 dilution, goat anti-SOX2 (#SC17320, Santa Cruz Biotechnology) at 1:50 dilution or rabbit anti-TOM-20 (#sc-11415, Santa Cruz Biotechnology) at 1: 50 were then incubated at 4 ºC, O.N. Cells were then washed with PBS and incubated for 1 h at RT with a solution containing the secondary antibodies: donkey anti-goat Alexa Fluor 568 (#A11004; Thermo Fisher Scientific) and donkey anti-rabbit Alexa Fluor 647 (#A31573, Thermo Fisher Scientific) at 1:200 dilution; Hoechst 33342 (Sigma-Aldrich) at 1:40 dilution and phalloidin Alexa Fluor 488 (#A12379, Thermo Fisher Scientific) at a dilution 1:40 dilution. Cells were then washed with PBS and fluorescent images were collected. Cells were imaged on a Nikon A1 confocal microscope, using a Plan Apo VC 60x water-immersion objective lens (Nikon), NA = 1.2, and controlled by Nikon Elements imaging software (NIS 4.0).

3.2.4. Phase-contrast imaging

Before RNA extraction, phase contrast images were acquired from each sample condition on an inverted Eclipse Ti microscope; Nikon, using a Plan Fluor 4x PhL DL objective lens (Nikon), NA = 0.13.

3.2.5. Mitochondrial modulation

In order to inhibit OXPHOS, the medium was replaced 24 h after plating with warm medium containing 50 nM Antimycin A (AA, Sigma-Aldrich) or 50 nM Myxothiazol (Mx, Sigma-Aldrich), complex III inhibitors. Cell medium was changed daily.

To indirectly increase mitochondrial metabolism, cells were cultured in galactose medium containing DMEM-no glucose (Thermo Fisher Scientific), supplemented with 15% Fetal Bovine Serum, ESC-qualified, USDA-approved regions (Thermo Fisher Scientific), 2 mM L-Glutamine (Thermo Fisher Scientific), 100 U/mL penicillin/streptomycin (Thermo Fisher Scientific), 0.1 mM 2-Mercapthoethanol (Thermo Fisher Scientific), 1 mM sodium pyruvate (Thermo Fisher Scientific) and 1.8 g/L galactose (Sigma-Aldrich).

3.2.6. Oxygen consumption rate (OCR) analysis

O_2 consumption was determined using a Seahorse XF24 extracellular flux analyzer (Seahorse) as previously described [111]. Briefly, 1 x10^4 ESC were seeded in a 24-well XF24 cell culture plate, in the respective culture medium, 12h prior the OCR acquisition. 1 h prior to the run, cell culture medium was replaced by XF assay medium modified DMEM (Seahorse), adjusted to pH 7.4 and supplemented with 4.5 g/L glucose (Sigma-Aldrich), 1 mM pyruvate (Thermo Fisher Scientific) and 2mM L-glutamine (Thermo Fisher Scientific). Three mitochondria inhibitors: 1 μM Oligomycin (Seahorse), 1.25 μM FCCP (Seahorse) and 1 μM rotenone + 1 μM AA (Seahorse) were sequentially injected after measurements cycles 3, 6 and 9, respectively. After all the measurements were completed, cells were dissociated and counted for condition normalization.

3.2.7. RNA extraction and purification

In order to extract RNA of each condition, cells were rinsed with PBS and then each hydrogel or coverslip was flipped on top of a trizol (Life Technologies) drop on a parafilm sheet, and left for at least 1 min at RT. The solution was then collected to eppendorfs and mechanical disruption was promoted by vortex each sample during 30 s. RNA extraction was proceed afterwards according to manufacturer's instructions (Direct-zol™ RNA MiniPrep, Zymo).

3.2.8. cDNA synthesis and quantitative real-time PCR (qPCR)

One microgram of total RNA was used for first-strand DNA synthesis through the iScriptTM cDNA Synthesis kit (Bio-Rad), accordingly to manufacturer's instructions.

qPCR was performed using mouse-specific primers – obtained in the Primer Bank database [188–190] – and iTaq SYBRE Green Universal Master Mix (Bio-Rad). Primers sequence are shown in Table 3.1. The expression of each target mRNA was calculated based on the threshold cycle (Ct) as $2^{-\Delta(\Delta CT)}$, where $\Delta Ct = Ct_{target} - Ct_{Rplp0}$ and $-\Delta(\Delta CT) = \Delta Ct_{test} - \Delta Ct_{control}$. Unless otherwise stated,

control condition refers to ESC cultured for 4 days, on stiff substrates, in the absence of pluripotent modulators in the medium in the last 3 days (referred in the text as "st").

Table 3.1 - Sequences of forward and reverse primers (5' to 3')

Target Gene	Forward	Reverse	PrimerBank ID
Dppa3	GACCCAATGAAGGACCCTGAA	GCTTGACACCGGGGTTTAG	21218416a1
Esrrb	GCACCTGGGCTCTAGTTGC	TACAGTCCTCGTAGCTCTTGC	31542617a1
Fgf5	AAGTAGCGCGACGTTTTCTTC	CTGGAAACTGCTATGTTCCGAG	3721900a1
Gata4	CCCTACCCAGCCTACATGG	ACATATCGAGATTGGGGTGTCT	6679953a1
Klf4	GTGCCCCGACTAACCGTTG	GTCGTTGAACTCCTCGGTCT	6754456a1
Lefty2	CAGCCAGAATTTTCGAGAGGT	CAGTGCGATTGGAGCCATC	28893031a1
Nanog	TCTTCCTGGTCCCCACAGTTT	GCAAGAATAGTTCTCGGGATGAA	31338864a1
Nestin	CCCTGAAGTCGAGGAGCTG	CTGCTGCACCTCTAAGCGA	15011851a1
Oct4	CGGAAGAGAAAGCGAACTAGC	ATTGGCGATGTGAGTGATCTG	356995852c3
Rex1	CCCTCGACAGACTGACCCTAA	TCGGGGCTAATCTCACTTTCAT	7110739a1
Rplp0	AGATTCGGGATATGCTGTTGGC	TCGGGTCCTAGACCAGTGTTC	6671569a1
T	GGATTCACATCGTGAGAGTTGG	GTCACAGCTATGAACTGGGTC	118130357c3
Zeb2	ATTGCACATCAGACTTTGAGGAA	ATAATGGCCGTGTCGCTTCG	7657695a1

3.2.9. RNA-Seq

RNA-Seq data was derived from two independent experiments. Total RNA was extracted by TRIzol from E14 cells cultured on stiff or soft substrates in the presence of different biochemical modulators (+LIF, AA, Gal+LIF, 2i). Total RNA was then subject to DNAse digestion to remove residual DNA and cleaned over a RNeasy (Qiagen 74104) column using the manufacturer's 'cleanup protocol' to remove contaminants and deplete RNAs < 200 nt. RNA quality was assessed using a RNA 6000 nano total RNA kit (Agilent 5067-1511) with a 2100 Bioanalyzer (Agilent G2938C); all samples had RNA integrity numbers of 10. RNA samples were depleted of mature ribosomal RNA (rRNA) transcripts with Ribo ZERO (Epicentre RZH1064) following the manufacturer's recommendation, using 2 μg of RNA as input. RNA depleted of rRNA was converted to indexed, strand-specific RNA sequencing libraries using the ScriptSeqv2 system (Epicentre SSV21106) following the manufacturer's recommendation, using 50 ng of rRNA-depleted RNA as input. These RNA-seq libraries were sequenced on a HiSeq 2000 (Illumina SY-401–1001) to a read depth of ~90,000,000 single end 97 bp

reads per sample. Raw reads were 'cleaned' using 'Fastq quality trimmer by sliding window' as described above. Cleaned reads were aligned to the mouse reference genome (mm9) with TopHat using strand-specific parameters [191]. Transcript abundance (measured as fragments per kilobase per million reads, FPKM) and differential expression estimates were generated by running Cuffdiff2.1.1 on the aligned reads using the protein-coding genes of RefSeq as the reference. All differential FPKM expression values are expressed as log2. All RNA-seq analysis was performed on Galaxy Cloudman using AWS [192]. FPKM/RPKM ratios were generated for each protein-coding RefSeq gene by dividing FPKM values of RNA-seq by RPKM values of GRO-seq.

The expression of the qPCR gene panel was compared with the RNA-Seq values. Both Spearman and Pearson correlations were above 0.6, suggesting that RNA-seq data is consistent with qPCR data (Table 3.2).

Table 3.2 – Validation of RNA-Seq data through Spearman and Pearson correlations

	(qPCR vs RNA-Seq)									
	so	**st**	**so_2i**	**st_2i**	**so_AA**	**st_AA**	**so_Gal+LIF**	**st_Gal+LIF**	**so_LIF**	**st_LIF**
Spearman Correlation	0.874	0.786	0.879	0.755	0.832	0.691	0.860	0.636	0.741	0.734
Pearson Correlation	0.989	0.917	0.931	0.710	0.956	0.936	0.880	0.748	0.981	0.746

3.2.10. LIF effect, AA effect, Gal effect and Stiffness effect

Heat maps were calculated taking into account the gene expression difference between (i) ESC cultured in the absence of LIF *vs.* ESC cultured in the presence of LIF (LIF effect); (ii) ESC cultured in the absence of AA *vs.* ESC cultured in the presence of AA (AA effect); (iii) ESC cultured in the absence of Gal *vs.* ESC cultured in the presence of Gal (Gal effect); (iv) ESC cultured on stiff substrates *vs.* ESC cultured on soft substrates (stiffness effect).

The degree of Pearson correlation in LIF effect was calculated through comparison of the different genes expression upon presence of LIF, when ESC were cultured on soft or stiff substrates, in the presence or absence of AA. The degree of Pearson correlation in AA effect was calculated through comparison of the different genes expression upon presence of AA, when ESC were cultured on soft or

stiff substrates, in the presence or absence of LIF. The degree of Pearson correlation in stiffness effect was calculated through comparison of the different genes expression upon ESC cultured on soft substrates, when ESC were cultured in the presence or absence of LIF, AA, Mx, Gal, Gal+LIF, AA + LIF, and 2i.

3.2.11. Data and statistical analysis

All data are presented as mean ± standard error of the mean (SEM). qPCR data is derived from three independent experiments. qPCR data analysis was performed using the Bio-Rad CFX manager software 3.1, and gene expression was considered significantly different to the control when regulation threshold was higher than 2.0 and p-value threshold was lower than 0.05. The principal component analysis and hierarchy clustering analysis of gene expression data were analyzed using MATLAB.

To identify enriched functional annotation gene categories, each RNA-Seq data condition was compared to the respective control. Genes with a regulation threshold higher than 1.3 and p-value threshold lower than 0.05 were analyzed in the database for annotation, visualization and integrated discovery web server (DAVID 6.8) [193,194]. Genes were tested for enrichment of Kyoto Encyclopedia of Genes and Genomes (KEGG) pathway. Cutoffs for enrichment were set at EASE score (modified Fisher Exact P-Value) of 0.01, with minimum of 2 genes per functional category. All significant genes were also analyzed for their intersections among the different conditions using the open source jvenn [195].

3.3. Results

LIF, 2i, mitochondria activity and substrate stiffness all have been shown to be key modulators of ESC fate [41,49,114–116,171–173]. To learn how different modulators could additively, subtractively or synergistically promote differentiation or stemness, we tested a cohort of unique mESC culture conditions established by combinations of stem-cell modulators. LIF, 2i, mitochondrial complex III inhibitors Antimycin A (AA) and Myxothiazol (Mx), and the monosaccharide sugar Galactose (Gal), known to indirectly increase OXPHOS by forcing cells to use the Krebs cycle, were selected as biochemical modulators. Substrate stiffness was controlled to expose ESC to different mechanical stimuli (see Experimental Procedure). These conditions were tested in two commonly used mouse embryonic stem cell lines, E14 and R1 (Figure 3.1). We considered stiff substrates without LIF, the "standard condition", as it is well known to promote differentiation [196]. With these different culture combinations, we covered the key modulators in ESC fate control described in the literature. A panel of six common pluripotency-associated genes and six early differentiation-associated genes measured by RT-qPCR, were selected to evaluate pluripotency status for each different condition tested.

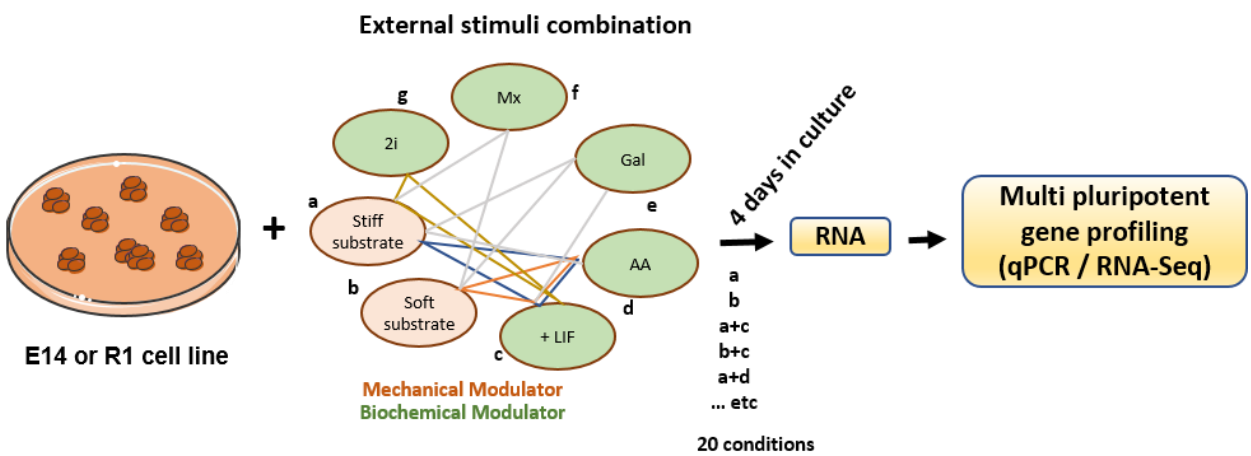

Figure 3.1 – Overview of the experimental design.

ESC exposed to substrates of different mechanical stiffness (denoted mechanical modulators in the text) in the presence/absence of different cell culture modulators of pluripotency (denoted biochemical modulators in the text). After 4 days in culture, the RNA was isolated and both RNA-Seq analysis and pluripotent gene profiling (qPCR) analysis were performed. The RNA data library was used to decouple the effects of the different

modulators on stem cell fate. Abbreviations: AA: Antimycin A; Gal: Galactose; Mx: Myxothiazol; LIF: Leukemia inhibitory factor; 2i: Serum-free Media with CHIR99021, PD0325901 and LIF.

To validate our systems analysis, we paired conditions that were only different in one ESC culture system variable, and selected the ones well known to maintain pluripotency, i.e., (i) cells cultured in the presence of LIF on glass (denoted st_LIF) *vs*. cells cultured in the absence of LIF on glass (denoted st) [196]; (ii) cells cultured in the absence of LIF on soft substrates (0.5 kPa, so) *vs*. cells cultured in the absence of LIF on stiff substrates (glass, st) [171]; and (iii) cells cultured in the presence of AA on glass (st_AA) *vs*. cells cultured in the absence of LIF on glass (st) [114]. As expected, ESC cultured in the presence of LIF on stiff substrates and ESC cultured on soft substrates without LIF both displayed oval, birefringent colony structures with clear boundaries and expressed the pluripotent markers *Oct4* and *Sox2* (Figure 3.2 A – C). In contrast, ESC cultured on stiff substrates in the absence of LIF formed flat colonies that had low expression of the pluripotent markers (Figure 3.2 A – D). In addition, when ESC were cultured on stiff substrates in the presence of the mitochondrial complex III inhibitor AA, oxygen consumption rate (OCR) was inhibited and differentiation was decreased, with AA maintaining the expression of *Oct4* and *Sox2* (Figure 3.2 A – B, D – E).

To uncover the effect of different modulators on gene expression, we grouped the results based on the modulators effects. For example, the "LIF effect" (- LIF *vs.* + LIF) showed that, as predicted, LIF promoted the expression of genes such as *Klf4*, *Esrrb* and *Rex1* and decreased the expression of differentiation genes such as *Fgf5* and *T* (Figure 3.3 A, C). Similarly, the "stiffness effect" (stiff *vs.* soft) presented an upregulation of pluripotent genes and a downregulation of differentiated genes. Nevertheless, this condition induced different expression of pluripotent and differentiated genes, when compared to the "LIF effect" (Figure 3.3 A, C).

In agreement with these results complex III inhibition by two different modulators, AA and Mx, also inhibited differentiation genes and maintained higher levels of pluripotency genes, showing that as expected "OXPHOS inhibition effect", or more precisely, "AA effect" and "Mx effect" regulate ESC fate (Figure 3.3 B, C). Although the OXPHOS inhibition effect, the LIF effect, and the stiffness effect promoted pluripotency, both conditions induced different expressions of pluripotent and

differentiated genes (Figure 3.2 C). These results suggest that different modulators maintain pluripotency through multiple gene regulation mechanisms. Interestingly, Gal, in spite of increasing OCR, was not capable by itself of inhibiting differentiation (Figure 3.4).

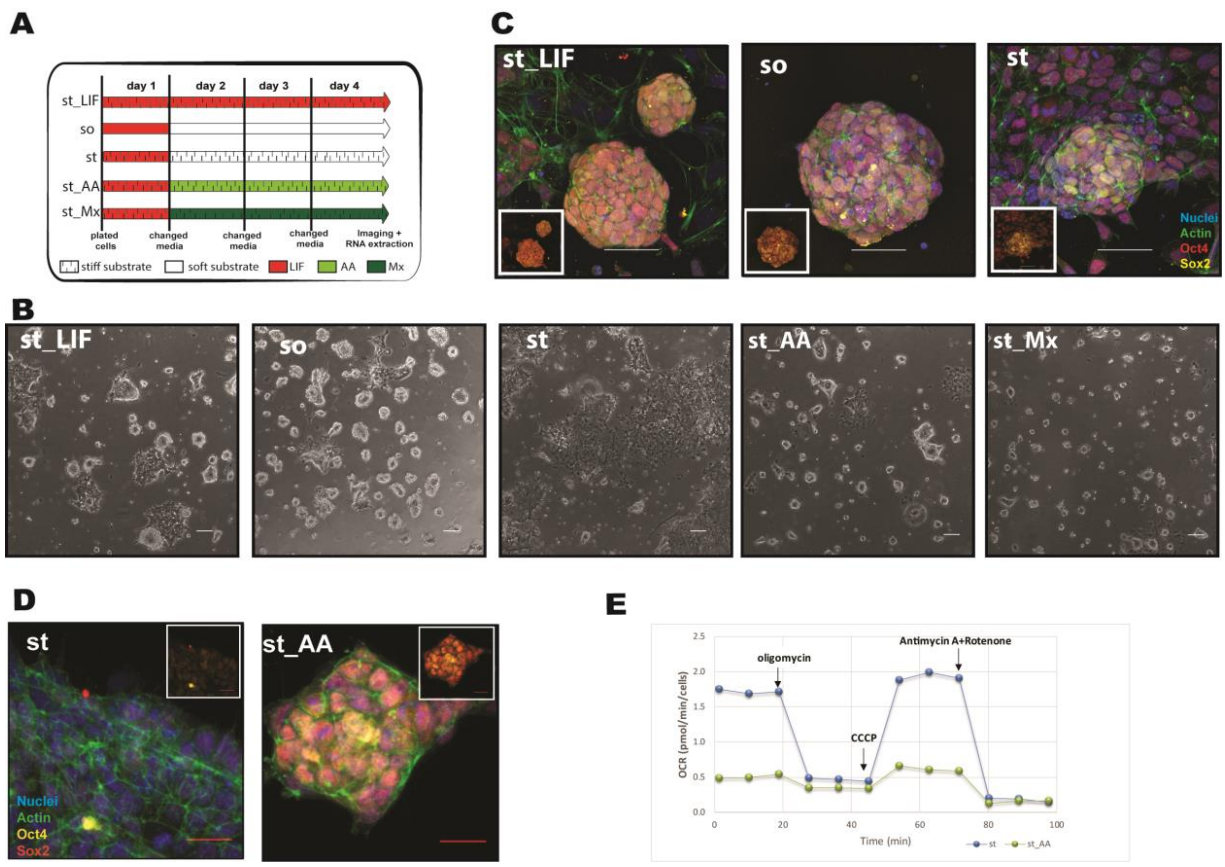

Figure 3.2 – LIF, AA and soft substrates maintain pluripotency.

(A) Experimental design. st: stiff substrate; st_LIF: stiff substrate in the presence of LIF; st_Mx: stiff substrate in the presence of Mx; st_AA: stiff substrate in the presence of AA; so: soft substrate. **(B)** Representative phase-contrast images of ESC cultured for 4 days in the presence of LIF, AA, Mx or subjected to substrates of different stiffness. **(C)** Representative immunofluorescence images of pluripotent transcription factors Oct4 (red) and Sox2 (yellow) after cells were cultured during 4 days in LIF, or on substrates of different stiffnesses. **(D)** Representative immunofluorescence images of pluripotent transcription factors Oct4 (yellow) and Sox2 (red) after 4 days in the presence or absence of Antimycin A (AA). Scale bar in panels A, B and C, 100 µm. **(E)** AA effect on OXPHOS activity – cells cultured on stiff conditions, without LIF, in the presence or absence of AA. Measurements of oxygen consumption rates (OCR, pMoles O_2/min). Abbreviations: AA: Antimycin A; Mx: Myxothiazol; LIF: Leukemia inhibitory factor; st: stiff substrate; so: soft substrate.

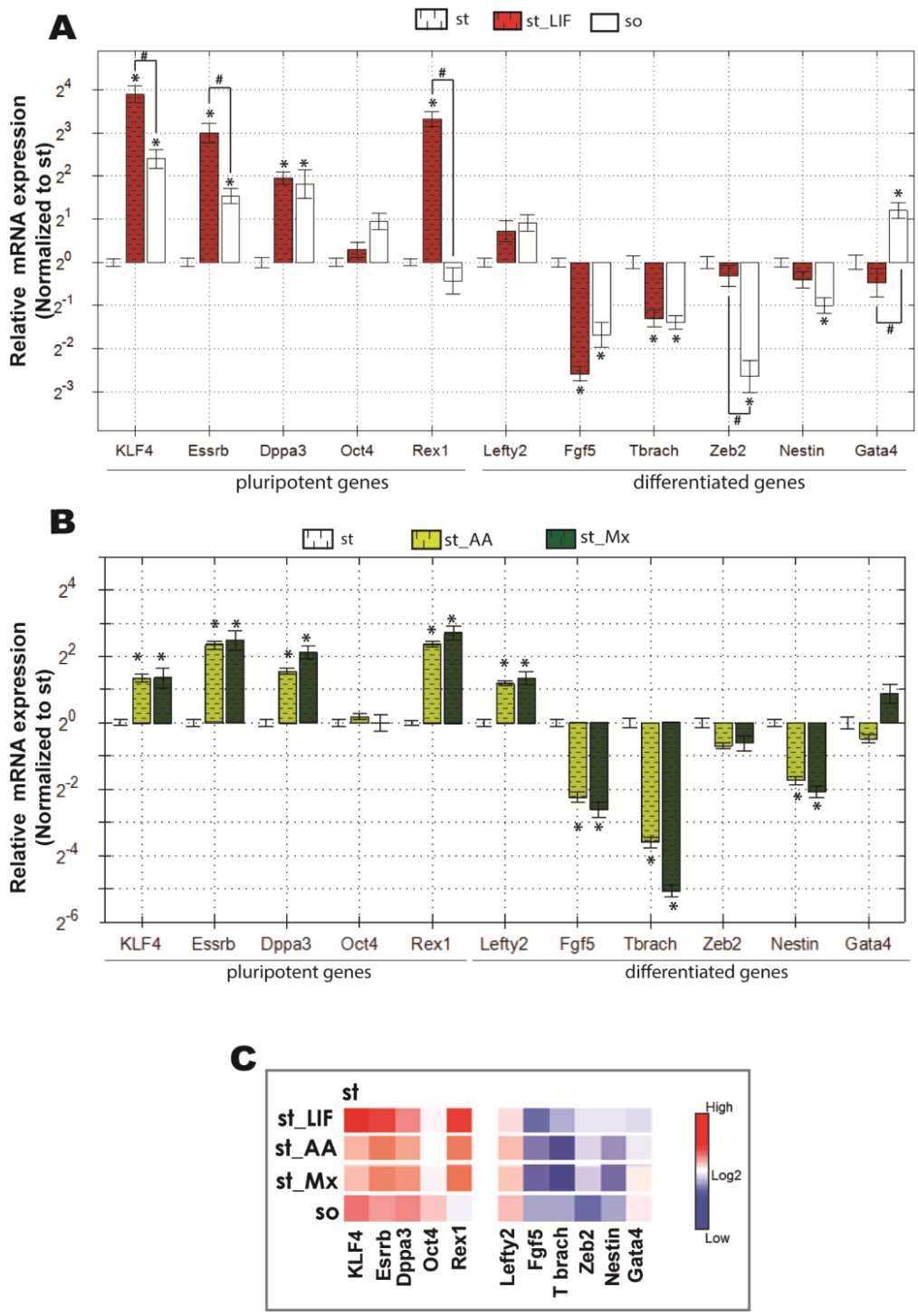

Figure 3.3 – The LIF, AA and stiffness effects maintain pluripotency through the regulation of different gene sets.

(A) mRNA expression fold change (as determined by qPCR analysis) induced by "LIF effect" or "stiffness effect" – ESC cultured in LIF or on soft substrate *vs.* ESC cultured in the absence of pluripotent modulators on stiff substrates. **(B)** mRNA expression fold change (as determined by qPCR analysis) induced by "AA effect" or "Mx effect" – ESC cultured in AA or Mx, respectively *vs.* ESC cultured in the absence of AA or Mx, respectively **(C)** Gene expression heat map of differentially expressed genes upon presence of LIF, AA or stiffness effects, when compared to ESC cultured on stiff substrates in the absence of biochemical modulators (determined by qPCR).

Abbreviations: so – Soft; st – stiff; st_AA – ESC cultured on stiff substrate in the presence of Antimycin A; st_Mx – ESC cultured on stiff substrate in the presence of Myxothiazol; st_LIF – ESC cultured on stiff substrate in the presence of LIF.

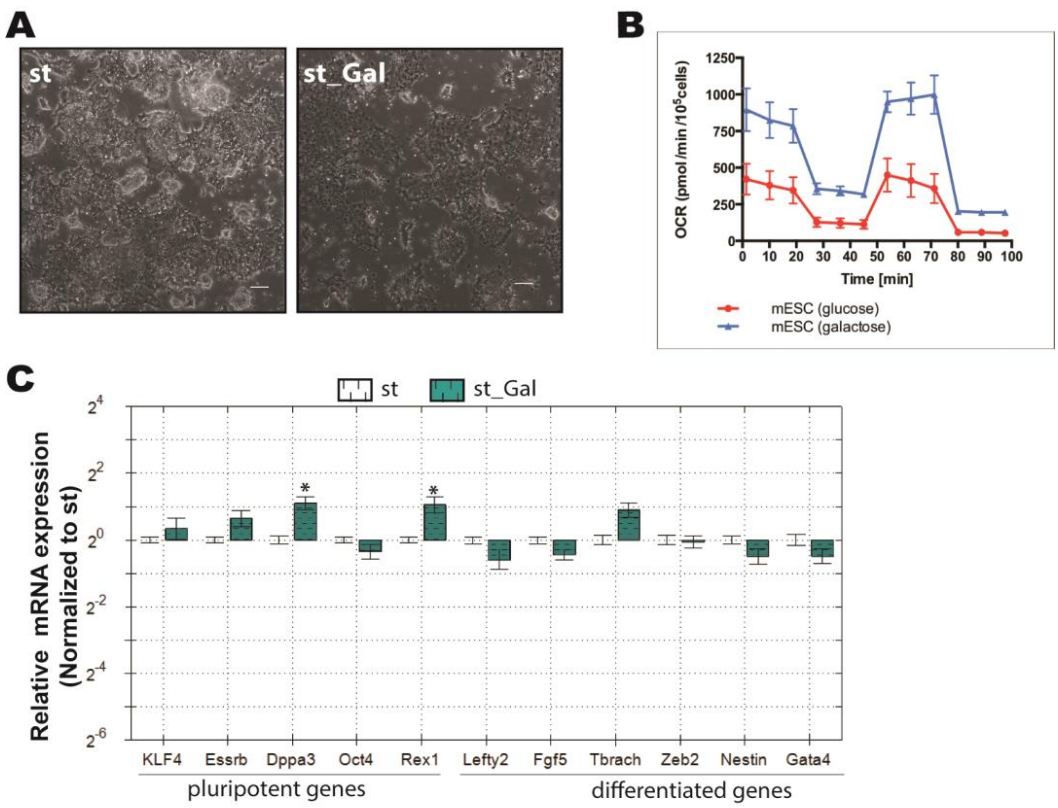

Figure 3.4 – The presence of galactose is not sufficient to maintain pluripotency.

(A) Representative phase-contrast images of ESC cultured for 4 days in the absence or presence of galactose. Scale bar: 100 µm. **(B)** Galactose effect on OXPHOS activity – cells cultured in the presence or absence of galactose. Measurements of oxygen consumption rates (OCR, pMoles O2/min). **(C)** Normalized mRNA expression fold change (determined by qPCR) induced by "Gal effect" – ESC culture in galactose *vs.* ESC cultured in the presence of glucose. st – stiff (cells cultured on soft substrates in the presence of glucose); st_Gal – ESC cultured on stiff substrate in the presence of galactose.

To uncover the underlying principles of how different modulators regulated pluripotency gene expression at a systems level, we quantitatively determined the inter-relationship between paired modulators (Figure 3.5 – Figure 3.9). The principles behind this analysis is to identify different paired modulators and study their effects on gene expression, revealing the effect of each ESC culture system modulator on ESC gene expression. To accomplish this, we compared the gene expression observed

from each paired modulator with and without the other modulator pair, i.e. effect of A with and without B, and the effect of B with and without A).

From this analysis, we observed that the magnitude in changes of gene expression due to the "LIF effect" did not change when ESC were cultured on substrates of different stiffness (st *vs.* st_LIF compared to so *vs.* so_LIF) (Figure 3.5 A), although gene expression values changed (Figure 3.5 C). Interestingly, the magnitude of the LIF effect changed when LIF was conjugated with AA (Figure 3.5 A). Thus, a positive correlation was observed between the LIF effect for substrates of different stiffness. The degree of correlation decreased when LIF was combined with AA treatment (Figure 3.5 B).

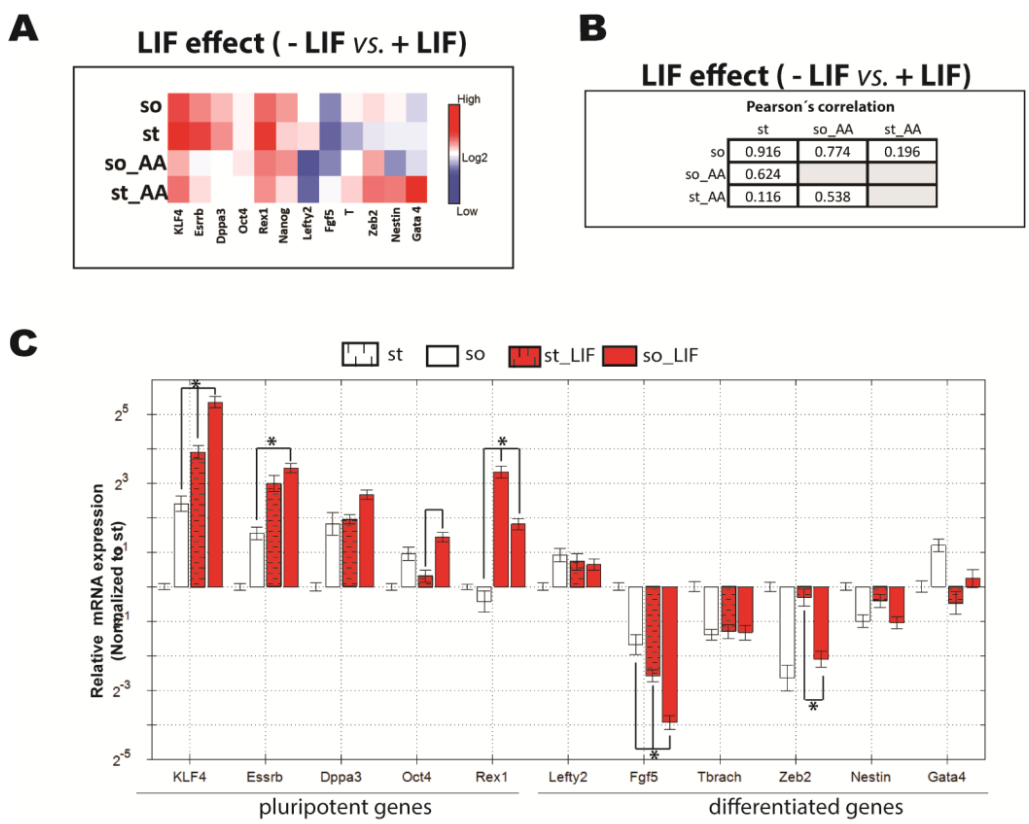

Figure 3.5 – The LIF effect is independent of substrate stiffness but depends on AA.

(A) Gene expression heat map (determined by qPCR) of cells cultured in the absence *vs.* presence of LIF, when multiple modulators are combined. **(B)** Decouple of LIF effect: Pearson correlation upon presence of AA, soft and stiff substrates. **(C)** Normalized mRNA expression fold change (as determined by qPCR analysis) of ESC cultured on soft / stiff substrate in the presence of LIF *vs.* ESC cultured in the absence of pluripotent modulators. Abbreviations: so – soft substrate; st – stiff substrate; AA – Antimycin A; Gal: Galactose; LIF: Leukemia inhibitory factor.

Thus, we decided to study the AA effect. AA stimulus combined with different substrate stiffness induced significant changes in gene expression (Figure 3.6 C). Nevertheless, the AA effect was independent of the substrate stiffness used, but dependent on the presence of LIF in the medium (Figure 3.6 A). When we measured the correlation of the AA effect with other stimuli, a positive correlation between the AA effect in different stiffnesses was observed (Figure 3.6 B). However, this correlation decreased when LIF was present (Figure 3.6 B).

Interestingly, although the LIF effect did not depend on Gal in the medium, the Gal effect depended on LIF (Figure 3. 7).

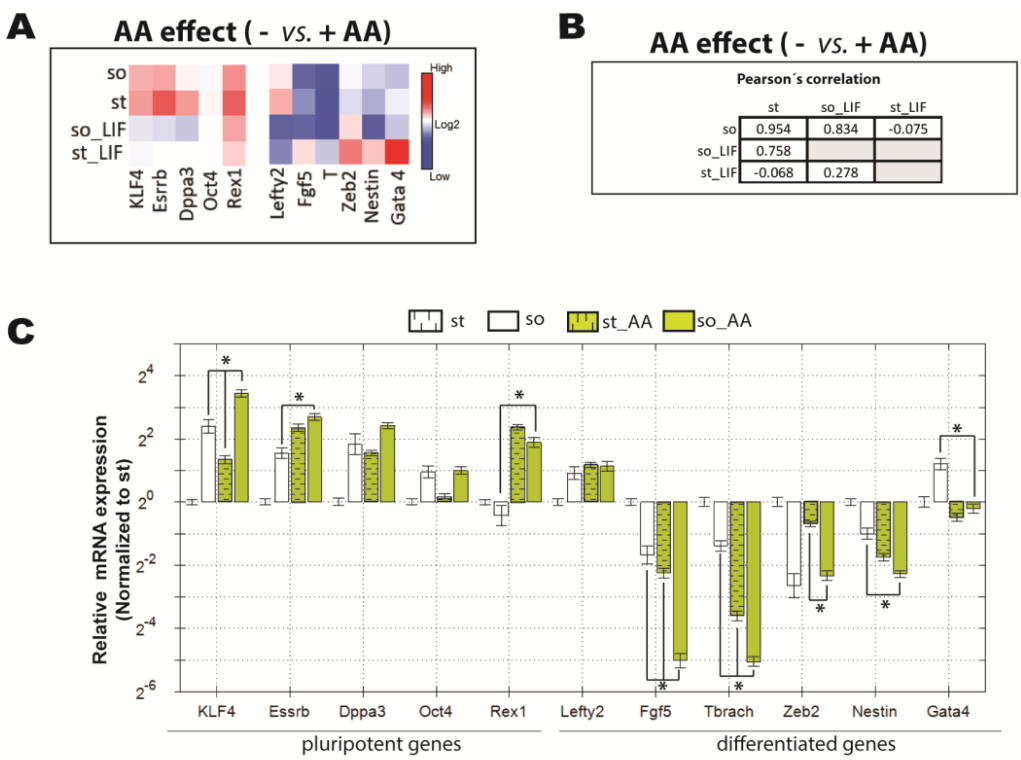

Figure 3.6 – The AA effect is independent of substrate stiffness but depends on LIF.

(A) Gene expression heat map (determined by qPCR) of ESC cultured in the absence *vs.* presence of AA, when multiple modulators are combined. **(B)** Decouple of AA effect: Pearson correlation upon presence of LIF, soft (so) and stiff (st) substrates. **(C)** Normalized mRNA expression fold change (as determined by qPCR analysis) of ESC cultured on soft / stiff substrate in the presence of AA *vs.* ESC cultured in the absence of pluripotent modulators. Abbreviations: so – soft substrate; st – stiff substrate; AA – Antimycin A; LIF: Leukemia inhibitory factor.

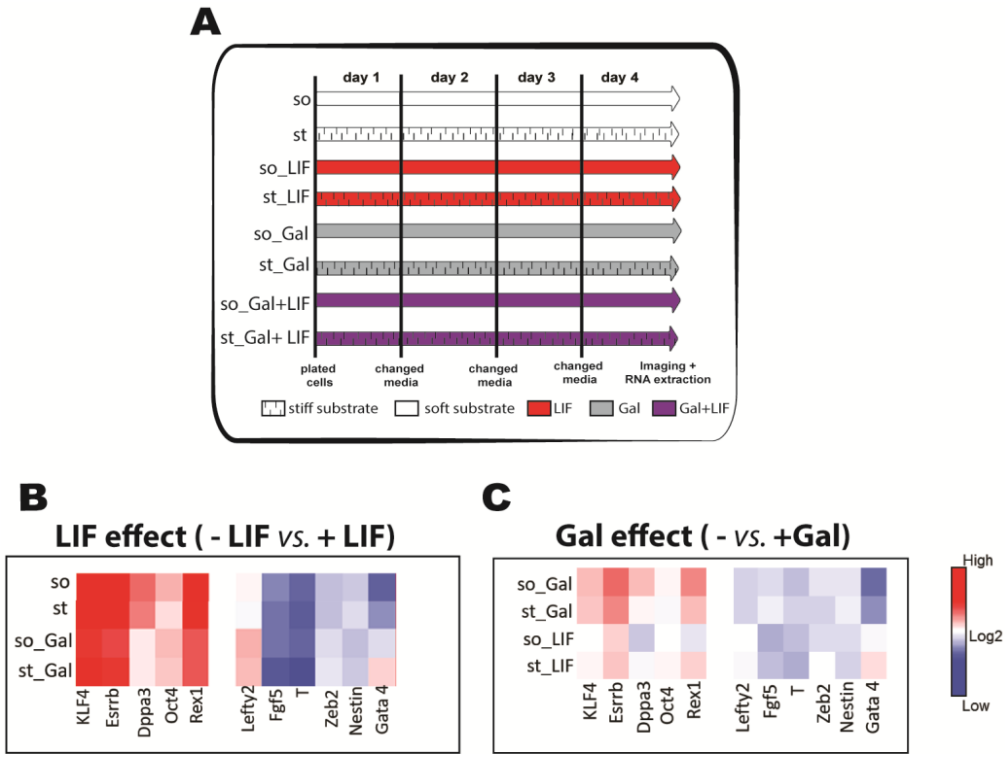

Figure 3.7 – The Galactose effect is independent of substrate stiffness but depends on LIF.

(A) Experimental design. st: stiff substrate; so: soft substrate; st_LIF: stiff substrate in the presence of LIF; st_Gal: stiff substrate in the presence of Gal; st_Gal+LIF: stiff substrate in the presence of Galactose and LIF; so: soft substrate; so_LIF: soft substrate in the presence of LIF; so_Gal: soft substrate in the presence of Gal; so_Gal+LIF: soft substrate in the presence of Galactose and LIF. **(B)** Gene expression heat map (as determined by qPCR analysis) of ESC cultured in the absence *vs.* presence of LIF, when different stiffness or presence of Gal are combined. **(C)** Gene expression heat map (determined by qPCR) of ESC cultured on the absence vs. presence of galactose, when different stiffness or presence of LIF are combined. Abbreviations: so – soft substrate; st – stiff substrate; Gal: Galactose; LIF: Leukemia inhibitory factor.

When we compared the inter-relationship between the stiffness effect in the presence of AA or LIF, we found that a positive correlation between these different conditions was maintained, with a gene expression magnitude identical when LIF or AA was present in the medium (Figure 3.8). Yet, soft substrates in combination with biochemical modulators such as LIF and AA promoted the downregulation of differentiated genes and the upregulation of pluripotency genes, when compared to the same conditions on stiff substrates (Figure 3.5 C and Figure 3.6 C).

Gene expression regulation showed a non-linear but monotonic change following a reduction in substrate stiffness. Importantly, the LIF and stiffness effects on gene regulation remained independent of each other for various substrate stiffness, suggesting that the LIF effect is robust and the pluripotency state is highly dependent of substrate stiffness (Figure 3.9). In addition, gene expression changed when cells were cultured in 2i medium on different stiffness, which demonstrates that gene expression promoted by 2i medium is also dependent of the substrate stiffness that cells are on (Figure 3.10). Nevertheless, the stiffness effect was also independent of 2i medium (Figure 3.8 A). Together, these results suggest that the effect of mechanical stiffness was robust in the presence of the biochemical pluripotency modulators, such as LIF, 2i, galactose, AA and Mx. In addition, mechanical stiffness of the environment seems to regulate stem cell pluripotency through a pathway independent from LIF and AA.

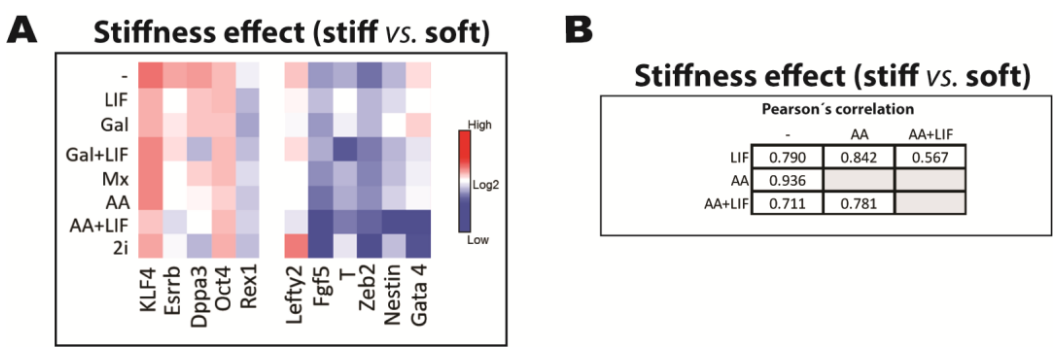

Figure 3.8 – The Stiffness effect is independent of pluripotent biochemical modulators.
(A) Gene expression heat map (determined by qPCR) of ESC cultured on stiff *vs.* soft substrates, when multiple modulators are combined. **(A)** Decouple of stiffness effect: Pearson correlation upon presence of AA and / or LIF. Abbreviations: so – soft substrate; st – stiff substrate; AA – Antimycin A; Gal: Galactose; LIF: Leukemia inhibitory factor; Mx – Myxothiazol; 2i - Serum-free Media with CHIR99021, PD0325901 and LIF.

We then decided to cluster gene expression patterns measured for different conditions in a hierarchical manner (Figure 3.11). As expected, ESC cultured in the presence of pluripotent modulators (such as 2i, AA, Mx and LIF) clustered on top, with high expression of pluripotent genes such as *KLF4*, *Esrrb*, *Dppa3*, and low expression of differentiated genes, such as *Fgf5* and *T*, when compared to ESC cultured in the absence of these biochemical pluripotent cues. Still, different biochemical modulators

on soft substrates clustered together, on top of the hierarchy. Thus, soft substrates in combination with pluripotent biochemical cues promote a more pluripotent state when compared to ESC cultured in the same biochemical conditions, but on stiff substrates (Figure 3.11 B). These results demonstrate that the substrate stiffness is likely to transform consistently the gene expression landscapes to regulate pluripotency, independently of various biochemical cues. In addition, we observed that ESC maintained a characteristic pluripotent morphology, albeit with colony borders defined when cultured on soft substrates in medium with pluripotent modulators (Figure 3.11 A). Importantly, similar results were obtained when another embryonic cell line (R1) was used, which demonstrates that stiffness and biochemical effects are not cell line-dependent (Figure 3.12). These results imply that the effects of ESC pluripotency modulators depend on the culture system context, which is responsible for a complex pattern of gene responses.

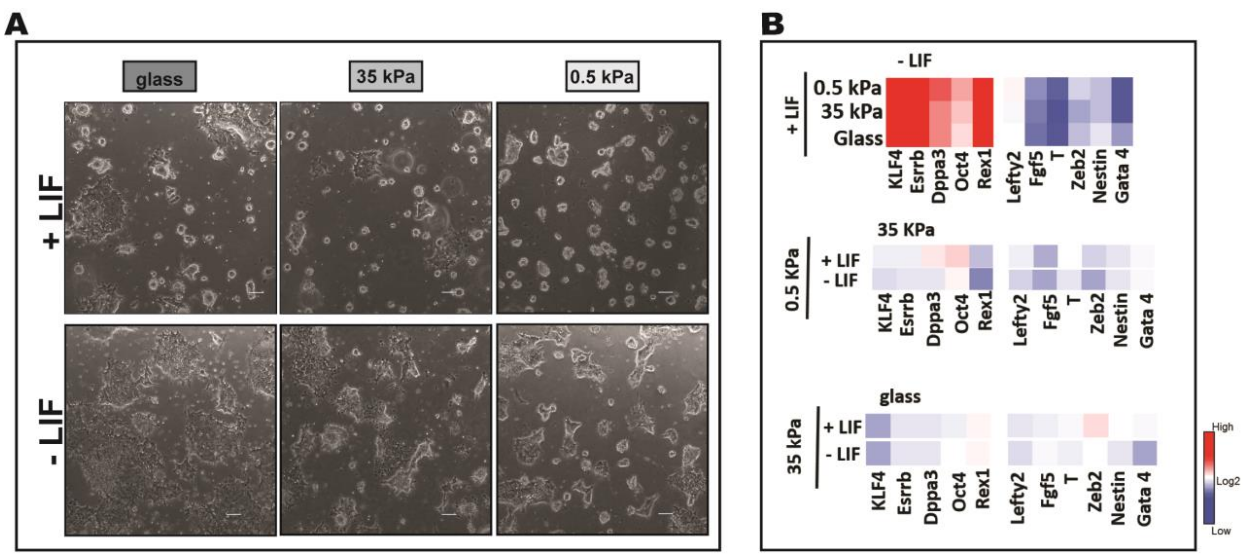

Figure 3.9 – The LIF and stiffness effects are independent.

(A) Representative phase-contrast images of ESC cultured for 4 days on glass (stiff substrates), 35 kPa polyacrylamide gels and 0.5 kPa polyacrylamide gels (soft substrates) in the presence or absence of LIF. Scale bar: 100 µm. **(B)** LIF response in different range of stiffness: 0.5 kPa, 35 kPa and glass.

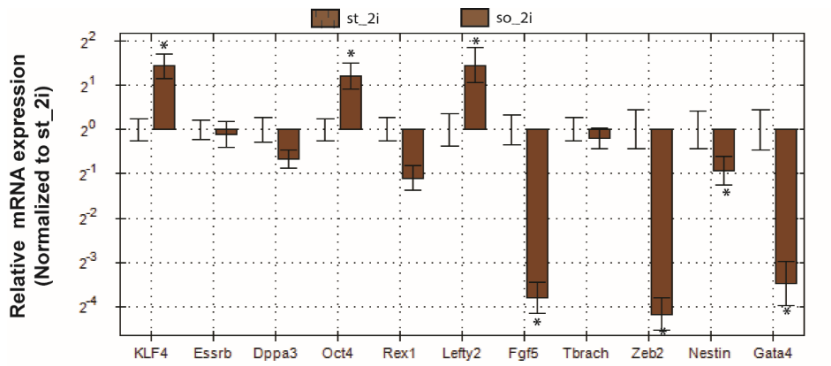

Figure 3.10 - ESC cultured on soft substrates in the presence of 2i have higher pluripotency levels.
Normalized mRNA expression fold change (as determined by qPCR analysis) of ESC cultured on soft substrate in the presence of 2i *vs.* ESC cultured on stiff substrates in the presence of 2i. Abbreviations: so – soft substrate; st – stiff substrate; 2i - Serum-free Media with CHIR99021, PD0325901 and LIF.

The fact that signaling pathways driving the LIF and stiffness effects did not interfere was further confirmed at the whole-genome level using RNA-seq analysis (Figure 3.13 A). The visualization of RNA-seq results, using the first two eigenvectors from a principal component analysis (PCA), showed that LIF and stiffness effects differently regulate ESC gene expression. The gene expression pattern exhibited by the LIF effect is distinct from the one exhibited by the stiffness effect. Yet, changes in ESC culture system conditions with LIF, AA, galactose, or 2i, did not affect the stiffness pattern effect on gene expression (Figure 3.13 A). Similar results were obtained when qPCR data was visualized using first two eigenvectors from principal component analysis both in E14 (Figure 3.13 B) and R1 cell lines (Figure 3.14). Interestingly, RNA-Seq analysis of AA effect was significantly different from LIF effect, suggesting that the AA can have a different role from LIF in regulating gene expression.

We then decided to examine the pool of genes altered upon change of substrate stiffness (st *vs.* so) or LIF stimuli (st *vs.* st_LIF). Our RNA-Seq data shows that soft substrates changed the expression of more than 4500 genes, from which only approximately 1100 genes were in common with LIF regulation (Figure 3.15 A). Thus, we took advantage of the RNA-Seq data analysis to investigate through Kyoto Encyclopedia of Genes and Genomes (KEGG) pathway analysis which pathways were associated with the differently expressed genes, and therefore, more prone to be activated or inhibited for each tested stimulus ("LIF effect" and "stiffness effect") (Figure 3.15 B, C). As expected, LIF effect

promoted an increased expression of genes associated with pluripotent signaling pathways, such as *Lifr* and *Stat3* (Figure 3.15 B, and Appendix 7.1).

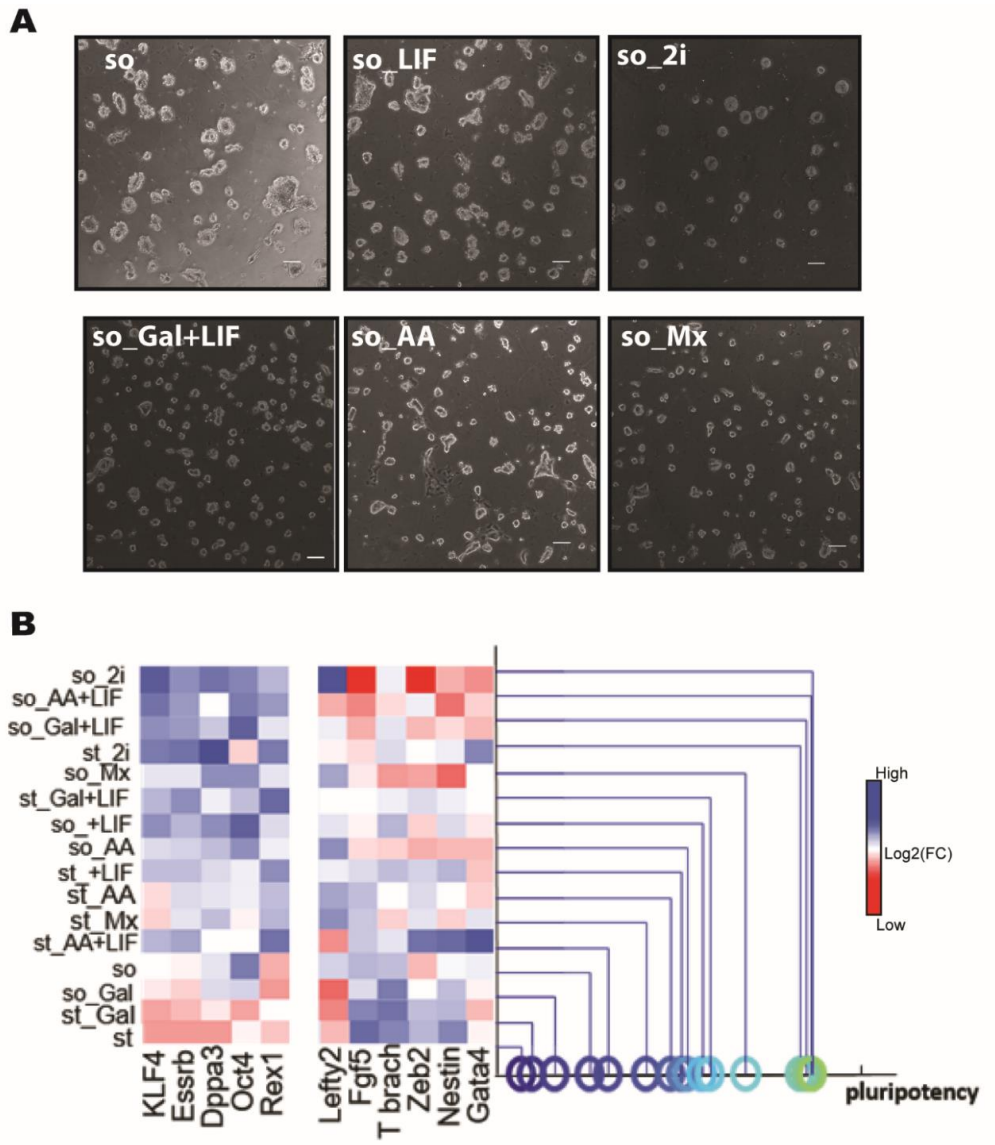

Figure 3.11 - ESC cultured on soft substrates in the presence of pluripotent modulators maintain their pluripotent morphology and are more pluripotent than ESC cultured on stiff substrates with the same pluripotent modulators.

(A) Representative phase-contrast images of ESC cultured for 4 days on soft substrates in the presence of LIF, AA, Mx, AA+LIF, Gal+LIF or 2i. Scale bar: 100 µm. **(B)** Cluster of all conditions, ranked by the highest pluripotency values, determined by qPCR analysis. Abbreviations: so – soft substrate; st – stiff substrate; AA – Antimycin A; Gal: Galactose; LIF: Leukemia inhibitory factor; Mx – Myxothiazol; 2i - Serum-free Media with CHIR99021, PD0325901 and LIF.

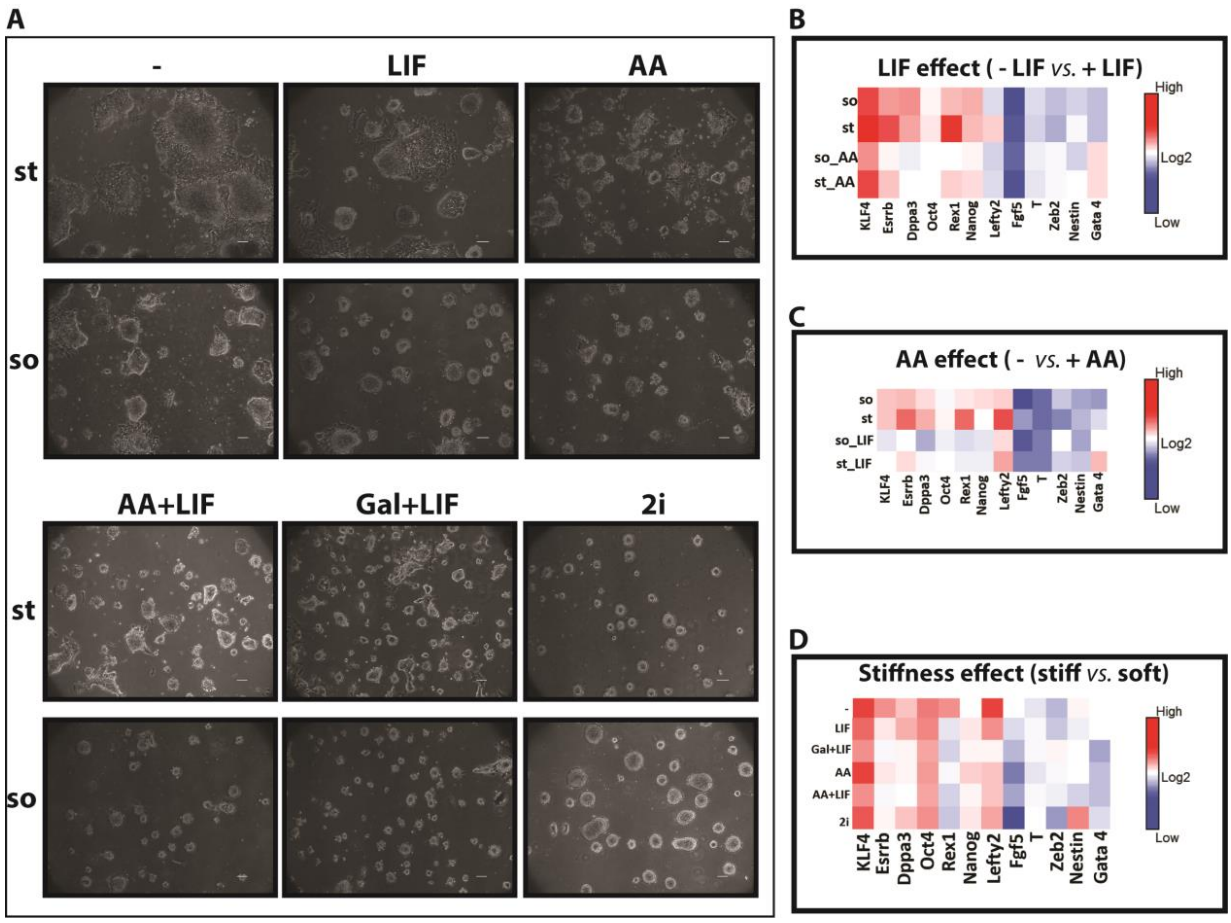

Figure 3.12 – Stiffness and biochemical modulators of pluripotency are cell line-independent.

(A) Representative phase-contrast images of ESC (R1 cell line) cultured for 4 days in the presence of LIF, AA, AA+LIF, Gal+LIF or 2i on stiff or soft substrates. Scale bar: 100 µm. **(B – D)** Gene expression heat map of R1 cell line to decouple the **(B)** LIF effect (cells cultured in the absence *vs.* presence of LIF, when multiple modulators are combined), **(C)** AA effect (cells cultured in the absence *vs.* presence of AA, when multiple modulators are combined), **(D)** stiffness effect (cells cultured on stiff *vs.* soft substrates, when multiple modulators are combined), Abbreviations: so – soft substrate; st – stiff substrate; AA – Antimycin A; Gal: Galactose; LIF: Leukemia inhibitory factor; 2i - Serum-free Media with CHIR99021, PD0325901 and LIF.

Soft substrates induced a downregulation of actin cytoskeleton genes (Figure 3.15 C). Accordingly, ESC cultured on soft substrates showed fewer stress fibers to adhere to their substrate, when compared to ESC cultured on stiff substrates (Figure 3.15 D). In addition, soft substrates promote the downregulation of genes associated with pluripotency signaling pathways, such as *Bmp* and *Smads* (Figure 3.15 C and Appendix 7.1). Nevertheless, soft substrates induced the upregulation of pluripotency associated genes such as *Klf4*, *Esrrb* and *Oct4* (Appendix 7.1). Surprisingly, metabolic pathways were enriched upon decrease of substrate stiffness, with the upregulation of genes associated

with oxidative phosphorylation (OXPHOS) and glycolysis, which did not occur with the LIF effect (Figure 3.15 B, C and Appendix 7.2 – 7.3). Yet, mitochondria structures did not change when ESC were cultured on different stiffness (Figure 3.15 D). These results suggest that the stiffness effect, oppositely to the LIF effect, promotes pluripotency through the regulation of cell metabolism and cytoskeleton.

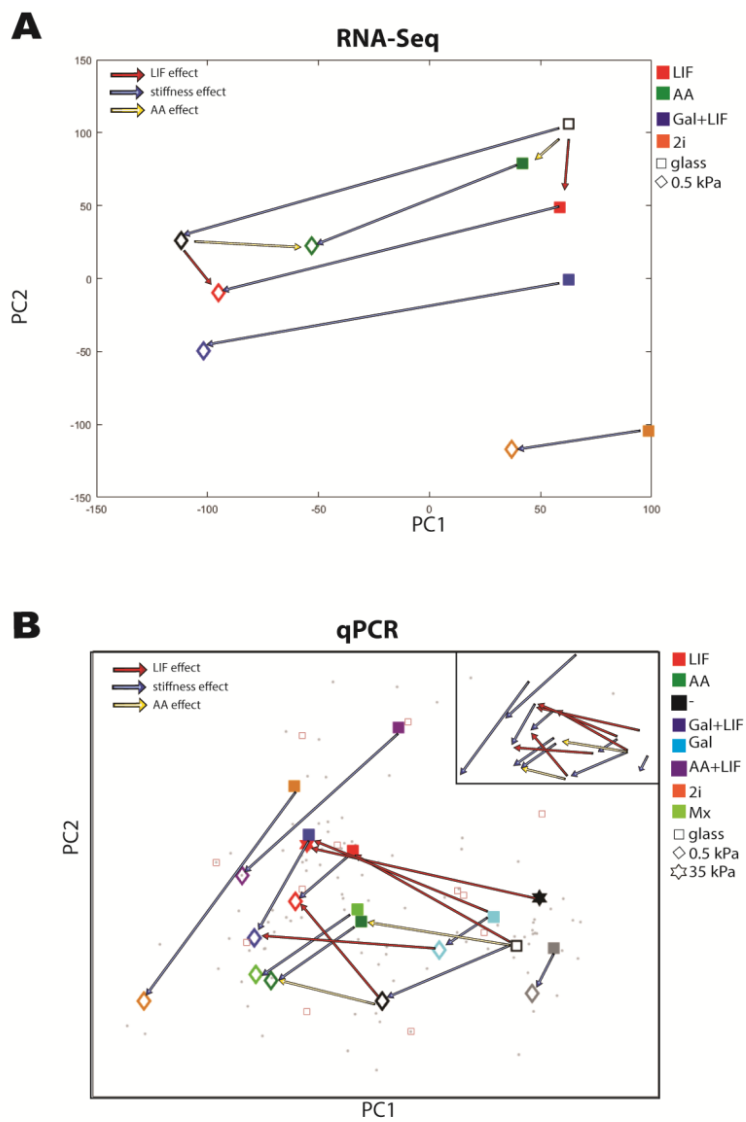

Figure 3.13 - LIF and stiffness effect regulate ESC gene expression differently.

Visualization of LIF, AA and stiffness effect determined by **(A)** RNA-Seq data and **(B)** qPCR data**,** using the first two eigenvectors from a principal component analysis (PCA). Abbreviations: AA – Antimycin A; Gal: Galactose; LIF: Leukemia inhibitory factor; 2i - Serum-free Media with CHIR99021, PD0325901 and LIF.

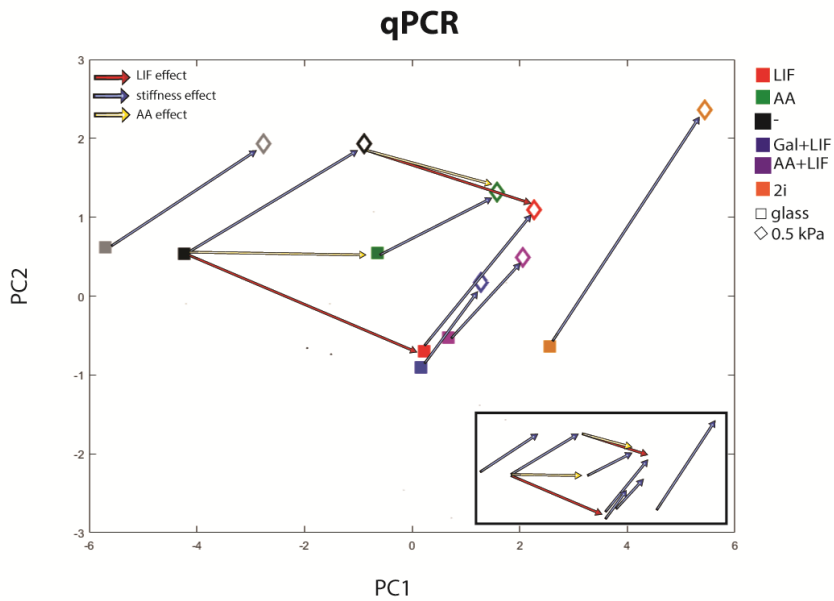

Figure 3.14 - LIF and stiffness effect is not ESC line dependent.

Visualization of LIF, AA and stiffness effect determined by qPCR data using the first two eigenvectors from a principal component analysis (PCA) from R1 cell line gene expression. Abbreviations: AA – Antimycin A; Gal: Galactose; LIF: Leukemia inhibitory factor; 2i - Serum-free Media with CHIR99021, PD0325901 and LIF.

A

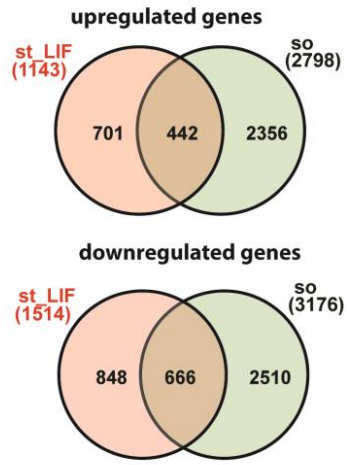

D

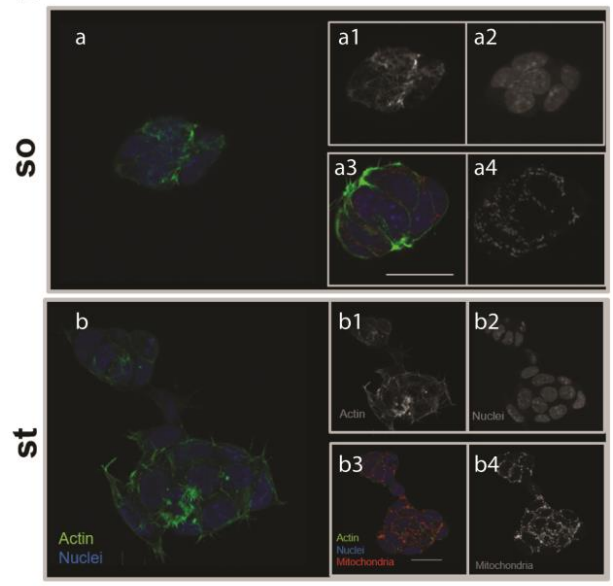

B

LIF effect (st *vs.* st_+LIF)

Upregulated	# Genes	%	P-Value	Fold Enrichment
Signaling pathways regulating pluripotency of stem cells	20	1.8	9.20E-05	2.8
PI3K-Akt signaling pathway	32	2.8	2.70E-03	1.7

Downregulated	# Genes	%	P-Value	Fold Enrichment
Rap1 signaling pathway	40	2.7	2.10E-07	2.4
Focal adhesion	37	2.5	2.00E-06	2.3
Hippo signaling pathway	29	1.9	7.90E-06	2.5
Adherens junction	17	1.1	7.70E-05	3.1
MAPK signaling pathway	38	2.5	8.00E-05	2
Tight junction	25	1.7	1.10E-04	2.4
Wnt signaling pathway	24	1.6	3.70E-04	2.2
Signaling pathways regulating pluripotency of stem cells	23	1.5	6.90E-04	2.2
ECM-receptor interaction	17	1.1	8.70E-04	2.5
Ras signaling pathway	32	2.1	1.10E-03	1.8
Cell adhesion molecules (CAMs)	25	1.7	1.20E-03	2
PI3K-Akt signaling pathway	41	2.7	6.20E-03	1.5
cAMP signaling pathway	26	1.7	7.70E-03	1.7

C

Stiffness effect (st *vs.* so)

Upregulated	# Genes	%	P-Value	Fold Enrichment
Ribosome	98	3.5	2.00E-44	4.3
Metabolic pathways	330	11.9	1.70E-24	1.6
Oxidative phosphorylation	69	2.5	2.50E-20	3.1
Spliceosome	58	2.1	5.90E-14	2.8
Carbon metabolism	52	1.9	3.80E-13	2.8
Biosynthesis of amino acids	39	1.4	8.50E-12	3.2
Proteasome	25	0.9	6.10E-09	3.5
Glycolysis / Gluconeogenesis	29	1	2.00E-07	2.8
RNA transport	54	2	3.10E-07	2
Amino sugar and nucleotide sugar metabolism	23	0.8	1.30E-06	3
DNA replication	17	0.6	2.80E-05	3.1
Citrate cycle (TCA cycle)	16	0.6	3.40E-05	3.2
Pyrimidine metabolism	33	1.2	7.20E-05	2
Aminoacyl-tRNA biosynthesis	24	0.9	1.10E-04	2.3
Ribosome biogenesis in eukaryotes	28	1	1.10E-04	2.1
Pyruvate metabolism	17	0.6	1.40E-04	2.8
Glutathione metabolism	21	0.8	1.50E-04	2.4
Glycine, serine and threonine metabolism	17	0.6	2.00E-04	2.7
Glyoxylate and dicarboxylate metabolism	13	0.5	8.60E-04	2.8
Arginine and proline metabolism	18	0.7	8.90E-04	2.3
2-Oxocarboxylic acid metabolism	10	0.4	1.20E-03	3.3
Fructose and mannose metabolism	14	0.5	1.30E-03	2.6
Valine, leucine and isoleucine degradation	19	0.7	1.40E-03	2.2
Peroxisome	25	0.9	1.70E-03	1.9
Cysteine and methionine metabolism	15	0.5	2.30E-03	2.4
Fatty acid degradation	17	0.6	2.60E-03	2.2
Fatty acid metabolism	17	0.6	4.00E-03	2.1
Mismatch repair	10	0.4	4.20E-03	2.9
RNA polymerase	12	0.4	4.40E-03	2.5
Pentose phosphate pathway	12	0.4	4.40E-03	2.5
Cell cycle	32	1.2	5.00E-03	1.6
Base excision repair	13	0.5	5.50E-03	2.4

Downregulated	# Genes	%	P-Value	Fold Enrichment
Focal adhesion	67	2.2	2.70E-13	2.5
PI3K-Akt signaling pathway	86	2.8	1.40E-09	1.9
Rap1 signaling pathway	60	1.9	3.20E-09	2.2
ECM-receptor interaction	33	1.1	1.20E-08	2.9
MAPK signaling pathway	65	2.1	2.80E-08	2
FoxO signaling pathway	40	1.3	3.40E-07	2.3
Endocytosis	64	2.1	2.40E-06	1.8
TGF-beta signaling pathway	27	0.9	1.20E-05	2.5
Signaling pathways regulating pluripotency of stem cells	37	1.2	1.50E-05	2.1
Ras signaling pathway	52	1.7	3.60E-05	1.8
Wnt signaling pathway	36	1.2	6.10E-05	2
Cell cycle	32	1	1.40E-04	2
Regulation of actin cytoskeleton	47	1.5	2.10E-04	1.7
mTOR signaling pathway	19	0.6	2.60E-04	2.5
Hippo signaling pathway	36	1.2	2.60E-04	1.9
Phosphatidylinositol signaling system	26	0.8	3.60E-04	2.1
TNF signaling pathway	28	0.9	4.30E-04	2
Adherens junction	20	0.6	1.30E-03	2.2
Gap junction	22	0.7	2.20E-03	2
AMPK signaling pathway	29	0.9	2.30E-03	1.8
Notch signaling pathway	15	0.5	2.50E-03	2.4
cAMP signaling pathway	40	1.3	3.10E-03	1.6
p53 signaling pathway	18	0.6	3.60E-03	2.1
Inositol phosphate metabolism	18	0.6	5.90E-03	2
Tight junction	29	0.9	8.70E-03	1.6

Figure 3.15 – The LIF and stiffness effect induce different gene signaling pathways in order to maintain ESC pluripotency.

(A) Venn diagrams of the RNA-Seq global pool of genes demonstrating the number of upregulated (top) and downregulated (bottom) genes ($P<0.05$, fold change >1.3) in ESC exposed to different pluripotent modulators (LIF or soft substrates) when compared to ESC cultured in the absence of pluripotent modulators (ESC cultured on stiff substrates). **(B)** KEGG (Kyoto Encyclopedia of Genes and Genomes) pathway analysis determined by DAVID functional annotation bioinformatics analysis of differentially expressed genes in ESC cultured in LIF, when compared to ESC cultured in the absence of LIF, on stiff substrates (LIF effect). **(C)** KEGG pathway analysis determined by DAVID functional annotation bioinformatics analysis of differentially expressed genes in ESC cultured on soft substrates when compared to ESC cultured on stiff substrates, in the absence of LIF (stiffness effect). **(D)** Representative immunofluorescence images of actin structure of ESC colony attached to (a) soft or on (b) stiff substrates. (a1/b1) z-tack representing the bottom of a colony. (a2/a3/a4 and b3/b3/b4) Z-slice representing an intermediate plane with mitochondria (red), actin (green) and nuclei (blue) represented. Scale bar: 50 µm. Abbreviations – st_LIF : ESC cultured on stiff substrates in the presence of LIF; st: ESC cultured on stiff substrates; so: ESC cultured on soft substrates.

3.4. Discussion

Mechanical and biochemical cues work together *in vivo* for proper embryonic development [197,198]. Although ESC *in vitro* are commonly cultured in contact with a stiff (glass or plastic) substrate, substrate stiffness is usually neglected, and only biochemical modulators present in the medium are taken into account for analysis. In this study, we decouple the importance of different, commonly used modulators of ESC pluripotency. We show that changes in gene expression induced by matrix stiffness (the "stiffness effect") is independent of biochemical modulators such as 2i, LIF and OXPHOS inhibition. Soft substrates with pluripotent biochemical modulators increase the expression of pluripotent genes and decrease the expression of differentiated genes. In addition, the magnitude of the LIF effect changes neither upon changes in substrate stiffness, nor with the indirect increase of mitochondrial respiratory chain by galactose. Nevertheless, the LIF effect was changed by the OXPHOS inhibitor, AA.

Mitochondria oxidative metabolism plays a key role in the regulation of ESC fate [114–116,119]. Stat3, a downstream effector of LIF, has recently been shown to promote pluripotency through the increase in pluripotent-associated transcription factors, while inducing proliferation through the increase of oxidative phosphorylation [107]. Yet, both pathways were shown to work distinctly, with oxidative phosphorylation inhibition not affecting naïve pluripotency identity [107].

In our study, we show that the LIF effect is altered when AA is present in the medium, with maintained pluripotency levels. Similarly, the AA effect is altered when LIF is present. Although the LIF effect alone without AA, and the AA effect alone without LIF on gene expression were similar, the effects when AA and LIF were combined, particularly on the expression of the selected pluripotent and differentiated genes, were neither additive nor synergetic. These results suggest that LIF and AA regulate these pluripotency genes through shared downstream pathways. Nevertheless, RNA-seq results suggest that AA effect and LIF effect have different roles in regulating global gene expression. In fact, AA has also been shown to induce mitochondrial reactive oxygen species (ROS) production and stabilization of HIF1-α under normoxia conditions [114]. Therefore, the results observed when AA is

present in the medium might reflect a combination of OXHPOS inhibitions, production of ROS, and HIF1-α expression.

ESC are known to have a bivalent energy metabolism, relying both on glycolysis and OXPHOS [106]. Interestingly, our results also show that soft substrates induce an increase expression of genes related with the OXPHOS and glycolysis pathway. In contrast, Gal, in spite of indirectly increasing OCR, was not able to maintain pluripotency. Although the Gal effect was not dependent of substrate stiffness, it was dependent on LIF. These results suggest that the increase of OXPHOS and glycolysis is not sufficient to maintain ESC in a pluripotent state, but the presence of a stimuli that induce both OXPHOS and glycolysis in combination with a pluripotent modulator, prone ESC into a more pluripotent state.

The MAPK signaling pathway promotes ESC differentiation [46]. Recently, ESC differentiation through substrate stiffness has been related to Src-MAPK pathway role via mechanotransduction [172]. In addition, soft substrates affect cell adhesion, cell spreading, and cytoskeleton assembly, when compared to stiff substrates [199]. In agreement with the literature, our RNA-seq results showed that both LIF- and stiffness- effect induce downregulation of MAPK pathway, with soft substrates also promoting alterations of actin cytoskeleton-related genes. Accordingly, ESC cultured on soft substrates had less actin stress fibers. Interestingly, soft substrates also induced a downregulation of BMP receptor and Smad proteins. Similar results were previously shown in bone marrow mesenchymal stem cells cultured on soft substrates [200]. But oppositely to bone marrow mesenchymal stem cells, ESC did not differentiate to neural cells.

Importantly, our study also demonstrates that the magnitude of the stiffness effect is independent of the pluripotent biochemical stimuli present in the medium. Soft substrates have been recently reported to promote a more efficient cell reprogramming to pluripotency [179]. In our study, cells cultured with different biochemical modulators induce higher expression of pluripotent markers and lower expression of differentiated markers when cultured on soft substrates. Interestingly, even in 2i, a medium that maintains a homogeneous ESC culture [49], a higher expression of pluripotency markers and a decrease expression of differentiated markers was observed when ESC were cultured on soft substrates. A parallel to these results has also been reported in cancer cells, notably stating that cancer cells cultured on different stiffness have been reported to react differently to chemotherapeutic drugs

[201,202], suggesting that the role of stiffness on cell fate is not specific to ESC. In addition, recent studies show that *in vivo*, mechanosensing is crucial for the correct position and specification of the ICM [160], whereas mechanical forces effects (stiffness), seem to be critical for post-implantation development [161,162]. Therefore, ESC gene expression is a combination between biochemical modulators and stiffness.

Taking into account that ESC are usually cultured in contact with a glass or plastic substrate, our results suggest that stiffness plays a dominant role in stem cell fate. Stiffness seems to control ESC fate by creating a homogeneous gene expression shift that is independent of the biochemical pluripotent cues. In contrast, the effect of biochemical modulators on ESC pluripotency are dependent on each other.

With this new approach to analyze gene expression, we were able to decouple, compare and rank-order different stimuli featured by ESC, and responsible to regulate their fate. We believe that our method can provide new insights to understand how different modulators additively, subtractively or synergetically affect gene expression and, consequently, cell fate, which can open the door to understanding mutual relationships among different pluripotency modulators, and provide guidelines to design new processes for cell-fate control.

Chapter 4

Pluri-IQ: Quantification of Embryonic Stem Cell Pluripotency Through an Image Based Analysis Software[3]

[3] Tânia Perestrelo*, Weitong Chen*, Marcelo Correia, Christopher Le, Sandro Pereira, Ana S. Rodrigues, Maria I. Sousa, João Ramalho-Santos and Denis Wirtz *(submitted)*
* co-first authors

Abstract

Image-based-assays, such as alkaline phosphatase staining or immunocytochemistry for pluripotent markers, are common methods used in the stem cell field to assess pluripotency. Although an increased number of image analysis approaches have been described, there is still a lack of software availability to automatically quantify pluripotency in large images after pluripotency staining. To address this need, we developed a robust and rapid image processing software, Pluri-IQ, that allows the automatic evaluation of pluripotency in large low magnification images. We combined an automated segmentation algorithm with a supervised machine learning platform to classify colonies as pluripotent, mixed or differentiated. In addition, Pluri-IQ allows the automatic comparison between different culture conditions. This efficient user-friendly open-source software can be easily implemented in images derived from different pluripotent cell line sources (e.g. iPSCs, EGs, ECs), or cells that express pluripotent markers (e.g. Oct4-GFP cells), and can be routinely used, decreasing image assessment bias.

4.1. Introduction

Embryonic stem cells (ESC) are characterized by their self-renewal and pluripotent capacities. Due to their properties, ESC serve as an important research model to study key factors that maintain pluripotency, as well as factors that trigger differentiation. ESC are morphologically distinct from differentiated cells, featuring a high nuclear-to-cytoplasmic ratio and growth as 3D colonies. In the undifferentiated state, ESC are characterized by high levels of pluripotency-related transcription factors, such as OCT 3/4, NANOG and SOX2 [14,60,203–205]. Additionally, the expression of enzyme alkaline phosphatase (AP) is another hallmark of pluripotency [196]. AP is an enzyme that catalyzes the hydrolysis of phosphate esters [206]. ESC have high levels of AP, which decreases upon ESC differentiation [196,206]. The expression specificity of AP and the transcription factors described above makes them crucial proteins to evaluate ESC pluripotency *in vitro*.

Image-based-assays are common methods used in stem cell research to evaluate maintenance and loss of pluripotency. AP staining is commonly used to assess maintenance/loss of pluripotency after different stimuli, such as drug treatments, gene silencing or overexpression [207]. Immunocytochemistry with antibodies specific to pluripotent markers is another image-based-method used to analyze stem cell fate [207]. Immunocytochemistry and AP assays are fast and easy to perform. Contrary to methods that require suspension cells, such as flow cytometry, these image-based-assays allow colony morphological analysis as they maintain the spatial information of each cell in the colony. Therefore, the increase of ESC image acquisitions creates a demand for image analysis programs suitable for ESC image quantification.

Considering that ESC cultures are usually heterogeneous, with varying degrees of pluripotency and irregular colony sizes, several imaging quantification programs have been developed specifically for ESC. Using phase contrast images, different imaging analysis pipelines have been reported to segment ESC colonies and automatically track their growth and morphology over time [208–211]. Despite their high ability to segment ESC in culture and monitor ESC growth and confluency, these pipelines do not provide any other pluripotency measurements. More recently, phase-contrast images have been used to evaluate induced pluripotent stem cells (iPSCs) quality [212–214]. However, in all these studies,

morphology is the key feature, where iPSCs are classified as good or bad quality colonies, but no other pluripotency measurement is obtained. In addition to phase-contrast images, other studies have been reported to segment ESC colonies using immunofluorescence images [215–218]. Although these pipelines allow the location analysis of labeled cells, which makes them suitable for pluripotency quantification, the pipelines developed by some groups rely in high magnification images to evaluate pluripotency marker expression [216,217], whereas others, in spite of analyzing labeled cells in low magnification, they only determine the signal location of different markers in a colony, constraining the automatic and global pluripotency determination [218].

Therefore, none of the current image analysis pipelines allow an easy and robust automatic quantification of ESC pluripotency in an environment where different degrees of pluripotency occur, i.e., presence of pluripotent colonies, mixed colonies, and differentiated cells. For instance, to even answer the simple question of whether or not a treatment induces loss of pluripotency, stem cell biologists rely on manual scoring, or culture observations after AP staining. This manual quantification not only limits reproducibility and objectivity, but it is also time-consuming.

Here, we present an accurate, open-source and user friendly software, Pluri-IQ, which can automatically quantify the percentage of pluripotent, mixed or differentiated cells through culture images. Pluri-IQ is able to analyze different low magnification image sizes, and through core cascade modules (segmentation, machine learning, validation, and automatic scoring) accurately quantifies pluripotency through the analysis of the pluripotency markers present in the image. Segmentation provides the outline of each colony and is performed automatically by Pluri-IQ. Classifiers are built through a machine learning interactive process. Manual validation provides the user with the classifier accuracy, while automatically updating the classifier, which guarantees high accuracy of automatic score classification of each colony as pluripotent, mixed, or differentiated, with low user input required.

4.2. Experimental Procedure

4.2.1. Cell culture

Mouse embryonic cell line (E14Tg2a.4, derived from 129P2/OlaHsd, RRID:MMRRC_015890-UCD) was cultured at 37ºC, 5% CO_2 and two different culture media were used for ESC maintenance and propagation: (1) media with serum (KODMEM), consisting in KnockOut-DMEM (Thermo Fisher Scientific) supplemented with 15% Fetal Bovine Serum, ESC-qualified, USDA-approved regions (Thermo Fisher Scientific), 2 mM L-Glutamine (Thermo Fisher Scientific), 1% non-essential amino acids (Sigma-Aldrich), 100 U/mL penicillin/streptomycin (Thermo Fisher Scientific), 0.1 mM 2-Mercapthoethanol (Thermo Fisher Scientific) and 1000 U/mL of ESGRO Leukemia inhibitory factor (LIF, Merck Millipore); and (2) serum free media (2i), consisting in 1:1 mix of DMEM/F12 (Thermo Fisher Scientific) and Neurobasal medium (Thermo Fisher Scientific), N2 (Clontech) and B27 (Thermo Fisher Scientific) supplements, 100 U/mL penicillin/streptomycin, 0.1 mM 2-Mercapthoethanol, 2 mM L-Glutamine and 1000x dilution of the supplements LIF and MEK/GSK3 inhibitors (Millipore). To induce spontaneous differentiation, ESC were maintained in KODMEM in the absence of LIF for 4 days. 50 nM of Antimycin A (AA) was used to block complex III mitochondria respiratory chain. AA was added to cells cultured in KODMEM medium in the absence of LIF.

In order to induce neuronal differentiation, 10,000 cells.cm^{-2} mESC were seeded on 0.1 % gelatin-coated plates and cultured in N2B27 serum free media for 5 days. Media was replaced every 2 days. N2B27 is a 1:1 mix of Neurobasal medium (Thermo Fisher Scientific), 1:2 mix of MEM (Thermo Fisher Scientific) and 1:2 mix of Ham's F12 Nutrient Mix (Thermo Fisher Scientific), supplemented with 1 mM L-Glutamine, 100 U/mL penicillin/streptomycin, 0.1 mM 2-Mercapthoethanol, 1.5 g/L D-glucose, 1.5 g/L, 1.5 g/L AlbuMAX I Lipid-Rich BSA (Thermo Fisher Scientific), 7.5 mM HEPES (Thermo Fisher Scientific), B27 (Thermo Fisher Scientific) and N2 (Thermo Fisher Scientific).

4.2.2. Alkaline Phosphatase Staining

mESC were fixed with 4 % paraformaldehyde (Electron Microscopy Sciences) at RT and stained with Vector Red alkaline phosphatase vector kit (#SK5100, Vector laboratories) as described in manufacturer's instruction. Briefly, after mESC were fixed, cells were washed twice with PBS and incubated with substrate working solution (2 drops of reagents 1, 2 and 3 diluted in 5 mL of Tris-HCl 150 mM, pH 8.5 buffer containing 0.1 % Tween (Sigma)) for 30 min on the dark. After incubation, cells were washed once with 150 mM Tris-HCl and then PBS was added. Fluorescence as well as phase-contrast images were taken.

4.2.3. Immunocytochemistry

mESC were fixed with 4 % paraformaldehyde for 15 min at room temperature (RT). Cells were then washed 3 times with phosphate-buffered saline (PBS), permeabilized with 0.1 % Triton X-100 (Sigma-Aldrich) in PBS for 10 min, and blocked for non-specific binding with 1% Bovine Serum Albumin (Sigma-Aldrich) in PBS for 1 h at RT, followed by incubation overnight at 4 ºC primary antibody: rabbit anti-Oct-4 (#2840, Cell Signaling Technology) at 1:100 dilution. Cells were then washed with PBS for 3 times and incubated for 1 h at RT with a solution containing secondary antibody: anti-rabbit Alexa Fluor 488 (Thermo Fisher Scientific) at 1:200 dilution; Hoechst 33342 (Sigma-Aldrich) at 1:50 dilution and phalloidin Alexa Fluor 647 (#A22287, Thermo Fisher Scientific) at a dilution 1:40 dilution. Cells were then washed three times with PBS and images were taken.

4.2.4. Imaging acquisition

All images were collected with Nikon DS-QiMc camera installed on a customized Nikon TE300 epifluorescent microscope (Nikon Melville, NY), equipped with a motorized stage and motorized excitation and emission filters (Prior Scientific, Rockland, MA) controlled by Nikon NIS Elements. Images were acquired with a 10 x Plan Fluor lens (N.A. 0.3, Nikon Melville, NY) and different grid numbers with a 20 % overlap were acquired in order to ensure that the entire well was

imaged. Image size from the camera was 1280 x 1280 pixels, and the pixel size 0.57 µm. For immunofluorescence images, three fluorescence channels for Hoechst 33342, Alexa Fluor 488 and Alexa Fluor 647 were recorded, while for AP staining the fluorescence channel Alexa Fluor 568 and phase-contrast channel were recorded.

4.2.5. RNA extraction and purification

RNA was extracted of each condition by incubating cells with trizol (Life Technologies) for 1 min at RT. The solution was then collected to eppendorf tubes and mechanical disrupted by vortex each sample for 30 s. Then, RNA extraction was performed accordingly to manufacturer's instructions (Direct-zol^{RM} RNA MiniPrep, Zymo).

4.2.6. cDNA synthesis and quantitative real-time PCR

One microgram of total RNA was used to synthesize first-strand DNA through the iScriptTM cDNA Synthesis Kit (Bio-Rad), accordingly to manufacturer´s instructions.

qPCR was performed using mouse-specific primers and iTaq SYBR Green Universal Master Mix (Bio-Rad). Primers sequence, which were obtained in the PrimerBank database [188–190] are described in Table 4.1. All samples were analyzed in technical duplicates. The expression of each target mRNA was calculated based on the threshold cycle (Ct) as $2^{-\Delta(\Delta CT)}$, where $\Delta Ct = Ct_{target} - Ct_{Rplp0}$ and $-\Delta(\Delta CT) = \Delta Ct_{test} - \Delta Ct_{control}$. Control condition refers to mESC cultured in the presence of LIF. All data are presented as mean ± standard error of the mean (SEM). qPCR data analysis was performed using the Bio-Rad CFX manager software 3.1, and gene expression was considered significantly different to the control when regulation threshold was higher than 2.0 and p-value threshold was lower than 0.05.

Table 4.1 - Sequences of forward and reverse primers (5' to 3')

Target Gene	Forward	Reverse	PrimerBank ID
Dppa3	GACCCAATGAAGGACCCTGAA	GCTTGACACCGGGGTTTAG	21218416a1
Esrrb	GCACCTGGGCTCTAGTTGC	TACAGTCCTCGTAGCTCTTGC	31542617a1
Fgf5	AAGTAGCGCGACGTTTTCTTC	CTGGAAACTGCTATGTTCCGAG	3721900a1
Klf4	GTGCCCCGACTAACCGTTG	GTCGTTGAACTCCTCGGTCT	6754456a1
Oct4	CGGAAGAGAAAGCGAACTAGC	ATTGGCGATGTGAGTGATCTG	356995852c3
Rex1	CCCTCGACAGACTGACCCTAA	TCGGGGCTAATCTCACTTTCAT	7110739a1
Rplp0	AGATTCGGGATATGCTGTTGGC	TCGGGTCCTAGACCAGTGTTC	6671569a1
T	GGATTCACATCGTGAGAGTTGG	GTCACAGCTATGAACTGGGTC	118130357c3

4.2.7. Recall, precision, specificity and dice index calculations

To compare FACT and Phantast segmentation we calculated recall, precision, specificity and dice index values defined in Equations 1 to 4, as previously described [219,220]. Briefly, TP (true positives) represents the number of segmented colonies in FACT that were also segmented in Phantast; FN (false negatives) represents the number of colonies not segmented in FACT but segmented in Phantast; FP (false positives) represents the number of colonies segmented in FACT and not segmented in Phantast; TN (true negatives) represents the number of pixel that are not considered a colony in both FACT and Phantast; X represents FACT segmentation regions and Y represents the Phantast segmentation regions.

(Equation 1)

$$Recall = \frac{TP}{TP + FN}$$

(Equation 2)

$$\text{Precision } = \frac{\text{TP}}{\text{TP} + \text{FP}}$$

(Equation 3)

$$Specificity = \frac{TN}{TN + FP}$$

(Equation 4)

$$Dice\ Index = \frac{2|X \cap Y|}{|X + Y|}$$

4.2.8. Classification accuracy

Classification accuracy was measured by comparing the colony prediction of the classifier to the classification given by the user through manual validation. The number of positive hits was then divided by the total number of colonies evaluated in order to obtain the accuracy percentage.

4.2.9. Data Comparison

The percentage of pluripotent, mixed and differentiated colonies, as well as the percentage of pluripotent, mixed and differentiated colony area are calculated for each large image. In addition, mean area, circularity and DNA/cytoplasm ratio, as well as standard error of the mean (SEM), are provided. The percentage of pluripotent, mixed, and differentiated colonies in an image is measured by calculating the number of colonies in each classification and dividing it by the total number of colonies present in the image. The pluripotent, mixed and differentiated area of each image is measured by the summation of each classifier area, followed by ratio between each sum of classifier area and the total area occupied by colonies. Mean area and mean circularity are calculated by averaging the pluripotent, mixed and differentiated area and circularity in each image, respectively. DNA/cytoplasm ratio of each large image is calculated using colony average area derived from DNA staining image, and colony average area derived from cytoplasm image.

4.2.10. SOFTWARE availability

Pluri-IQ was implemented using MATLAB on a 64-bit Windows OS laptop with intel i7 processor with 8GB of RAM memory. The software will be hosted at CNC website (**www.cnbc.pt**) both as a compiled MATLAB standalone application (requires installation of 64bit MATLAB runtime,

available for free at **www.mathworks.com/products/compiler/mcr.html**) and MATLAB .m files. In our application, we made use of Custom GINPUT by Jiro Doke, Nov 07, 2012 (**https://www.mathworks.com/matlabcentral/fileexchange/38703-custom-ginput/content/ginputc.m**, retrieved June 2016) and uipickfiles: uigetfile on steroids by Douglas Schwarz, Apr 25, 2006 (**https://www.mathworks.com/matlabcentral/fileexchange/10867-uipickfiles--uigetfile-on-steroids**, retrieved May 2016).

4.3. Results

4.3.1. Image based analysis outlines

To evaluate the performance of Pluri-IQ, we tested its classification precision over a set of mouse ESC (mESC) images. These mESC were cultured in different media conditions that promote maintenance of pluripotency or induce mESC differentiation. Cells were stained with AP. Subsequently, low magnification phase contrast images and a fluorescence channel for AP staining were acquired.

AP staining was selected as a method for pluripotency assessment since it is a fast and common protocol to evaluate pluripotency [207]. To confirm that the AP assay utilized only stained pluripotent cells, we performed the AP assay followed by immunostaining against the pluripotent marker Oct-4 (Figure 4.1). Phase contrast images, as well as nuclear staining, were used to provide a general outlook of all colonies. Then, Oct-4 expression was compared to AP staining and colonies positive for Oct-4 were also positive for AP (Figure 4.1, red arrow), while the portions of colonies that fail to express Oct-4 do not stain for AP (Figure 4.1, yellow arrow). These results show that the AP assay utilized in these experiments is specific for pluripotent cells.

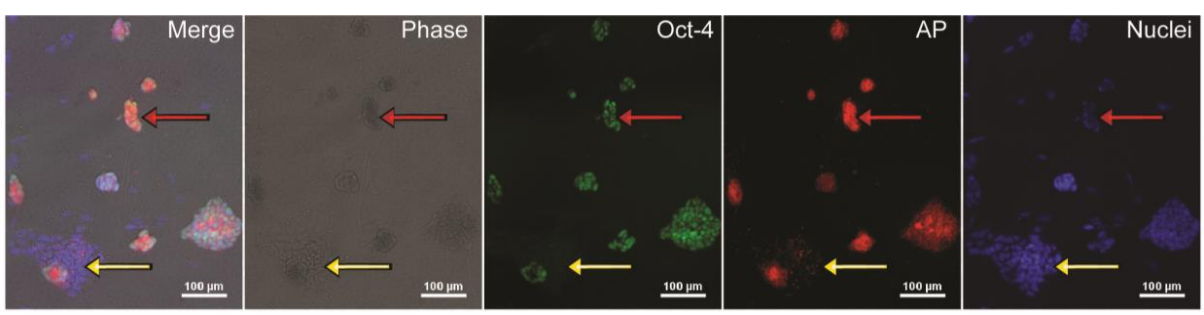

Figure 4.1 AP co-localizes with OCT-4 expression.

Cropped image of ESC cultured for four days in pluripotent conditions and stained for AP assay and the pluripotent marker Oct-4. Yellow arrow shows a portion of a colony differentiated, where no Oct-4 neither AP staining is visible; red arrow shows a pluripotent colony positive to Oct-4 and AP staining. Scale bar: 100 µm. Abbreviations: AP: alkaline phosphatase.

One of the challenges in characterizing pluripotency automatically is that the majority of image-based-assays, including AP staining, are specific for pluripotent cells, which gives a positive signal when a colony is pluripotent. However, differentiated colonies are only defined as such when the positive signal is non-detectable (Figure 4.1). In addition, pluripotent colonies acquire different morphologies upon different treatments, and usually, during ESC differentiation, pluripotent staining is firstly reduced before it is completely lost. Therefore, mixed colonies, which we consider a mixture of pluripotent cells and differentiated cells, are prevalent in most cultures and difficult to impartially classify. Taking all these factors into consideration, we developed an image analysis approach that incorporates three major steps in order to automatically quantify pluripotency: a fast segmentation algorithm capable of identifying different colony types in both large phase-contrast and fluorescent images, an interactive machine learning algorithm to classify colonies as pluripotent, mixed or differentiated, and a validation algorithm responsible for the measurement of classification accuracy to increase the trust on the automatic pluripotency quantification and the comparison of different conditions (Figure 4.2).

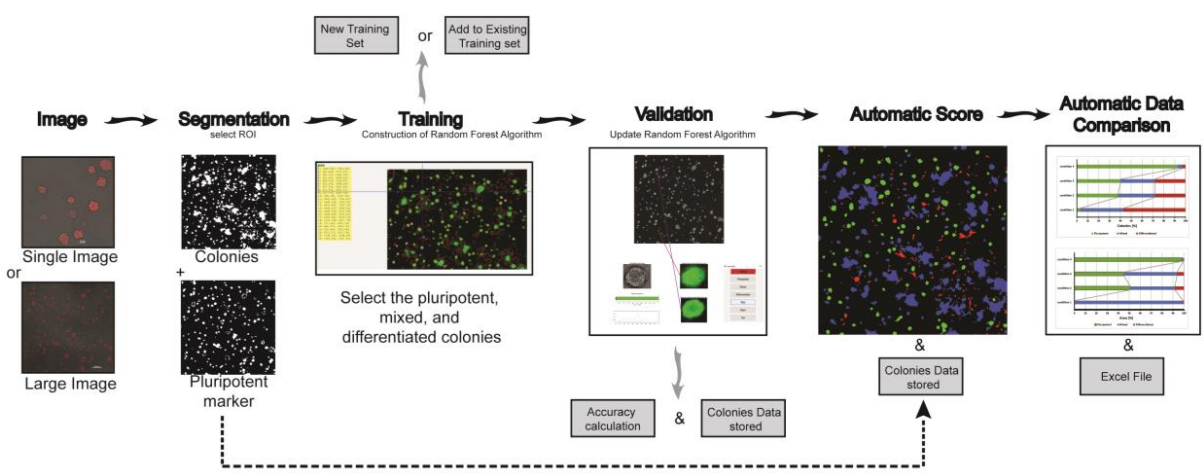

Figure 4.2 - Pluri-IQ approach to quantify ESC pluripotency.

Users provide a single image or a large image input, as shown. Upon selection of the ROI, Pluri-IQ segments both phase contrast image channel to get all colonies, and the pluripotent marker channel. After segmentation, training is required, through selection of what is considered pluripotent, mixed, and differentiated colonies, in order to construct a random forest algorithm, which can be added to an existing training system or to a new training system. Validation is performed by the user and accuracy of the Pluri-IQ is calculated. The random forest algorithm is updated and colonies features are stored in both Excel and Matlab files. After all these steps completed, and

segmentation performed to all images, automatic score is then available. Finally, automatic data comparison is available and allows the comparison of different conditions automatically, providing figures with the percentage of colonies or area pluripotent, mixed and differentiated, in addition to storage as Excel file the data comparisons.

4.3.2 Image properties and colony segmentation

A reliable pluripotency evaluation requires an overview of the entire well plate. However, automatic image acquisition often leads to colonies on the border of the image, and consequently, loss of partial colony information. Such colonies are thus, not suitable for quantification. Therefore, we designed a pipeline that allows the analysis of single or multiple TIFF images combined (stitched together during or after single image acquisition) in order to fulfill the criteria described above (Figure 4.2).

To detect and segment the colonies, we developed a custom script written in Matlab (MathWorks ®), FACT (Fast and Accurate Colony Tracing), which does not require user input (Figure 4.3). Colony detection and segmentation is primarily performed in the phase contrast image. The image background is first calculated: Fast Fourier transform is applied to the raw image; the transformed image obtained is filtered with a cut off frequency of 0.2 in the Fourier domain, followed by an inverse Fast Fourier transform, resulting in a reconstructed image with only low frequency features. The background is removed from the raw image through subtraction of the low frequency image from the raw image, which isolates the high frequency information, cells, and colonies (Figure 4.3). Then, the local contrast is highlighted using a 3x3 high frequency filter and binarized using Otsu thresholding, which separates the foreground from the background. A sobel filter is applied to the subtracted background image to obtain the image gradient. Raw images are also processed by morphological operations erosion and dilation, and the difference between these two processes is used to obtain a binary mask. The binary mask from the local contrast, gradient, and morphological operations applied to the raw image is added together and the final mask is produced when the value of the cumulative mask is greater than 1 (Figure 4.3). Given that ESC grow in colonies, we added two particular restrictions in the algorithm: (1) the segmentation algorithm was adapted to ignore single cells, however, single cells can be included by manually adapting this segmentation algorithm parameter; (2) differentiated and mixed colonies tend

to occupy a large area and, by eliminating all colonies on the periphery of the ROI, biased results were obtained. Therefore, colonies in the periphery are only discarded if their pixel size is bellow $7x10^4$ pixels. After colony segmentation is completed, all colonies detected are assigned with a specific number (ID), with the colony ID derived from the phase contrast image applied to the pluripotent marker image (Figure 4.3). A similar procedure is applied for fluorescence images, with a small nuance: if there are saturated pixel in the image, the software will automatically fill them in as a positive hint for a colony. After segmentation is performed, the results are saved as new TIFF images, which allows for segmentation inspection.

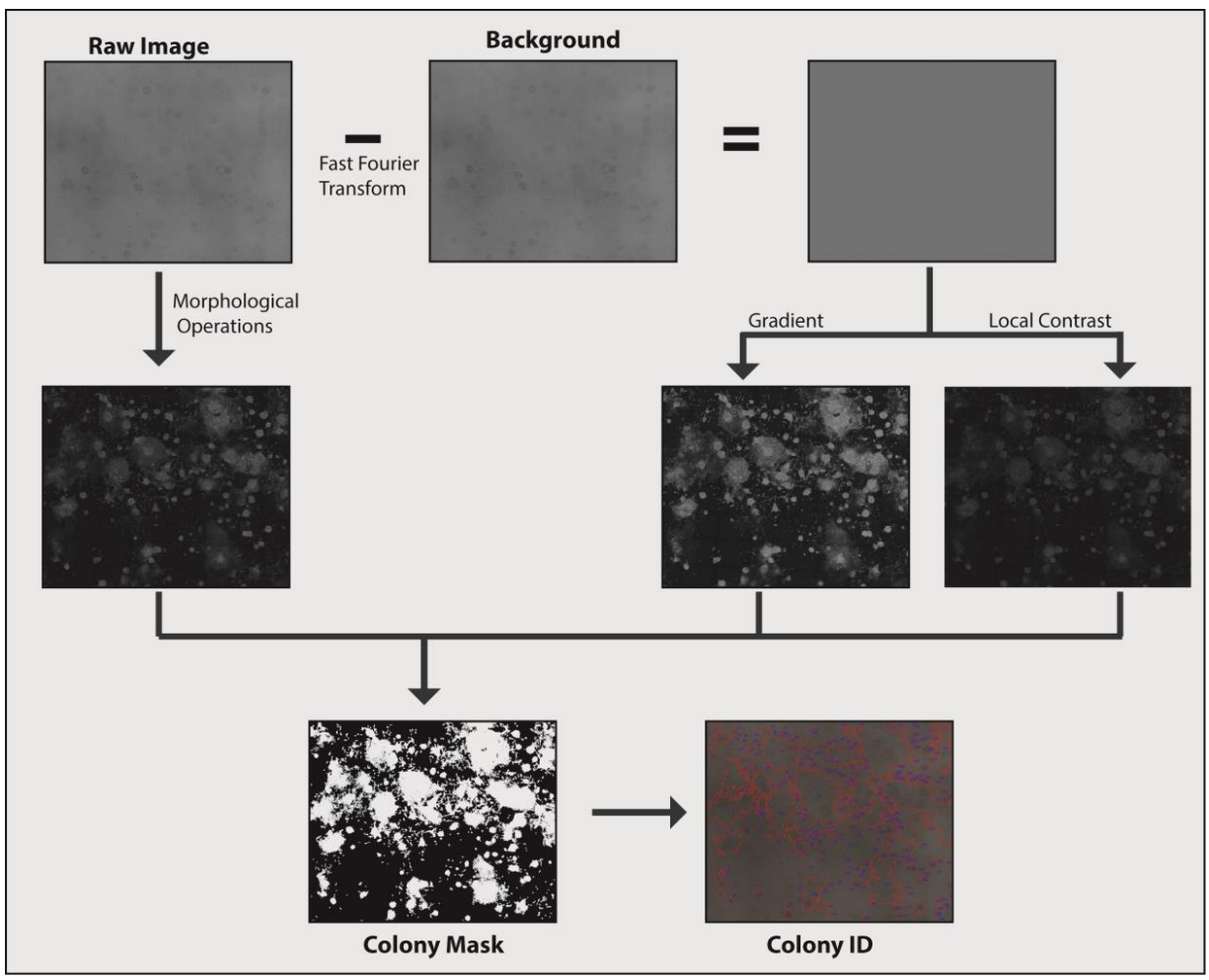

Figure 4.3 – Colony detection and segmentation pipeline.

The raw image is processed by the difference of erosion and dilation followed by Otsu thresholding to create the first mask. The raw image is also processed by removing the background level through Fast Fourier transform, creating a background subtracted image, from which we extract the gradient and local contrast and produce two more masks through Otsu thresholding. The three masks are added together and if the pixel value is greater than

1, the object is incorporated into the final mask. The outline and label of the final mask is added to the raw image to show the outcome of the segmentation.

4.3.3 Segmentation accuracy

To evaluate segmentation accuracy, large phase contrast images (10078 x 10054 pixel), with different degrees of pluripotency, morphology, and confluency were analyzed by FACT and compared with previously published segmentation algorithms: Phantast [208], and Empirical Gradient Threshold (EGT) [215] (Figure 4.4 A). We selected Phantast and EGT as they have both been shown to successfully segment ESC images. While Phantast requires user input for accurate segmentation, EGT does not. Our results show that both Phantast and FACT are able to segment large images, whereas EGT fails to segment some image fractions (Figure 4.4 A). We then decided to directly compare FACT segmentation with Phantast segmentation, and calculate FACT precision, recall, specificity, and dice index (Figure 4.4 B, C). Quantitatively, we achieved an average precision of 94.24 ± 0.02; an average recall of 93.95 ± 0.02; an average specificity of 96.35 ± 0.03, and an average dice index of 94.06 ± 0.01. These results show that our segmentation method (FACT) can provide accurate image segmentation on a wide range of cell colony morphologies, from a large sheet of cells to individualized colonies, without any additional user input. Moreover, these results demonstrate that our segmentation algorithm, without tuning requirements, is as robust and accurate as Phantast.

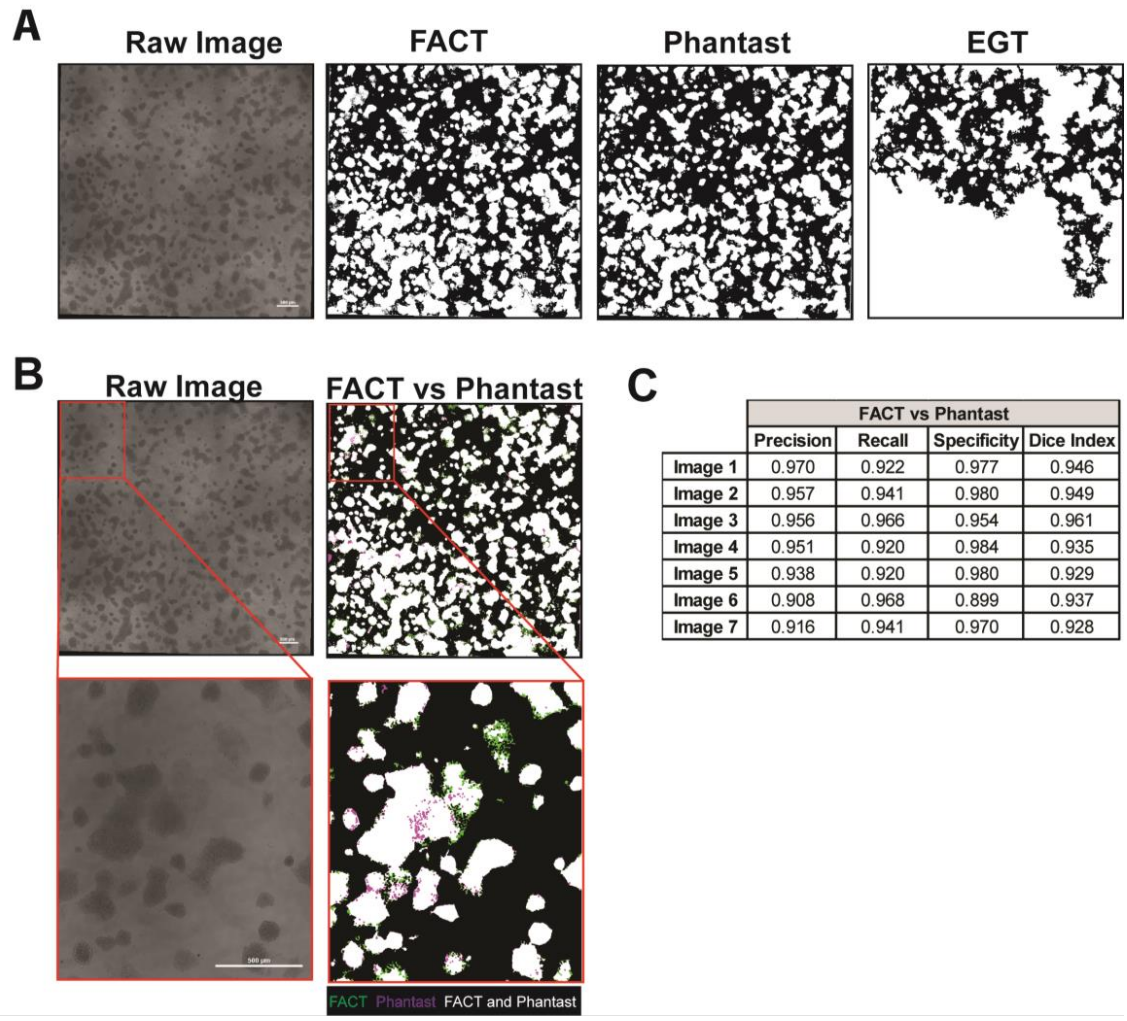

	FACT vs Phantast			
	Precision	Recall	Specificity	Dice Index
Image 1	0.970	0.922	0.977	0.946
Image 2	0.957	0.941	0.980	0.949
Image 3	0.956	0.966	0.954	0.961
Image 4	0.951	0.920	0.984	0.935
Image 5	0.938	0.920	0.980	0.929
Image 6	0.908	0.968	0.899	0.937
Image 7	0.916	0.941	0.970	0.928

Figure 4.4 – Comparison between FACT algorithm segmentation and Phantast and EGT segmentation algorithms.

(A) FACT, Phantast and EGT segmentation results. Binary images, where white is representative of presence of a colony. Scale bar: 500 µm. **(B)** Direct comparison between FACT and Phantast segmentation. White regions represent segmentation overlap between Phantast and FACT; purple regions represent pixel only positively segmented by Phantast; and green regions represent pixel only positively segmented by FACT. Scale bar: 500 µm. **(C)** Precision, recall, specificity and dice index of FACT segmentation was compared with Phantast segmentation. Abbreviations: EGT - Empirical Gradient Threshold. FACT - Fast and Accurate Colony Tracing.

4.3.4 Machine Learning Classification

Once segmentation is performed, automatic pluripotency classification poses a further challenge. Pluripotent cells in culture conditions have different colony height, area, and circularity. To classify a colony as pluripotent, the intensity of the pluripotent marker must be high, whereas a differentiated colony has low or undetectable pluripotent signal. Mixed colonies are described to (1)

have a combination of high and low intensity pluripotency markers, or (2) have a dim positive signal, above the positive staining threshold. However, intensity signal is dependent on the colony morphology, which makes automatic pluripotency classification through image-based analysis a challenge. To tackle this issue, we used a supervised colony classification approach to differentiate between the three colony types. We selected the random forest classifier [221], due to its robustness and computational simplicity. We designed an interactive classification approach, where users can build a classifier by interactively training and validating their own image sets (Figure 4.5 A). During this cycle, users are expected to after selecting the training set images, to pick the best subset of colonies that fit the pluripotent, mixed and differentiated standard parameters from each image. After selecting the colonies, the classifier is built taking into account different colony features from both phase-contrast and pluripotent marker images (Table 4.2) and an Excel file is created with each colony feature (Figure 4.5 A). Thus, when a new colony is presented to the program, the software evaluates all the features of the new colony and classifies this colony accordingly with the classifier pool where its features best fit. Since fluorescence intensity is one of the features to characterize pluripotency, and intensity is dependent on microscopy settings upon acquisition, different training sets can be created and uploaded to attenuate the misclassification due to the difference between independent experiments.

Table 4.2: Features used to train the random forest classifier and discriminate between pluripotent, mixed and differentiated colonies

Feature	Feature type
Colony circularity	Morphological
Intensity mode	Intensity
Intensity mean	Intensity
Intensity variance	Texture
Intensity Histogram Skew	Intensity
Variation of intensity histogram peaks	Intensity

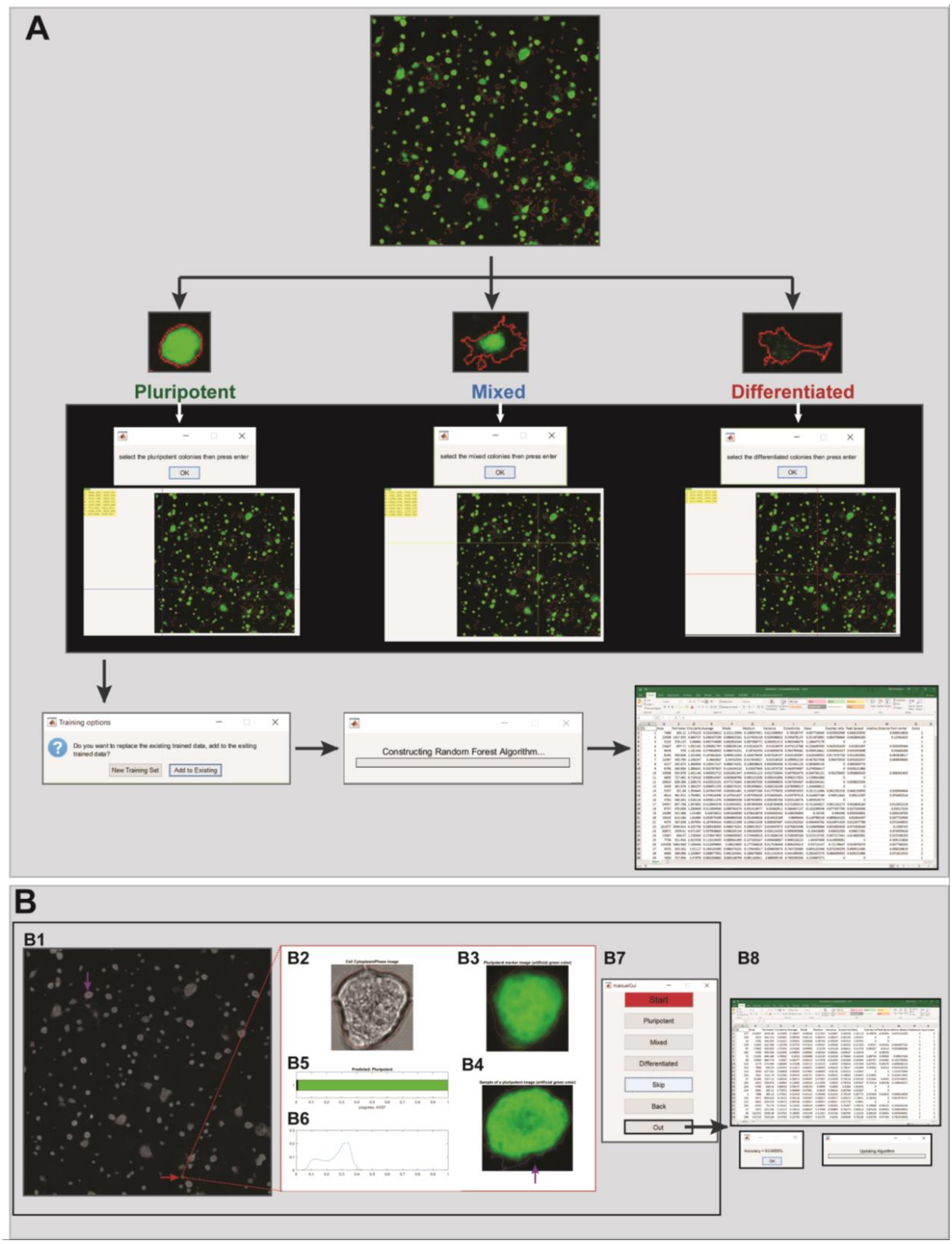

Figure 4.5 – Machine learning and manual validation overview.

(A) Machine learning overview. Upon selection of the images to use as training set, the user interactively selects first the pluripotent colonies, then the mixed colonies and finally, the differentiated colonies presented in the image. After this procedure is complete for all the images in the training set, the classifier is built, with the possibility to add the training set to a previous classifier, or create a new training set. An Excel file with all the colony features as well as the pluripotency score is created, where score 1 is pluripotent, 2 mixed and 3

differentiated colony. Green: pluripotent marker AP; red: colony border obtained by the phase contrast segmentation image **(B)** Manual validation overview: **(B1)** Image overview. Purple arrow shows an example of a pluripotent colony. Red arrow shows the colony picked to validate the classifier prediction. **(B2)** Phase-contrast image and **(B3)** pluripotent marker image of the colony picked to validate the classifier prediction. **(B4)** Example of a pluripotent colony. **(B5)** Classifier prediction and progress bar with the total number of colonies present in the image and the number of colonies already validated. **(B6)** Normalized number of pixel versus pluripotent marker intensity. **(B7)** Graphical user interface used to validate each colony as pluripotent, mixed or differentiated. **(B8)** After manual validation completed, the manual accuracy is automatic shown, and the random forest algorithm is updated. Segmentation information summary is saved as an Excel file.

4.3.5 Manual Validation Algorithm

In order to evaluate the accuracy of colony classification, we developed an interactive validation algorithm that allows the user to validate the classification of the selected training set (Figure 4.5 B). After the selection of different images, a phase contrast and fluorescent marker image derived from a random selected colony is shown in addition to its intensity pluripotent marker plot (Figure 4.5 B1 – B6). Manual validation is allowed through the selection of the pluripotent, mixed, or differentiated button (Figure 4.5 B7), with the opportunity to go back to a previous colony and overwrite the previous classification (back button), to skip a colony (skip button), or to finalize the manual validation process without the need to validate the entire image (out button) (Figure 4.5 B7). The classification results are exported with each colony ID to Excel and Matlab files. These files provide a detailed summary of each colony feature, as well as the classifier prediction and user manual validation (Figure 5 B8). In addition, the accuracy score is shown at the end of each large image analysis. Finally, in order to increase precision, every time that manual validation is completed, the classifier is updated.

4.3.6 Performance Evaluation

To evaluate our colony classification approach, we used six large images derived from different mESC cultures, with a wide range of pluripotent percentages and colony shapes. We started by creating a training set selecting 15 pluripotent colonies, 15 mixed colonies, and 20 differentiated colonies from one of the large images (Figure 4.6 A1). Then, we ran the manual validation on the same image, evaluating all the colonies, and we achieved an accuracy of 97.6 %. Afterwards, we ran the automatic

score on the other 5 large images and manually evaluated 100 colonies from each image to obtain the pluripotency classification accuracy (Figure 4.6 A1). All images had an accuracy classification above 90 %. To test the number of colonies that should be selected to train the classifier, we went back and selected only 5 pluripotent, 5 mixed, and 5 differentiated colonies, and created a new classification set (Figure 4.6 A2). The accuracy decreased to 59 % when we manually validated 150 colonies from the same image. After the manual validation classifier update, we ran the automatic score on the 5 large images that we had previously ran, and manually validated the results. All images had similar accuracy values to the previous classifier set (Figure 4.6 A2). These results demonstrate that our manual validation is important and capable of maintaining high accuracy values, without the need to tune the training system multiple times, since manual validation updates the classifier.

To validate Pluri-IQ pipeline, mESC were cultured in medium with serum and LIF, and seeded with different densities (6000 cells.cm^{-2}, 8000 cells.cm^{-2}, 10 000 cells.cm^{-2}), in medium with serum but in absence of LIF (referred as – LIF), in medium with serum and Antimycin A (referred as AA), and in serum-free media with CHIR99021 and PD0325901 (referred as 2i). After validation and automatic score, automatic comparison between different conditions was performed, with an Excel file as output (Figure 4.6 B1). Our results show that the highest number of pluripotent colonies is obtained when mESC are cultured in 2i medium, whereas the absence of LIF in medium with serum induces the highest differentiation (Figure 4.6 B2). In addition, the increase in mESC density induces a decrease in the percentage of pluripotent colonies and an increase in differentiated colonies. Finally, when mESC are cultured in the absence of LIF but in the presence of a complex III mitochondria inhibitor, AA, ESC differentiation is decreased (Figure 4.6 B2). In order to confirm the cells' fate in different conditions, we performed qRT-PCR analysis in mESC cultured in the presence of LIF (6000 cells.cm^{-2}), 2i, AA, and in the absence of LIF (Figure 6 C). To evaluate mESC fate, we selected four pluripotent genes (Klf4, Dppa3, Esrrb and Oct4) and two early differentiation genes (Fgf5 and T) and compared the relative mRNA expression of the different conditions to + LIF condition. Cells cultured in the absence of LIF had a low expression of pluripotent markers (Klf4, Dppa3, Esrrb) and an increased expression of differentiated markers (Fgf5 and T) (Figure 6 C), which suggests that this cell culture condition had a high percentage of differentiated colonies and low percentage of pluripotent colonies, in agreement

with the results obtained by Pluri-IQ software (Figure 6B2). Cells cultured in the presence of 2i had a significant increase of the pluripotent marker Klf4, and low expression of the differentiated markers Fgf5 and T (Figure 6C). This result suggests that these cells have a higher percentage of pluripotent colonies than mESC cultured in the presence of LIF, which is in accordance to the results obtained by Pluri-IQ (Figure 6B2). Finally, when cells were cultured in the presence of AA they had low expression of Klf4, when compared to cells cultured in the presence of LIF (Figure 6C), which suggests that AA culture conditions promotes a decrease of pluripotent colonies when compared to mESC cultured in the presence of LIF. Thus, through qRT-PCR, we also verify that mESC cultured in the presence of 2i medium have the highest pluripotency levels, whereas mESC cultured in the absence of LIF promote colony differentiation. These results are in agreement with the literature [49,114,196], which demonstrates that our pipeline is able to accurately classify colony pluripotency even in the presence of different colony densities and morphologies.

We decided to use the same rationale, and evaluate Pluri-IQ accuracy in fluorescence images (Figure 4.7). We utilized images from mESC cultured in serum with LIF (pluripotency medium) or in a neuronal differentiation medium (referred as N2B27). Cells were stained for the pluripotent marker Oct-4. After uploading the images and their segmentation performed, the classifier was created utilizing 16 pluripotent colonies, 14 mixed colonies and 10 differentiated colonies selected from two large images (Figure 4.7 C, upper panel). Manual validation was performed on the same images, and an accuracy of 87 % was achieved. We then used the training set to automatic score two new images (Figure 4.7 C, bottom panel). The mESC classification accuracy was approximately 90%. After comparing both conditions, we saw that, in agreement with the literature, mESC cultured in the presence of neuronal differentiation medium have more differentiated and mixed colonies than cells cultured in the presence of LIF (Figure 4.7 D). In addition, when we measured colony parameters such as DNA cytoplasmic ratio, the results obtained were in agreement with previous studies: DNA/cytoplasm ratio decreased with colony differentiation (Figure 4.8). These results demonstrate that our pipeline also accurately classifies pluripotency in fluorescence images.

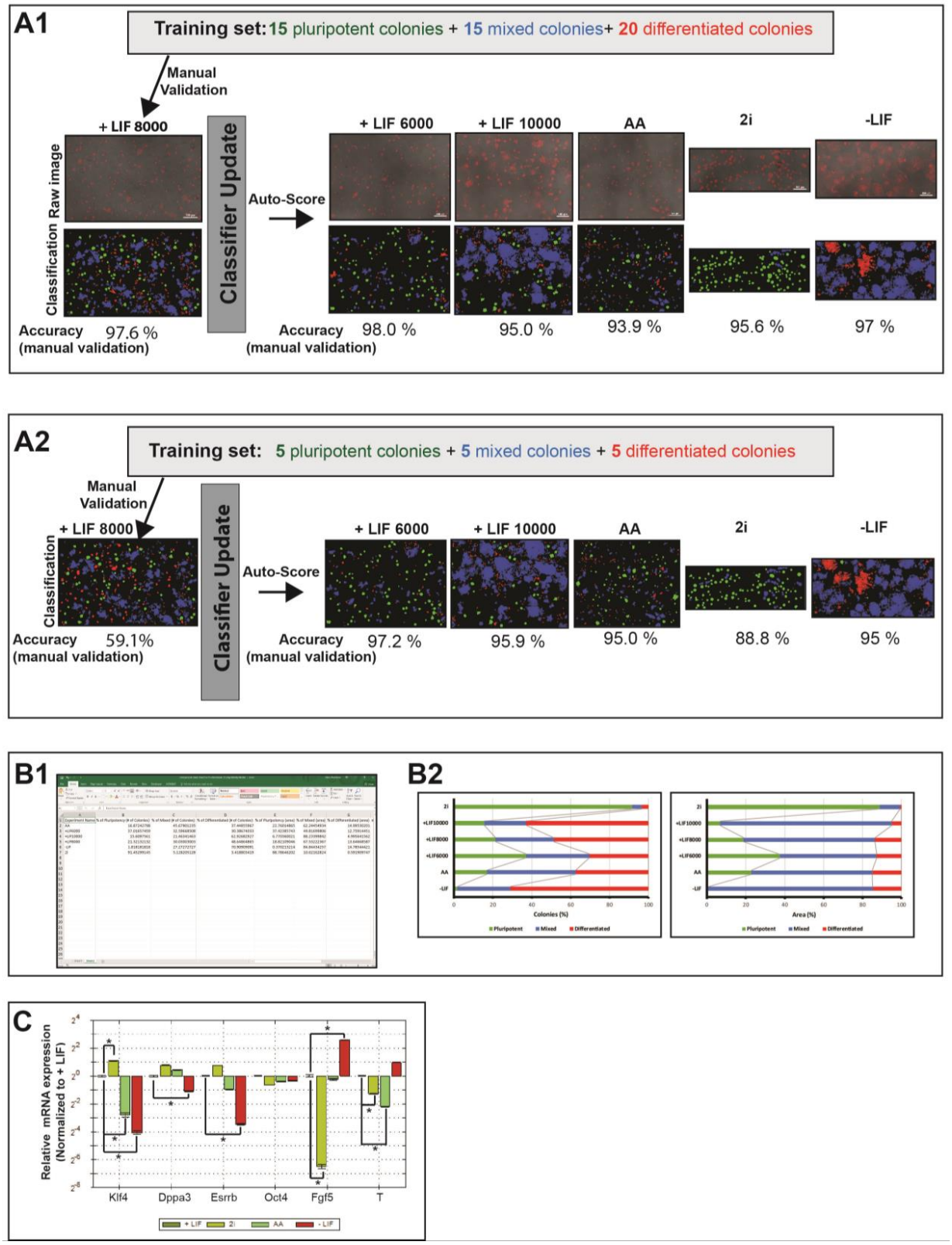

Figure 4.6 – Pluri-IQ performance evaluation in different ESC culture conditions.

(A1) The training set was built by selecting 15 pluripotent, 15 mixed and 20 differentiated colonies. Manual validation showed that accuracy of the classifier is ~ 97 %. Classifier was updated after manual validation and automatic score was run in 5 different large images. Manual validation performed afterwards showed accuracy values all above 90 %. Scale bar in raw images: 500 µm. **(A2)** After selection of a reduced number of colonies to

train the classifier, the manual accuracy decreased to ~ 59%. However, the update of the classifier after the manual training leads to an increase of accuracy classification. **(B1)** Excel sheet output derived from the automatic data comparison. **(B2)** Percentage of pluripotent, mixed and differentiated colonies (left) and area (right) of each condition. Color code: green – pluripotent colonies; blue – mixed colonies; red – differentiated colonies. (C) Normalized mRNA expression fold change (determined by RT-qPCR) of ESC cultured for four days in the presence of 2i medium, LIF, 50 nM AA or in the absence of LIF. Abbreviations: AA – Antimycin A; LIF – Leukemia Inhibitory Factor; 2i – Serum-free Media with CHIR99021, PD0325901 and LIF.

4.3.7 Performance Evaluation

We created a simple and straightforward graphical user interface (GUI), which confers an easy comprehension of the processing pipeline (Figure 4.7 A, B). Users are first required to select their type of image staining, AP or immunofluorescence, and upload two images: a single channel image of phase contrast (or fluorescence cytoplasmic) image, and a single channel pluripotent marker image. In addition to these two images, nuclear staining can also be uploaded in order to calculate the nucleus to cytoplasmic ratio. After successfully uploading the images and selecting the ROI, segmentation is performed and the results are saved as new TIFF images, which allows for segmentation inspection (Figure 4.7 C). To proceed to the automatic pluripotency quantification, the interface requires the uploading of a training classifier set and selection of each condition folder (Figure 4.7 B). The colony quantification results are exported as color coded images and Excel files. Finally, data comparison interface, automatically quantifies the colony pluripotency percentage, pluripotency colony area percentage, pluripotency mean area and circularity, and DNA/cytoplasm ratio, exporting these results to an Excel file.

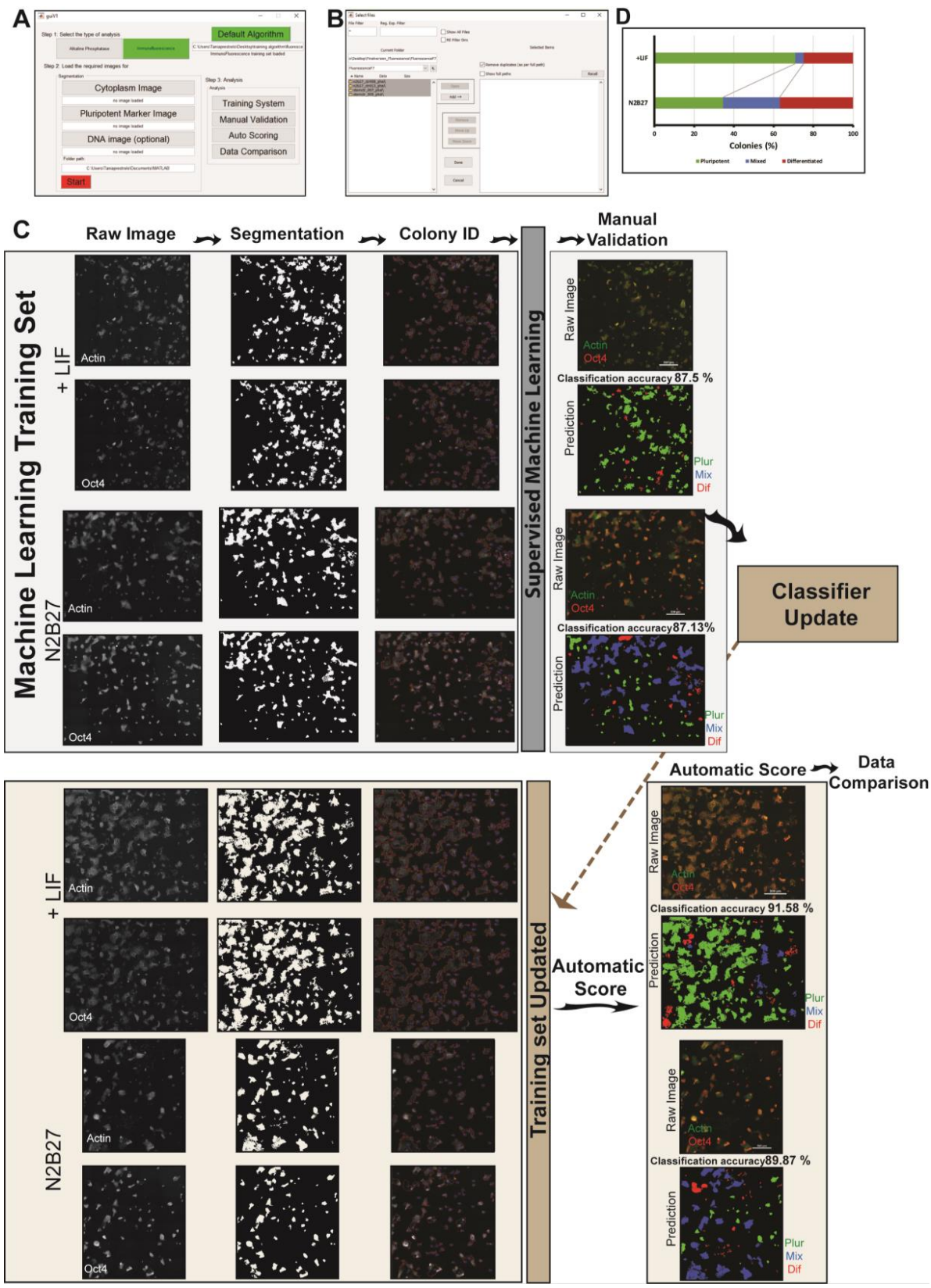

Figure 4.7 – Pluri-IQ application pipeline and its performance evaluation in immunofluorescence images.

(A) The main GUI of Pluri-IQ. **(B)** GUI used to select different folders containing the images to perform manual validation, autoscoring or data comparison. **(C)** Pluri-IQ pipeline: Two different images with different degrees of pluripotency were used to create the machine learning training set (upper panel). After each channel segmentation

and colony identification, a fluorescence training set was created and manually validated. After the classifier automatic update, two new images were scored automatically by Pluri-IQ and classification accuracy was evaluated (bottom panel). Scale bar in raw images: 500 µm. Color code on the raw images: green – actin; red – Oct4. Color code on the images prediction: green – pluripotent colonies (Plur); blue – mixed colonies (Mix); red – differentiated colonies (Dif). **(D)** Percentage of pluripotent, mixed and differentiated colonies in the two different experimental conditions. Data derived from the automatic data comparison in Pluri-IQ.

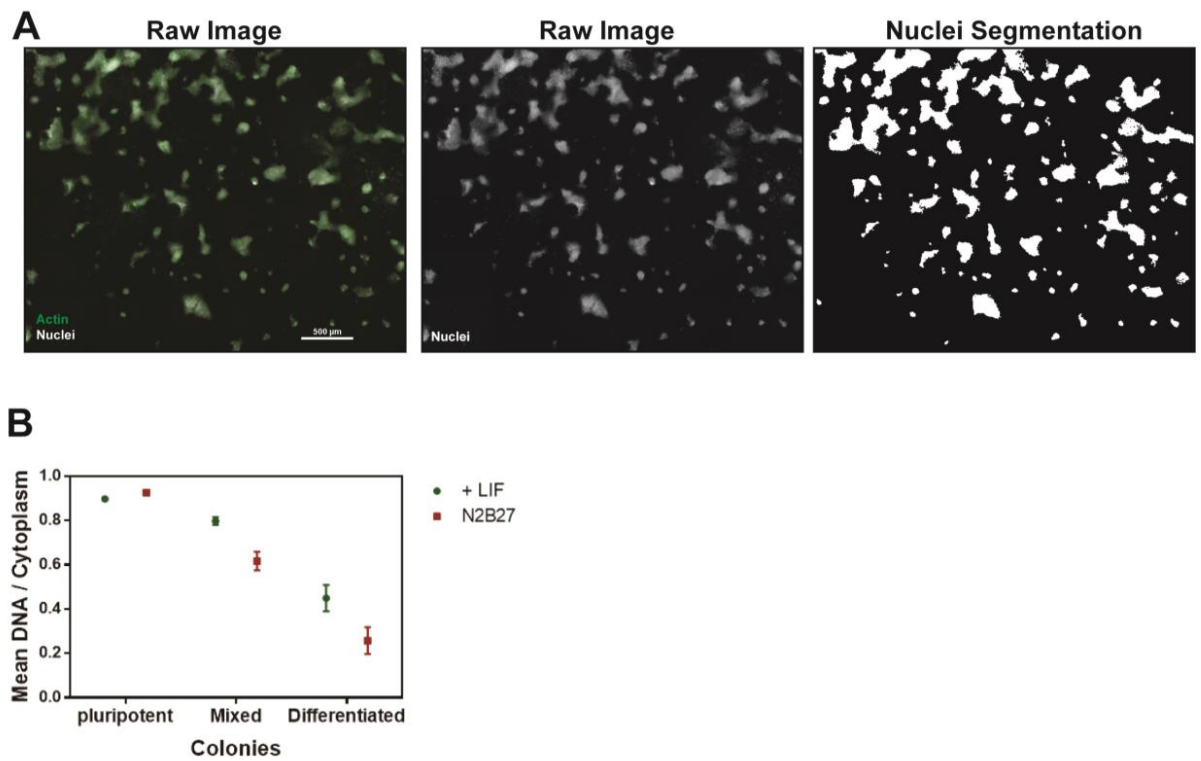

Figure 4.8 – Nuclei cytoplasm ratio decreases upon differentiation.

(A) Representative image of the nuclei segmentation through FACT algorithm. Raw image color code: green – actin; white – nuclei. Scale bar: 500 µm. **(B)** Average nuclei cytoplasm ratio, calculated by Pluri-IQ, of pluripotent, mixed and differentiated cells when cultured in a pluripotent medium (+LIF) and in a neuronal differentiation medium (N2B27). Result is expressed as mean ± SEM.

4.4 Discussion

Considering the widespread practice in stem cell laboratories to quantify pluripotency through image-based-assays, we sought to develop a software that allows the automatic quantification of pluripotency, with a low requirement of user input. Here, we report the development of an efficient, accurate, open-source, and user-friendly pipeline for pluripotency quantification of low magnification images, Pluri-IQ. This software segments colonies from large images with high precision, without the requirement of user input. Subsequently, through a machine learning process, automatically and accurately classifies pluripotent, mixed, and differentiated colonies. In parallel, we implemented a manual validation algorithm, which allows for the validation of the program by the user, through visualization of each colony and its corresponding pluripotent marker expression. The storage of each colony features, as well as its pluripotency score in Excel file, enables post-data treatment result analysis.

Importantly, we developed a user-friendly software that is accurate and efficient, with low user input requirements. Pluri-IQ uses as input large images, and present relevant advantages as compared with others since it does not require segmentation parameters to be refined in order to discharge background or detect and segment colonies, as in ilastik (http://ilastik.org/), and does not require users to create a specific pipeline of analysis as in CelProfiler (http://cellprofiler.org/). Although the training data is required, the software interactivity allows the user to quickly select the best colonies of each classification, without requiring the selection of the best features to tune machine learning, as in ilastik. After machine learning is complete, manual validation promotes the evaluation of the classifier accuracy at the same time that the classifier is updated. Finally, after high accuracy is achieved, it is possible to run a fast automatic score, followed by data comparison. Pluri-IQ was already tested in two independent laboratories and high precision classification of ESC colonies was achieved. Nevertheless, it is important to take into account that Pluri-IQ relies on image quality and user experience of pluripotency classification.

Different approaches to characterize cell fate have been developed in order to increase data consistency and reproducibility [222]. Although Pluri-IQ is specifically designed to measure pluripotency

percentage in images, image-based-assays to evaluate pluripotency are routinely performed. The necessity to infer if a different medium, shRNA, or other stimuli maintain pluripotency or induces differentiation makes quantification of pluripotency a common and required practice in stem cell laboratories [222]. Usually, fast and easy assays, such as image based assays, are performed in order to quantify pluripotency; however, this quantification is still evaluated manually. We have presented a new and robust method to evaluate the pluripotency of colonies through a Fast Fourier transform based segmentation, which works both in phase contrast as well as in fluorescence images. Using the information produced by the segmentation, we can very efficiently classify the colonies as pluripotent, mixed or differentiated without using time consuming methodologies that are currently employed. Based on our case study, we can conclude that Pluri-IQ is applicable in both large phase contrast and fluorescence low magnification images. Moreover, Pluri-IQ is able to analyze conditions that promote or destabilize pluripotency, allowing result collection in a faster and more impartial manner, thus increasing unbiased reproducibility. Nevertheless, to accurately assess pluripotency levels and cell state, further molecular analyzes techniques are required, such as qRT-PCR or Western-blot.

Chapter 5

Future Perspectives

Similarly to what takes place in embryonic development, embryo-derived ESC are regulated by biochemical and mechanical cues. Here it was demonstrated that ESC cultured on soft substrates in the presence of pluripotency modulators expressed higher levels of pluripotency markers and decreased levels of differentiated markers when compared to ESC cultured in the same biochemical conditions on stiff substrates. In addition, the stiffness effect was demonstrated to be independent of the presence of soluble pluripotent modulators in the medium. Thus, stiffness was shown to be a key modulator of ESC fate regulation, working independently of biochemical modulators such as LIF or AA. Considering that ESC are commonly cultured in contact with substrates, in the future it will be important to understand the molecular pathways involved in the regulation of ESC fate by substrate stiffness.

As a possible starting point in this endeavor, Src activity was previously shown to be responsible for the mechanical regulation of mESC [172]. To assess if the Src-MAP pathway is involved in the substrate stiffness effect, it would be interesting to evaluate Src activity in the different conditions tested – soft *vs.* stiff in the presence of different pluripotent modulators. Then, utilizing the Src inhibitor CGP77675, analyze if the stiffness effect is lost.

In addition, it would also be important to evaluate the roles of stiffness, LIF, AA and galactose in ESC state. Naïve cells are now accepted to rely on both glycolysis and OXPHOS, whereas primed cells shift their metabolism towards glycolysis [106]. Thus, a more comprehensive gene analysis pattern in addition to chimera assays should give the first answers of how these different modulators combined affect ESC state. Moreover, considering the results obtained when LIF and AA were combined, it would also be relevant to evaluate Stat3 and Hif1 α protein levels and their signaling pathways in order to clarify the pathways involved in the maintenance of pluripotency through AA.

Moreover, biocompatible scaffolds that mimic tissue mechanics are seen as a promise tool both in tissue engineering as well as in tumor and tissue 3D models [223,224]. Importantly, stiffness has been recognized as a vital characteristic responsible for different cell's response, especially in tissue engineering, where it has been used to trigger different cell types such as hepatocytes, cardiomyocytes, and neurons; and thereby generating enriched cultures in specific cell types [223]. Our results suggest that stiffness triggers different cell fates by inducing specific mechanotransduction pathways that are crucial in cell fate regulation, and are independent of biochemical pathways. Thus, it would be interesting to

evaluate the stiffness effect utilizing specific lineage differentiation biochemical modulators on biocompatible substrates. To trigger embryonic stem cell differentiation to cardiomyocytes, different biochemical cocktails have been described, with activin, BMP, VEGF, and FGF as crucial factors [225–227]. In addition, hydrogels have been used as scaffold material to promote cardiomyocyte differentiation and survival [228]. Taking into account that healthy myocardium has been reported to have a stiffness of approximately 10 kPa, while ischemic or fibrotic myocardium, a stiffness between 35 kPa and 70 kPa [229], it would be interesting to evaluate the conjugation of time-specific biochemical modulators (utilizing previous published protocols) [226,227] and hydrogel scaffolds with different stiffness (ranging from 10 kPa to 40 kPa) in ESC-derived cardiomyocytes. Then, evaluate the efficiency of cardiomyocytes derived from ESC cultures in the different stiffness, through specific transcription markers, such as myofilaments genes *Tnnt2*, cardiac α-actin (*Actc1*), and calcium-ATPase (*Atp2a2*), and cardiomyocyte functionality through electrical activity assessment. Following the same rationale, it would be also relevant to culture fibroblasts on different hydrogels stiffness, induce their direct reprogramming into cardiomyocytes [230], and then evaluate the efficiency of reprogramming and cardiomyocytes' functionality. These results may imply that stiffness is as important as biochemical modulators and to achieve the correct cell fate in an efficient manner, substrate stiffness cannot be neglected. Thus, these results open the door to understanding the relationship between stiffness and biochemical cues and their impact in cell fate, crucial findings for the advance of tissue engineering.

Chapter 6

References

1. Chazaud, C. & Yamanaka, Y. Lineage specification in the mouse preimplantation embryo. *Development* **143,** 1063–74 (2016).

2. Schrode, N. *et al.* Anatomy of a blastocyst: Cell behaviors driving cell fate choice and morphogenesis in the early mouse embryo. *Genesis* **51,** 219–233 (2013).

3. Tam, P. P. L. & Loebel, D. a F. Gene function in mouse embryogenesis: get set for gastrulation. *Nat Rev Genet* **8,** 368–81 (2007).

4. Evans, M. J. & Kaufman, M. H. Establishment in culture of pluripotential cells from mouse embryos. *Nature* **292,** 154–156 (1981).

5. Martin, G. R. Isolation of a pluripotent cell line from early mouse embryos cultured in medium conditioned by teratocarcinoma stem cells. *Proc. Natl. Acad. Sci. U. S. A.* **78,** 7634–8 (1981).

6. Thomson, J. A. *et al.* Embryonic stem cell lines derived from human blastocysts. *Science* **282,** 1145–7 (1998).

7. Brons, I. G. M. *et al.* Derivation of pluripotent epiblast stem cells from mammalian embryos. *Nature* **448,** 191–195 (2007).

8. Tesar, P. J. *et al.* New cell lines from mouse epiblast share defining features with human embryonic stem cells. *Nature* **448,** 196–199 (2007).

9. Takahashi, K. & Yamanaka, S. Induction of Pluripotent Stem Cells from Mouse Embryonic and Adult Fibroblast Cultures by Defined Factors. *Cell* **126,** 663–676 (2006).

10. Okita, K., Ichisaka, T. & Yamanaka, S. Generation of germline-competent induced pluripotent stem cells. *Nature* **448,** 313–317 (2007).

11. Ducibella, T. & Anderson, E. Cell Shape and Membrane Changes in the Eight-Cell Mouse Embryo : Prerequisites for Morphogenesis of the Blastocyst ’. *Dev. Biol.* **47,** 45–58 (1975).

12. Sasaki, H. Position- and polarity-dependent Hippo signaling regulates cell fates in preimplantation mouse embryos. *Semin. Cell Dev. Biol.* **48,** 1–8 (2015).

13. Niwa, H. *et al.* Interaction between Oct3/4 and Cdx2 determines trophectoderm differentiation. *Cell* **123,** 917–929 (2005).

14. Chambers, I. *et al.* Functional expression cloning of Nanog, a pluripotency sustaining factor in embryonic stem cells. *Cell* **113,** 643–55 (2003).

15. Avilion, A. A. *et al.* Multipotent cell lineages in early mouse development on SOX2 function. *Genes Dev.* **17,** 126–140 (2003).

16. Mitsui, K. *et al.* The homeoprotein nanog is required for maintenance of pluripotency in mouse epiblast and ES cells. *Cell* **113,** 631–642 (2003).

17. Chazaud, C., Yamanaka, Y., Pawson, T. & Rossant, J. Early Lineage Segregation between Epiblast and Primitive Endoderm in Mouse Blastocysts through the Grb2-MAPK Pathway. *Dev. Cell* **10,** 615–624 (2006).

18. Plusa, B., Piliszek, A., Frankenberg, S., Artus, J. & Hadjantonakis, A.-K. Distinct sequential cell behaviours direct primitive endoderm formation in the mouse blastocyst. *Development* **135,** 3081–91 (2008).

19. McLaren, A. Blastocysts in the mouse uterus: the effect of ovariectomy, progesterone and oestrogen. *J. Endocrinol.* **50,** 515–526 (1971).

20. Paria, B. C., Huet-Hudson, Y. M. & Dey, S. K. Blastocyst's state of activity determines the 'window' of implantation in the receptive mouse uterus. *Proc. Natl. Acad. Sci. U. S. A.* **90,** 10159–62 (1993).

21. Hamatani, T. *et al.* Global gene expression analysis identifies molecular pathways distinguishing blastocyst dormancy and activation. *Proc. Natl. Acad. Sci. U. S. A.* **101,** 10326–31 (2004).

22. Wang, H. & Dey, S. K. Roadmap to embryo implantation: clues from mouse models. *Nat Rev Genet* **7,** 185–199 (2006).

23. Stewart, C. L. *et al.* © 19 9 2 Nature Publishing Group. *Nature* **355,** 242–244 (1992).

24. Bedzhov, I. & Zernicka-Goetz, M. Self-organizing properties of mouse pluripotent cells initiate morphogenesis upon implantation. *Cell* **156,** 1032–1044 (2014).

25. Tanaka, S., Kunath, T., Hadjantonakis, A. K., Nagy, A. & Rossant, J. Promotion of trophoblast stem cell proliferation by FGF4. *Science* **282,** 2072–2075 (1998).

26. Guzman-Ayala, M. *et al.* Nodal protein processing and fibroblast growth factor 4 synergize to maintain a trophoblast stem cell microenvironment. *Proc. Natl. Acad. Sci. U. S. A.* **101,** 15656–15660 (2004).

27. Murohashi, M. *et al.* An FGF4-FRS2α-Cdx2 axis in trophoblast stem cells induces Bmp4 to regulate proper growth of early mouse embryos. *Stem Cells* **28,** 113–121 (2010).

28. Brennan, J. *et al.* Nodal signalling in the epiblast patterns the early mouse embryo. *Nature* **411,** 965–969 (2001).

29. Srinivas, S., Rodriguez, T., Clements, M., Smith, J. C. & Beddington, R. S. P. Active cell migration drives the unilateral movements of the anterior visceral endoderm. *Development* **131,** 1157–64 (2004).

30. Perea-Gomez, A. *et al.* Nodal antaginists in the anterior visceral endoderm prevent the formation of multiple primitive streaks. *Dev. Cell* **3,** 745–756 (2002).

31. Rossant, J. & Tam, P. P. L. Blastocyst lineage formation, early embryonic asymmetries and axis patterning in the mouse. *Development* **136,** 701–13 (2009).

32. Arnold, S. J. & Robertson, E. J. Making a commitment: cell lineage allocation and axis patterning in the early mouse embryo. *Nat. Rev. Mol. Cell Biol.* **10,** 91–103 (2009).

33. Bradley, a, Evans, M., Kaufman, M. H. & Robertson, E. Formation of germ-line chimaeras from embryo-derived teratocarcinoma cell lines. *Nature* **309,** 255–6 (1984).

34. Doetschman, T. C., Eistetter, H., Katz, M., Schmidt, W. & Kemler, R. The in vitro development of blastocyst-derived embryonic stem cell lines: formation of visceral yolk sac, blood islands

and myocardium. *J. Embryol. Exp. Morphol.* **87,** 27–45 (1985).

35. Itskovitz-Eldor, J. *et al.* Differentiation of human embryonic stem cells into embryoid bodies compromising the three embryonic germ layers. *Mol. Med.* **6,** 88–95 (2000).

36. De Los Angeles, A. *et al.* Hallmarks of pluripotency. *Nature* **525,** 469–478 (2015).

37. Solter, D. From teratocarcinomas to embryonic stem cells and beyond: a history of embryonic stem cell research. *Nat. Rev. Genet.* **7,** 319–27 (2006).

38. Smith, a G. *et al.* Inhibition of pluripotential embryonic stem cell differentiation by purified polypeptides. *Nature* **336,** 688–90 (1988).

39. Williams, R. L. *et al.* Myeloid leukaemia inhibitory factor maintains the developmental potential of embryonic stem cells. *Nature* **336,** 684–687 (1988).

40. Pease, S., Braghetta, P., Gearing, D., Grail, D. & Williams, R. L. Isolation of embryonic stem (ES) cells in media supplemented with recombinant leukemia inhibitory factor (LIF). *Dev. Biol.* **141,** 344–352 (1990).

41. Nichols, J., Evans, E. P. & Smith, a G. Establishment of germ-line-competent embryonic stem (ES) cells using differentiation inhibiting activity. *Development* **110,** 1341–1348 (1990).

42. Dejosez, M. & Zwaka, T. P. *Pluripotency and Nuclear Reprogramming*. *Annual Review of Biochemistry* **81,** (2012).

43. Ying, Q. L., Stavridis, M., Griffiths, D., Li, M. & Smith, A. Conversion of embryonic stem cells into neuroectodermal precursors in adherent monoculture. *Nat. Biotechnol.* **21,** 183–186 (2003).

44. Ying, Q. L., Nichols, J., Chambers, I. & Smith, A. BMP induction of Id proteins suppresses differentiation and sustains embryonic stem cell self-renewal in collaboration with STAT3. *Cell* **115,** 281–292 (2003).

45. Qi, X. *et al.* BMP4 supports self-renewal of embryonic stem cells by inhibiting mitogen-activated protein kinase pathways. *Proc. Natl. Acad. Sci. U. S. A.* **101,** 6027–6032 (2004).

46. Kunath, T. *et al.* FGF stimulation of the Erk1/2 signalling cascade triggers transition of pluripotent embryonic stem cells from self-renewal to lineage commitment. *Development* **134,** 2895–902 (2007).

47. Hao, J., Li, T. G., Qi, X., Zhao, D. F. & Zhao, G. Q. WNT/β-catenin pathway up-regulates Stat3 and converges on LIF to prevent differentiation of mouse embryonic stem cells. *Dev. Biol.* **290,** 81–91 (2006).

48. Martello, G. *et al.* Esrrb is a pivotal target of the Gsk3/Tcf3 axis regulating embryonic stem cell self-renewal. *Cell Stem Cell* **11,** 491–504 (2012).

49. Ying, Q. L. *et al.* The ground state of embryonic stem cell self-renewal. *Nature* **453,** 519–523 (2008).

50. Buehr, M. *et al.* Capture of Authentic Embryonic Stem Cells from Rat Blastocysts. *Cell* **135,** 1287–1298 (2008).

51. Kiyonari, H., Kaneko, M., Abe, S. I. & Aizawa, S. Three inhibitors of FGF receptor, ERK, and GSK3 establishes germline-competent embryonic stem cells of C57BL/6N mouse strain with high efficiency and stability. *Genesis* **48,** 317–327 (2010).

52. Li, P. *et al.* Germline Competent Embryonic Stem Cells Derived from Rat Blastocysts. *Cell* **135,** 1299–1310 (2008).

53. Boroviak, T., Loos, R., Bertone, P. & Smith, A. Cell The ability of inner-cell-mass cells to self-renew as embryonic stem cells is acquired upon epiblast specification. *Nat. Cell Biol.* **16,** 513–528 (2014).

54. Kim, H. *et al.* Modulation of β-catenin function maintains mouse epiblast stem cell and human embryonic stem cell self-renewal. *Nat. Commun.* **4,** 2403 (2013).

55. Huang, Y., Osorno, R., Tsakiridis, A. & Wilson, V. In Vivo Differentiation Potential of Epiblast Stem Cells Revealed by Chimeric Embryo Formation. *Cell Rep.* **2,** 1571–1578 (2012).

56. Weinberger, L., Ayyash, M., Novershtern, N. & Hanna, J. H. Dynamic stem cell states: naive to primed pluripotency in rodents and humans. *Nat. Rev. Mol. Cell Biol.* 30676 (2016). doi:10.1101/030676

57. Yamanaka, S. A Fresh Look at iPS Cells. *Cell* **137,** 13–17 (2009).

58. Takahashi, K. *et al.* Induction of Pluripotent Stem Cells from Adult Human Fibroblasts by Defined Factors. *Cell* **131,** 861–872 (2007).

59. Scholer, H. R., Dressler, G. R., Rohdewohid, H. & Gruss, P. Oct-4: a germline-specific transcription factor mapping to the mouse t-complex. *EMBO J.* **9,** 2185–2195 (1990).

60. Nichols, J. *et al.* Formation of Pluripotent Stem Cells in the Mammalian Embryo Depends on the POU Transcription Factor Oct4. *Cell* **95,** 379–391 (1998).

61. Palmieri, S. L., Werner, P., Hess, H. & Scholer, H. R. Oct-4 Transcription Factor is Differentially Expressed in the Mouse Embryo during Establishment of the two first Extraembryonic Cell Lineages Involved in Implantation. *Developmental Biology* **166,** 259–267 (1994).

62. Niwa, H., Miyazaki, J. & Smith, A. G. Quantitative expression of Oct-3/4 defines differentiation, dedifferentiation or self-renewal of ES cells. *Nat. Genet.* **24,** 372–376 (2000).

63. Radzisheuskaya, A. *et al.* A defined Oct4 level governs cell state transitions of pluripotency entry and differentiation into all embryonic lineages. *Nat. Cell Biol.* **15,** 579–90 (2013).

64. Masui, S. *et al.* Pluripotency governed by Sox2 via regulation of Oct3/4 expression in mouse embryonic stem cells. *Nat Cell Biol* **9,** 625-U26 (2007).

65. Zhao, S., Nichols, J., Smith, A. G. & Li, M. SoxB transcription factors specify neuroectodermal lineage choice in ES cells. *Mol. Cell. Neurosci.* **27,** 332–342 (2004).

66. Okumura-Nakanishi, S., Saito, M., Niwa, H. & Ishikawa, F. Oct-3/4 and Sox2 regulate Oct-3/4 gene in embryonic stem cells. *J. Biol. Chem.* **280,** 5307–5317 (2005).

67. Rodda, D. J. *et al.* Transcriptional regulation of Nanog by OCT4 and SOX2. *J. Biol. Chem.* **280,** 24731–24737 (2005).

68. Tomioka, M. *et al.* Identification of Sox-2 regulatory region which is under the control of Oct-3/4-Sox-2 complex. *Nucleic Acids Res.* **30,** 3202–13 (2002).

69. Yuan, H., Corbi, N., Basilico, C. & Dailey, L. Developmental-specific activity of the FGF-4 enhancer requires the synergistic action of Sox2 and Oct-3. *Genes Dev.* **9,** 2635–2645 (1995).

70. Chambers, I. *et al.* Nanog safeguards pluripotency and mediates germline development. *Nature* **450,** 1230–1234 (2007).

71. van den Berg, D. L. C. *et al.* Estrogen-related receptor beta interacts with Oct4 to positively regulate Nanog gene expression. *Mol. Cell. Biol.* **28,** 5986–95 (2008).

72. Zhang, X., Zhang, J., Wang, T., Esteban, M. A. & Pei, D. Esrrb activates Oct4 transcription and sustains self-renewal and pluripotency in embryonic stem cells. *J. Biol. Chem.* **283,** 35825–35833 (2008).

73. Festuccia, N. *et al.* Esrrb is a direct Nanog target gene that can substitute for Nanog function in pluripotent cells. *Cell Stem Cell* **11,** 477–490 (2012).

74. Ivanova, N. *et al.* Dissecting self-renewal in stem cells with RNA interference. *Nature* **442,** 533–538 (2006).

75. Festuccia, N. *et al.* Mitotic binding of Esrrb marks key regulatory regions of the pluripotency network. *Nat. Cell Biol.* **1,** (2016).

76. Jiang, J. *et al.* A core Klf circuitry regulates self-renewal of embryonic stem cells. *Nat. Cell Biol.* **10,** 353–360 (2008).

77. Niwa, H., Ogawa, K., Shimosato, D. & Adachi, K. A parallel circuit of LIF signalling pathways maintains pluripotency of mouse ES cells. *Nature* **460,** 118–22 (2009).

78. Hall, J. *et al.* Oct4 and LIF/Stat3 Additively Induce Kruppel Factors to Sustain Embryonic Stem

Cell Self-Renewal. *Cell Stem Cell* **5,** 597–609 (2009).

79. Yeo, J. C. *et al.* Klf2 is an essential factor that sustains ground state pluripotency. *Cell Stem Cell* **14,** 864–872 (2014).

80. Martello, G., Bertone, P. & Smith, A. Identification of the missing pluripotency mediator downstream of leukaemia inhibitory factor. *EMBO J.* **32,** 2561–74 (2013).

81. Ye, S., Li, P., Tong, C. & Ying, Q.-L. Embryonic stem cell self-renewal pathways converge on the transcription factor Tfcp2l1. *EMBO J.* **32,** 2548–60 (2013).

82. Pelton, T. a, Sharma, S., Schulz, T. C., Rathjen, J. & Rathjen, P. D. Transient pluripotent cell populations during primitive ectoderm formation: correlation of in vivo and in vitro pluripotent cell development. *J. Cell Sci.* **115,** 329–39 (2002).

83. Toyooka, Y., Shimosato, D., Murakami, K., Takahashi, K. & Niwa, H. Identification and characterization of subpopulations in undifferentiated ES cell culture. *Development* **135,** 909–918 (2008).

84. Masui, S. *et al.* Rex1/Zfp42 is dispensable for pluripotency in mouse ES cells. *BMC Dev. Biol.* **8,** 45 (2008).

85. Shi, W. *et al.* Regulation of the Pluripotency Marker Rex-1 by Nanog and Sox2. *J. Biol. Chem.* **281,** 23319–23325 (2006).

86. Hayashi, K., Lopes, S. M. C. de S., Tang, F. & Surani, M. A. Dynamic Equilibrium and Heterogeneity of Mouse Pluripotent Stem Cells with Distinct Functional and Epigenetic States. *Cell Stem Cell* **3,** 391–401 (2008).

87. Payer, B. *et al.* Generation of stella-GFP transgenic mice: a novel tool to study germ cell development. *Genesis* **44,** 75–83 (2006).

88. Guo, G. *et al.* Klf4 reverts developmentally programmed restriction of ground state pluripotency. *Development* **136,** 1063–9 (2009).

89. Hayashi, K., Ohta, H., Kurimoto, K., Aramaki, S. & Saitou, M. Reconstitution of the mouse germ cell specification pathway in culture by pluripotent stem cells. *Cell* **146,** 519–532 (2011).

90. Hébert, J. M., Boyle, M. & Martin, G. R. mRNA localization studies suggest that murine FGF-5 plays a role in gastrulation. *Development* **112,** 407–415 (1991).

91. Buecker, C. *et al.* Reorganization of enhancer patterns in transition from naive to primed pluripotency. *Cell Stem Cell* **14,** 838–853 (2014).

92. Song, L., Chen, J., Peng, G., Tang, K. & Jing, N. Dynamic heterogeneity of brachyury in mouse epiblast stem cells mediates distinct response to extrinsic bone morphogenetic protein (bmp) signaling. *J. Biol. Chem.* **291,** 15212–15225 (2016).

93. Lolas, M., Valenzuela, P. D. T., Tjian, R. & Liu, Z. Charting Brachyury-mediated developmental pathways during early mouse embryogenesis. *Proc. Natl. Acad. Sci. U. S. A.* **111,** 4478–83 (2014).

94. Lowe, L. a, Yamada, S. & Kuehn, M. R. Genetic dissection of nodal function in patterning the mouse embryo. *Development* **128,** 1831–1843 (2001).

95. Meno, C. *et al.* Mouse lefty2 and zebrafish antivin are feedback inhibitors of nodal signaling during vertebrate gastrulation. *Mol. Cell* **4,** 287–298 (1999).

96. Kim, D.-K., Cha, Y., Ahn, H.-J., Kim, G. & Park, K.-S. Lefty1 and lefty2 control the balance between self-renewal and pluripotent differentiation of mouse embryonic stem cells. *Stem Cells Dev.* **23,** 457–66 (2014).

97. Stryjewska, A. *et al.* Zeb2 Regulates Cell Fate at the Exit from Epiblast State in Mouse Embryonic Stem Cells. *Stem Cells* (2016). doi:10.1002/stem.2521

98. Chng, Z., Teo, A., Pedersen, R. A. & Vallier, L. SIP1 Mediates Cell-Fate Decisions between Neuroectoderm and Mesendoderm in Human Pluripotent Stem Cells. *Cell Stem Cell* **6,** 59–70 (2010).

99. Kawaguchi, A. *et al.* Nestin-EGFP transgenic mice: visualization of the self-renewal and multipotency of CNS stem cells. *Mol. Cell. Neurosci.* **17,** 259–73 (2001).

100. Stavridis, M. P., Lunn, J. S., Collins, B. J. & Storey, K. G. A discrete period of FGF-induced Erk1/2 signalling is required for vertebrate neural specification. *Development* **134,** 2889–2894 (2007).

101. Pereira, S. L. *et al.* From gametogenesis and stem cells to cancer: common metabolic themes. *Hum. Reprod. Update* **20,** 924–43 (2014).

102. Ramalho-Santos, J. & Rodrigues, A. S. in *Mitochondrial DNA, Mitochondria, Disease and Stem Cells* (ed. St. John, J. C.) 69–86 (Humana Press, 2013). doi:10.1007/978-1-62703-101-1_4

103. Ramalho-Santos, J. & Amaral, S. Mitochondria and mammalian reproduction. *Mol. Cell. Endocrinol.* **379,** 74–84 (2013).

104. Ramalho-Santos, J. *et al.* Mitochondrial functionality in reproduction: From gonads and gametes to embryos and embryonic stem cells. *Hum. Reprod. Update* **15,** 553–572 (2009).

105. Folmes, C. D. L. & Terzic, A. Metabolic determinants of embryonic development and stem cell fate. *Reprod. Fertil. Dev.* **27,** 82–88 (2015).

106. Zhou, W. *et al.* HIF1α induced switch from bivalent to exclusively glycolytic metabolism during ESC-to-EpiSC/hESC transition. *EMBO J.* **31,** 2103–2116 (2012).

107. Carbognin, E., Betto, R. M., Soriano, M. E., Smith, A. G. & Martello, G. Stat3 promotes mitochondrial transcription and oxidative respiration during maintenance and induction of naive pluripotency. *EMBO J.* **35,** 618–634 (2016).

108. Zhang, J. *et al.* UCP2 regulates energy metabolism and differentiation potential of human pluripotent stem cells. *EMBO J.* **30,** 4860–4873 (2011).

109. Seagroves, T. N. *et al.* Transcription factor HIF-1 is a necessary mediator of the pasteur effect in mammalian cells. *Mol. Cell. Biol.* **21,** 3436–44 (2001).

110. Takehara, T., Teramura, T., Onodera, Y., Hamanishi, C. & Fukuda, K. Reduced oxygen concentration enhances conversion of embryonic stem cells to epiblast stem cells. *Stem Cells Dev.* **21,** 1239–49 (2012).

111. Rodrigues, A. S. *et al.* Dichloroacetate, the pyruvate dehydrogenase complex and the modulation of mESC pluripotency. *PLoS One* **10,** (2015).

112. Rodrigues, A. S. *et al.* Differentiate or die: 3-Bromopyruvate and pluripotency in mouse embryonic stem cells. *PLoS One* **10,** (2015).

113. Varum, S. *et al.* Enhancement of human embryonic stem cell pluripotency through inhibition of the mitochondrial respiratory chain. *Stem Cell Res.* **3,** 142–156 (2009).

114. Pereira, S. L. *et al.* Inhibition of mitochondrial complex III blocks neuronal differentiation and maintains embryonic stem cell pluripotency. *PLoS One* **8,** 1–16 (2013).

115. Spitkovsky, D. *et al.* Activity of complex III of the mitochondrial electron transport chain is essential for early heart muscle cell differentiation. *FASEB J.* **18,** 1300–1302 (2004).

116. Chung, S. *et al.* Mitochondrial oxidative metabolism is required for the cardiac differentiation of stem cells. *Natl. Institutes Heal.* **4,** 1–12 (2011).

117. Facucho-Oliveira, J. M., Alderson, J., Spikings, E. C., Egginton, S. & St John, J. C. Mitochondrial DNA replication during differentiation of murine embryonic stem cells. *J. Cell Sci.* **120,** 4025–34 (2007).

118. Cho, Y. M. *et al.* Dynamic changes in mitochondrial biogenesis and antioxidant enzymes during the spontaneous differentiation of human embryonic stem cells. *Biochem. Biophys. Res. Commun.* **348,** 1472–1478 (2006).

119. Mandal, S., Lindgren, A. G., Srivastava, A. S., Clark, A. T. & Banerjee, U. Mitochondrial function controls proliferation and early differentiation potential of embryonic stem cells. *Stem Cells* **29,** 486–495 (2011).

120. Pernas, L. & Scorrano, L. Mito-Morphosis: Mitochondrial Fusion, Fission, and Cristae Remodeling as Key Mediators of Cellular Function. *Annu. Rev. Physiol.* **78,** 505–31 (2016).

121. Lunt, S. Y. & Vander Heiden, M. G. Aerobic Glycolysis: Meeting the Metabolic Requirements of Cell Proliferation. *Annu. Rev. Cell Dev. Biol.* **27,** 441–464 (2011).

122. Moussaieff, A., Kogan, N. M. & Aberdam, D. Concise Review : Energy Metabolites : Key Mediators of the Epigenetic State of Pluripotency. *Stem Cells* 2374–2380 (2015).

123. Wellen, K. E. *et al.* ATP-citrate lyase links cellular metabolism to histone acetylation. *Sci. (New York, NY)* **324,** 1076–1080 (2009).

124. Moussaieff, A. *et al.* Glycolysis-mediated changes in acetyl-CoA and histone acetylation control the early differentiation of embryonic stem cells. *Cell Metab.* **21,** 392–402 (2015).

125. Carey, B. W., Finley, L. W. S., Cross, J. R., Allis, C. D. & Thompson, C. B. Intracellular α-ketoglutarate maintains the pluripotency of embryonic stem cells. *Nature* **518,** 413–416 (2015).

126. Ware, C. B. *et al.* Histone Deacetylase Inhibition Elicits an Evolutionarily Conserved Self-Renewal Program in Embryonic Stem Cells. *Cell Stem Cell* **4,** 359–369 (2009).

127. Lee, J.-H., Hart, S. R. L. & Skalnik, D. G. Histone deacetylase activity is required for embryonic stem cell differentiation. *Genesis* **38,** 32–8 (2004).

128. Correia, M. *et al.* Sirtuins in metabolism, stemness and differentiation. *Biochim. Biophys. Acta - Gen. Subj.* (2016). doi:10.1016/j.bbagen.2016.09.008

129. Ryall, J. G., Cliff, T., Dalton, S. & Sartorelli, V. Metabolic Reprogramming of Stem Cell Epigenetics. *Cell Stem Cell* **17,** 651–662 (2015).

130. Tsumura, A. *et al.* Maintenance of self-renewal ability of mouse embryonic stem cells in the absence of DNA methyltransferases Dnmt1, Dnmt3a and Dnmt3b. *Genes to Cells* **11,** 805–814 (2006).

131. Jackson, M. *et al.* Severe global DNA hypomethylation blocks differentiation and induces

histone hyperacetylation in embryonic stem cells. *Mol. Cell. Biol.* **24,** 8862–71 (2004).

132. Sousa, M. I. *et al.* Mitochondrial Mechanisms of Metabolic Reprogramming in Proliferating Cells. *Curr. Med. Chem.* **22,** (2015).

133. Zhu, S. *et al.* Reprogramming of human primary somatic cells by OCT4 and chemical compounds. *Cell Stem Cell* **7,** 651–655 (2010).

134. Son, M. J., Jeong, B. R., Kwon, Y. & Cho, Y. S. Interference with the mitochondrial bioenergetics fuels reprogramming to pluripotency via facilitation of the glycolytic transition. *Int. J. Biochem. Cell Biol.* **45,** 2512–2518 (2013).

135. Varum, S. *et al.* Energy metabolism in human pluripotent stem cells and their differentiated counterparts. *PLoS One* **6,** (2011).

136. Folmes, C. D. L. *et al.* Somatic oxidative bioenergetics transitions into pluripotency-dependent glycolysis to facilitate nuclear reprogramming. *Cell Metab.* **14,** 264–271 (2011).

137. Prigione, A. *et al.* HIF1α modulates cell fate reprogramming through early glycolytic shift and upregulation of PDK1-3 and PKM2. *Stem Cells* **32,** 364–376 (2014).

138. LaCroix, A. S., Rothenberg, K. E. & Hoffman, B. D. *Molecular-Scale Tools for Studying Mechanotransduction*. *Annual Review of Biomedical Engineering* **17,** (2015).

139. Wang, N., Tytell, J. D. & Ingber, D. E. Mechanotransduction at a distance: mechanically coupling the extracellular matrix with the nucleus. *Nat Rev Mol Cell Biol* **10,** 75–82 (2009).

140. Butcher, D. T., Alliston, T. & Weaver, V. M. A tense situation: forcing tumour progression. *Nat Rev Cancer* **9,** 108–122 (2009).

141. Wang, N., Butler, J. P. & Ingber, D. E. Mechanotransduction across the cell surface and through the cytoskeleton. *Science* **260,** 1124–1127 (1993).

142. Sheehy, S. P. & Parker, K. K. in *Tissue Engineering in Regenerative Medicine* (ed. Bernstein, H. S.) 77–97 (Humana Press, 2011). doi:10.1007/978-1-61779-322-6_5

143. Leckband, D. E., le Duc, Q., Wang, N. & de Rooij, J. Mechanotransduction at cadherin-mediated adhesions. *Curr. Opin. Cell Biol.* **23,** 523–530 (2011).

144. Cavallaro, U. & Christofori, G. Cell adhesion and signalling by cadherins and Ig-CAMs in cancer. *Nat. Rev. Cancer* **4,** 118–132 (2004).

145. Mammoto, T., Mammoto, A. & Ingber, D. E. Mechanobiology and Developmental Control. *Annu. Rev. Cell Dev. Biol* **29,** 27–61 (2013).

146. Gupta, S. K. Role of zona pellucida glycoproteins during fertilization in humans. *J. Reprod. Immunol.* **108,** 90–97 (2015).

147. Clift, D. & Schuh, M. Restarting life: fertilization and the transition from meiosis to mitosis. *Nat Rev Mol Cell Biol* **14,** 549–562 (2013).

148. Drobnis, E. Z., Andrew, J. B. & Katz, D. F. Biophysical properties of the zona pellucida measured by capillary suction: is zona hardening a mechanical phenomenon? *J. Exp. Zool.* **245,** 206–19 (1988).

149. Sun, Y., Wan, K.-T., Roberts, K. P., Bischof, J. C. & Nelson, B. J. Mechanical property characterization of mouse zona pellucida. *IEEE Trans. Nanobioscience* **2,** 279–286 (2003).

150. Murayama, Y. *et al.* Mouse zona pellucida dynamically changes its elasticity during oocyte maturation, fertilization and early embryo development. *Hum. cell Off. J. Hum. Cell Res. Soc.* **19,** 119–125 (2006).

151. Khalilian, M., Navidbakhsh, M., Valojerdi, M. R., Chizari, M. & Yazdi, P. E. Estimating Young's modulus of zona pellucida by micropipette aspiration in combination with theoretical models of ovum. *J. R. Soc. Interface* **7,** 687–94 (2010).

152. Yanez, L. Z., Han, J., Behr, B. B., Pera, R. A. R. & Camarillo, D. B. Human oocyte developmental potential is predicted by mechanical properties within hours after fertilization. *Nat. Commun.* **7,** 10809 (2016).

153. Andolfi, L. *et al.* Investigating the mechanical properties of zona pellucida of whole human oocytes by atomic force spectroscopy. *Integr. Biol.* **8,** 886–893 (2016).

154. Maître, J.-L., Niwayama, R., Turlier, H., Nédélec, F. & Hiiragi, T. Pulsatile cell-autonomous contractility drives compaction in the mouse embryo. *Nat. Cell Biol.* **17,** 849–855 (2015).

155. Larue, L., Ohsugi, M., Hirchenhain, J. & Kemler, R. E-cadherin null mutant embryos fail to form a trophectoderm epithelium. *Proc. Natl. Acad. Sci. U. S. A.* **91,** 8263–8267 (1994).

156. Fierro-González, J. C., White, M. D., Silva, J. C. & Plachta, N. Cadherin-dependent filopodia control preimplantation embryo compaction. *Nat. Cell Biol.* **15,** 1424–1433 (2013).

157. Ducibella, T., Ukena, T., Karnovsky, M. & Anderson, E. Changes in cell surface and cortical cytoplasmic organization during early embryogenesis in the preimplantation mouse embryo. *J. Cell Biol.* **74,** 153–167 (1977).

158. Anani, S., Bhat, S., Honma-Yamanaka, N., Krawchuk, D. & Yamanaka, Y. Initiation of Hippo signaling is linked to polarity rather than to cell position in the pre-implantation mouse embryo. *Development* **141,** 2813–24 (2014).

159. Samarage, C. R. *et al.* Cortical Tension Allocates the First Inner Cells of the Mammalian Embryo. *Dev. Cell* **34,** 435–447 (2015).

160. Maître, J.-L. *et al.* Asymmetric division of contractile domains couples cell positioning and fate specification. *Nature* **536,** 344–348 (2016).

161. Hiramatsu, R. *et al.* External mechanical cues trigger the establishment of the anterior-posterior axis in early mouse embryos. *Dev. Cell* **27,** 131–144 (2013).

162. Matsuo, I. & Hiramatsu, R. Mechanical perspectives on the anterior-posterior axis polarization of mouse implanted embryos. *Mech. Dev.* (2016). doi:10.1016/j.mod.2016.09.002

163. Bedzhov, I. *et al.* Development of the anterior-posterior axis is a self-organizing process in the absence of maternal cues in the mouse embryo. *Cell Res.* **25,** 1368–71 (2015).

164. Ferreira, R. R. & Vermot, J. The balancing roles of mechanical forces during left-right patterning and asymmetric morphogenesis. *Mech. Dev.* (2016). doi:10.1016/j.mod.2016.11.001

165. Sutherland, A. E. Tissue morphodynamics shaping the early mouse embryo. *Semin. Cell Dev. Biol.* 1–10 (2016). doi:10.1016/j.semcdb.2016.01.033

166. Ingber, D. E. Mechanical control of tissue morphogenesis during embryological development. *Int. J. Dev. Biol.* **50,** 255–266 (2006).

167. Engler, A. J., Sen, S., Sweeney, H. L. & Discher, D. E. Matrix Elasticity Directs Stem Cell Lineage Specification. *Cell* **126,** 677–689 (2006).

168. Kolahi, K. S. *et al.* Effect of substrate stiffness on early mouse embryo development. *PLoS One* **7,** (2012).

169. Evans, N. D. & Gentleman, E. The role of material structure and mechanical properties in cell–matrix interactions. *J. Mater. Chem. B* **2,** 2345 (2014).

170. Trappmann, B. *et al.* Extracellular-matrix tethering regulates stem-cell fate. *Nat. Mater.* **11,** 742–742 (2012).

171. Chowdhury, F. *et al.* Soft substrates promote homogeneous self-renewal of embryonic stem cells via downregulating cell-matrix tractions. *PLoS One* **5,** (2010).

172. Shimizu, T. *et al.* Dual inhibition of Src and GSK3 maintains mouse embryonic stem cells, whose differentiation is mechanically regulated by Src signaling. *Stem Cells* **30,** 1394–1404 (2012).

173. Evans, N. D. *et al.* Substrate Stiffness Affects Early Differentiation Events in Embryonic Stem Cells. *Eur. Cell. Mater.* **18,** 1–14 (2009).

174. Shkumatov, A., Baek, K. & Kong, H. Matrix rigidity-modulated cardiovascular organoid formation from embryoid bodies. *PLoS One* **9,** 1–10 (2014).

175. Zoldan, J. *et al.* The influence of scaffold elasticity on germ layer specification of human

embryonic stem cells. *Biomaterials* **32,** 9612–9621 (2011).

176. Keung, A. J., Asuri, P., Kumar, S. & Schaffer, D. V. Soft microenvironments promote the early neurogenic differentiation but not self-renewal of human pluripotent stem cells. *Integr. Biol.* **100,** 130–134 (2012).

177. Chowdhury, F. *et al.* Material properties of the cell dictate stress-induced spreading and differentiation in embryonic stem cells. *Nat Mater* **9,** 82–88 (2010).

178. Lv, H. *et al.* Mechanism of regulation of stem cell differentiation by matrix stiffness. *Stem Cell Res. Ther.* **6,** 103 (2015).

179. Choi, B. *et al.* Stiffness of Hydrogels Regulates Cellular Reprogramming Efficiency Through Mesenchymal-to-Epithelial Transition and Stemness Markers. *Macromol. Biosci.* **16,** 199–206 (2016).

180. Higuchi, S., Watanabe, T. M., Kawauchi, K., Ichimura, T. & Fujita, H. Culturing of mouse and human cells on soft substrates promote the expression of stem cell markers. *J. Biosci. Bioeng.* **117,** 749–755 (2014).

181. Downing, T. L. *et al.* Biophysical regulation of epigenetic state and cell reprogramming. *Nat. Mater.* **12,** 1154–1162 (2013).

182. Wang, Z., Gerstein, M. & Snyder, M. RNA-Seq: a revolutionary tool for transcriptomics. *Nat. Rev. Genet.* **10,** 57–63 (2009).

183. Kukurba, K. R. & Montgomery, S. B. RNA Sequencing and Analysis. *Cold Spring Harb. Protoc.* **2015,** 951–969 (2015).

184. Tarazona, S., García-Alcalde, F., Dopazo, J., Ferrer, A. & Conesa, A. Differential expression in RNA-seq: A matter of depth. *Genome Res.* **21,** 2213–2223 (2011).

185. McBurney, M. W. *et al.* The absence of SIR2alpha protein has no effect on global gene silencing in mouse embryonic stem cells. *Mol. Cancer Res.* **1,** 402–409 (2003).

186. Tse, J. R. & Engler, A. J. Preparation of hydrogel substrates with tunable mechanical properties. *Curr. Protoc. cell Biol.* **Chapter 10,** Unit 10.16 (2010).

187. Cretu, A., Castagnino, P. & Assoian, R. Studying the effects of matrix stiffness on cellular function using acrylamide-based hydrogels. *J. Vis. Exp.* (2010). doi:10.3791/2089

188. Spandidos, A. *et al.* A comprehensive collection of experimentally validated primers for Polymerase Chain Reaction quantitation of murine transcript abundance. *BMC Genomics* **9,** 633 (2008).

189. Spandidos, A., Wang, X., Wang, H. & Seed, B. PrimerBank: a resource of human and mouse PCR primer pairs for gene expression detection and quantification. *Nucleic Acids Res.* **38,** D792-9 (2010).

190. Wang, X. & Seed, B. A PCR primer bank for quantitative gene expression analysis. *Nucleic Acids Res.* **31,** e154 (2003).

191. Trapnell, C., Pachter, L. & Salzberg, S. L. TopHat: discovering splice junctions with RNA-Seq. *Bioinformatics* **25,** 1105–1111 (2009).

192. Goecks, J., Nekrutenko, A. & Taylor, J. Galaxy: a comprehensive approach for supporting accessible, reproducible, and transparent computational research in the life sciences. *Genome Biol.* **11,** R86 (2010).

193. Huang, D. W., Lempicki, R. a & Sherman, B. T. Systematic and integrative analysis of large gene lists using DAVID bioinformatics resources. *Nat. Protoc.* **4,** 44–57 (2009).

194. Huang, D. W., Sherman, B. T. & Lempicki, R. A. Bioinformatics enrichment tools: Paths toward the comprehensive functional analysis of large gene lists. *Nucleic Acids Res.* **37,** 1–13 (2009).

195. Bardou, P., Mariette, J., Escudié, F., Djemiel, C. & Klopp, C. jvenn: an interactive Venn diagram viewer. *BMC Bioinformatics* **15,** 293 (2014).

196. Palmqvist, L. *et al.* Correlation of murine embryonic stem cell gene expression profiles with

functional measures of pluripotency. *Stem Cells* **23,** 663–680 (2005).

197. Mammoto, T. & Ingber, D. E. Mechanical control of tissue and organ development. *Development* **137,** 1407–1420 (2010).

198. Davidson, L. A. Mechanical design in embryos: mechanical signalling, robustness and developmental defects. *Philos. Trans. R. Soc. London B Biol. Sci.* **372,** (2017).

199. Discher, D. E., Janmey, P. & Wang, Y.-L. Tissue cells feel and respond to the stiffness of their substrate. *Science* **310,** 1139–1143 (2005).

200. Du, J. *et al.* Integrin activation and internalization on soft ECM as a mechanism of induction of stem cell differentiation by ECM elasticity. *Proc. Natl. Acad. Sci.* **108,** 9466–9471 (2011).

201. Nguyen, T. V., Sleiman, M., Moriarty, T., Herrick, W. G. & Peyton, S. R. Sorafenib resistance and JNK signaling in carcinoma during extracellular matrix stiffening. *Biomaterials* **35,** 5749–5759 (2014).

202. Schrader, J. *et al.* Matrix stiffness modulates proliferation, chemotherapeutic response, and dormancy in hepatocellular carcinoma cells. *Hepatology* **53,** 1192–1205 (2011).

203. Avilion, A. A. *et al.* Multipotent cell lineages in early mouse development depend on SOX2 function. *Genes Dev.* **17,** 126–40 (2003).

204. Hart, A. H., Hartley, L., Ibrahim, M. & Robb, L. Identification, cloning and expression analysis of the pluripotency promoting Nanog genes in mouse and human. *Dev. Dyn.* **230,** 187–98 (2004).

205. Hay, D. C., Sutherland, L., Clark, J. & Burdon, T. Oct-4 knockdown induces similar patterns of endoderm and trophoblast differentiation markers in human and mouse embryonic stem cells. *Stem Cells* **22,** 225–35 (2004).

206. Stefková, K., Procházková, J. & Pachernik, J. Alkaline phosphatase in stem cells. *Stem Cells Int.* **2015,** (2015).

207. Martello, G. & Smith, A. The nature of embryonic stem cells. *Annu Rev Cell Dev Biol* **30,** 647–

675 (2014).

208. Jaccard, N. *et al.* Automated method for the rapid and precise estimation of adherent cell culture characteristics from phase contrast microscopy images. *Biotechnol. Bioeng.* **111,** 504–517 (2014).

209. Narkilahti, S. *et al.* Monitoring and analysis of dynamic growth of human embryonic stem cells: comparison of automated instrumentation and conventional culturing methods. *Biomed. Eng. Online* **6,** 11 (2007).

210. Jaccard, N. *et al.* Automated and online characterization of adherent cell culture growth in a microfabricated bioreactor. *J. Lab. Autom.* **19,** 437–443 (2014).

211. Scherf, N. *et al.* Imaging, quantification and visualization of spatio-temporal patterning in mESC colonies under different culture conditions. *Bioinformatics* **28,** i556–i561 (2012).

212. Tokunaga, K. *et al.* Computational image analysis of colony and nuclear morphology to evaluate human induced pluripotent stem cells. *Sci. Rep.* **4,** 6996 (2014).

213. Joutsijoki, H., Haponen, M., Rasku, J., Aalto-Setala, K. & Juhola, M. Machine Learning Approach to Automated Quality Identification of Human Induced Pluripotent Stem Cell Colony Images. *Comput. Math. Methods Med.* **2016,** 3091039 (2016).

214. Maddah, M., Shoukat-Mumtaz, U., Nassirpour, S. & Loewke, K. A system for automated, noninvasive, morphology-based evaluation of induced pluripotent stem cell cultures. *J. Lab. Autom.* **19,** 454–460 (2014).

215. Chalfoun, J. *et al.* Empirical gradient threshold technique for automated segmentation across image modalities and cell lines. *J. Microsc.* **260,** 86–99 (2015).

216. Gorman, B. R. *et al.* Multi-scale imaging and informatics pipeline for in situ pluripotent stem cell analysis. *PLoS One* **9,** (2014).

217. Lou, X., Kang, M., Xenopoulos, P., Muñoz-Descalzo, S. & Hadjantonakis, A.-K. A Rapid and

Efficient 2D/3D Nuclear Segmentation Method for Analysis of Early Mouse Embryo and Stem Cell Image Data. *Stem Cell Reports* **2,** 382–397 (2014).

218. Paduano, V., Tagliaferri, D., Falco, G. & Ceccarelli, M. Automated identification and location analysis of marked stem cells colonies in optical microscopy images. *PLoS One* **8,** 1–11 (2013).

219. Intawong, K., Scuturici, M. & Miguet, S. in *Computer Analysis of Images and Patterns: 15th International Conference, CAIP 2013, York, UK, August 27-29, 2013, Proceedings, Part I* (eds. Wilson, R., Hancock, E., Bors, A. & Smith, W.) 188–195 (Springer Berlin Heidelberg, 2013). doi:10.1007/978-3-642-40261-6_22

220. Zou, K. H. *et al.* Statistical validation of image segmentation quality based on a spatial overlap index. *Acad. Radiol.* **11,** 178–189 (2004).

221. Breiman, L. Random Forests. *Mach. Learn.* **45,** 5–32 (2001).

222. French, A. *et al.* Enabling consistency in pluripotent stem cell-derived products for research and development and clinical applications through material standards. *Stem Cells Transl. Med.* **4,** 217–223 (2015).

223. Xia, T., Liu, W. & Yang, L. A review of gradient stiffness hydrogels used in tissue engineering and regenerative medicine. *J. Biomed. Mater. Res. A* **105,** 1799–1812 (2017).

224. Gomes, M. E., Rodrigues, M. T., Domingues, R. M. A. & Reis, R. L. Tissue Engineering and Regenerative Medicine: New trends and directions/A Year in Review. *Tissue Eng. Part B. Rev.* (2017). doi:10.1089/ten.TEB.2017.0081

225. Mummery, C. L. *et al.* Differentiation of human embryonic stem cells and induced pluripotent stem cells to cardiomyocytes: a methods overview. *Circ. Res.* **111,** 344–358 (2012).

226. Palpant, N. J. *et al.* Generating high-purity cardiac and endothelial derivatives from patterned mesoderm using human pluripotent stem cells. *Nat. Protoc.* **12,** 15–31 (2017).

227. Burridge, P. W., Keller, G., Gold, J. D. & Wu, J. C. Production of de novo cardiomyocytes:

human pluripotent stem cell differentiation and direct reprogramming. *Cell Stem Cell* **10,** 16–28 (2012).

228. Hasan, A. *et al.* Engineered Biomaterials to Enhance Stem Cell-Based Cardiac Tissue Engineering and Therapy. *Macromol. Biosci.* **16,** 958–977 (2016).

229. Engler, A. J. *et al.* Embryonic cardiomyocytes beat best on a matrix with heart-like elasticity: scar-like rigidity inhibits beating. *J. Cell Sci.* **121,** 3794 LP-3802 (2008).

230. Efe, J. A. *et al.* Conversion of mouse fibroblasts into cardiomyocytes using a direct reprogramming strategy. *Nat. Cell Biol.* **13,** 215–222 (2011).

Chapter 7

Appendix

A

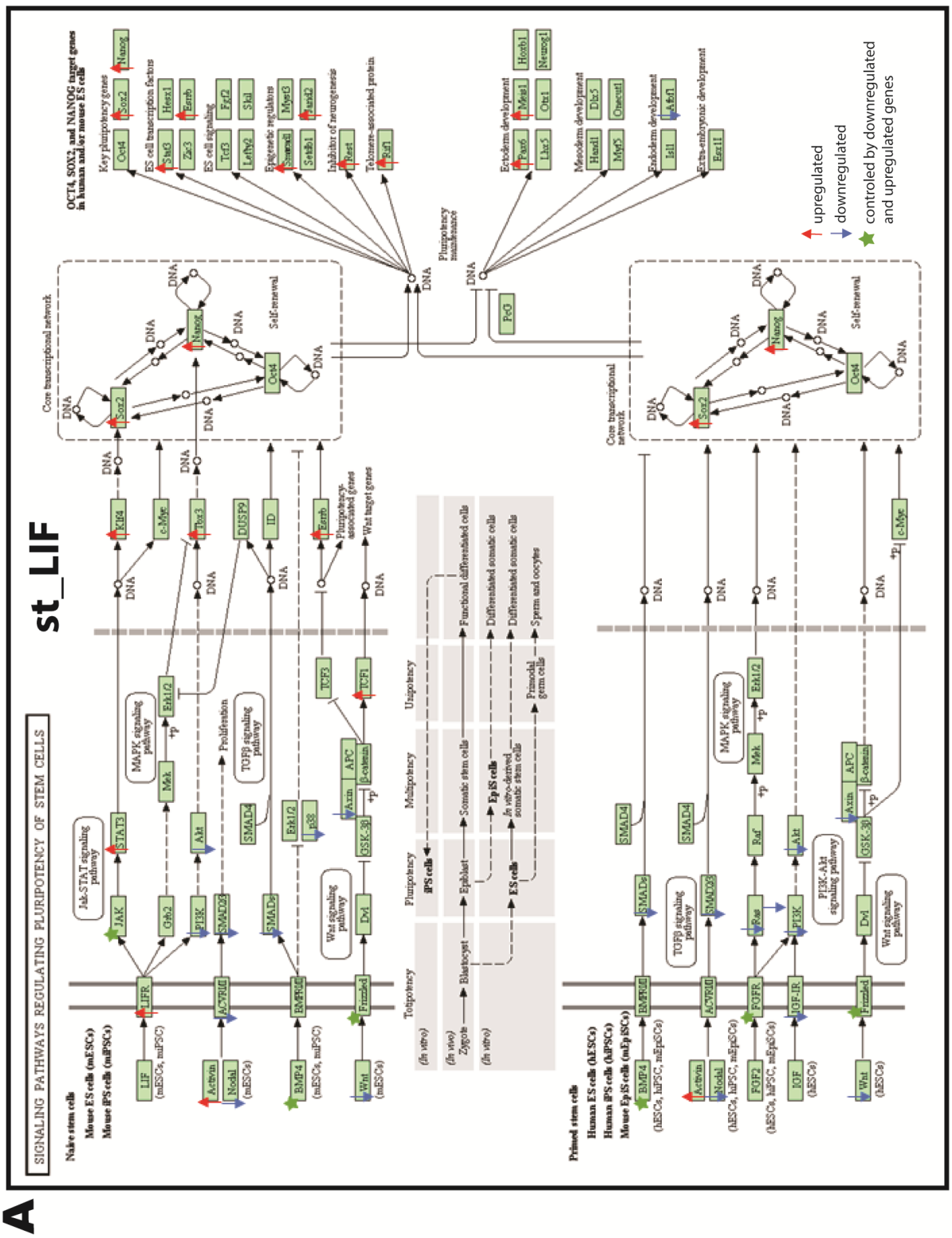
SIGNALING PATHWAYS REGULATING PLURIPOTENCY OF STEM CELLS
st_LIF
upregulated
downregulated
controled by downregulated and upregulated genes
Naive stem cells
Mouse ES cells (mESCs)
Mouse iPS cells (miPSC)
Primed stem cells
Human ES cells (hESCs)
Human iPS cells (hiPSCs)
Mouse EpiS cells (miEpiSCs)
Totipotency
Pluripotency
Multipotency
Unipotency
Core transcriptional network
Self-renewal
Pluripotency maintenance
Jak-STAT signaling pathway
MAPK signaling pathway
TGFβ signaling pathway
Wnt signaling pathway
PI3K-Akt signaling pathway
Proliferation
Somatic stem cells
Epiblast
Blastocyst
Zygote
Functional differentiated cells
Differentiated somatic cells
Primordial germ cells
Sperm and oocytes
Pluripotency-associated genes
Wnt target genes

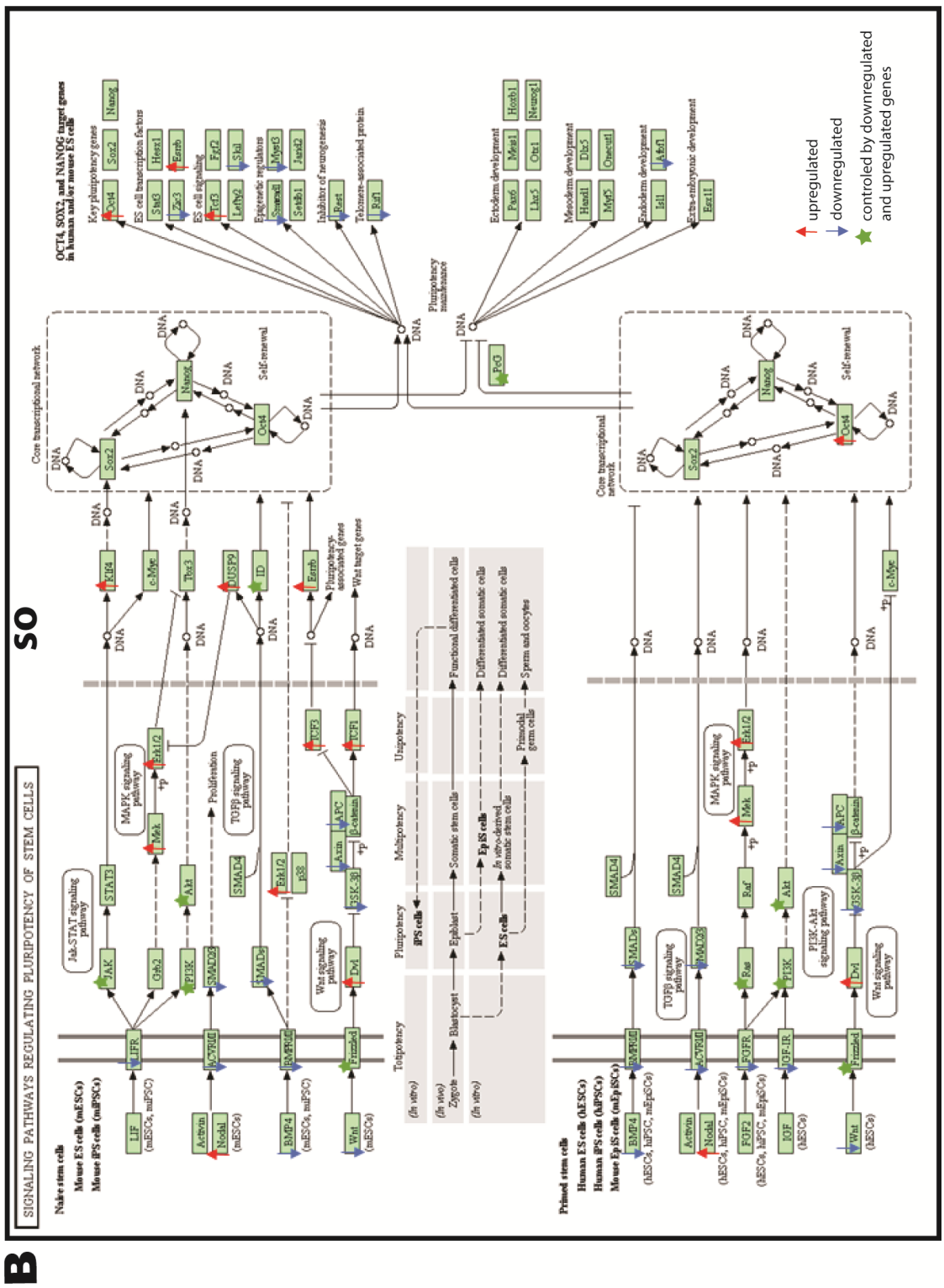

Appendix 7.1 - Pathways differentially expressed in ESC exposed to different stimuli
(A) Pluripotent signaling pathway determined by KEGG pathway analysis. Upregulated and downregulated genes represented: ESC cultured on stiff substrate in presence of LIF *vs.* ESC cultured on stiff substrates in the absence of LIF. **(B)** Pluripotent signaling pathway determined by KEGG pathway analysis. Upregulated and downregulated genes represented: ESC cultured on soft substrate in the absence of LIF *vs.* ESC cultured on stiff substrates in the absence of LIF.

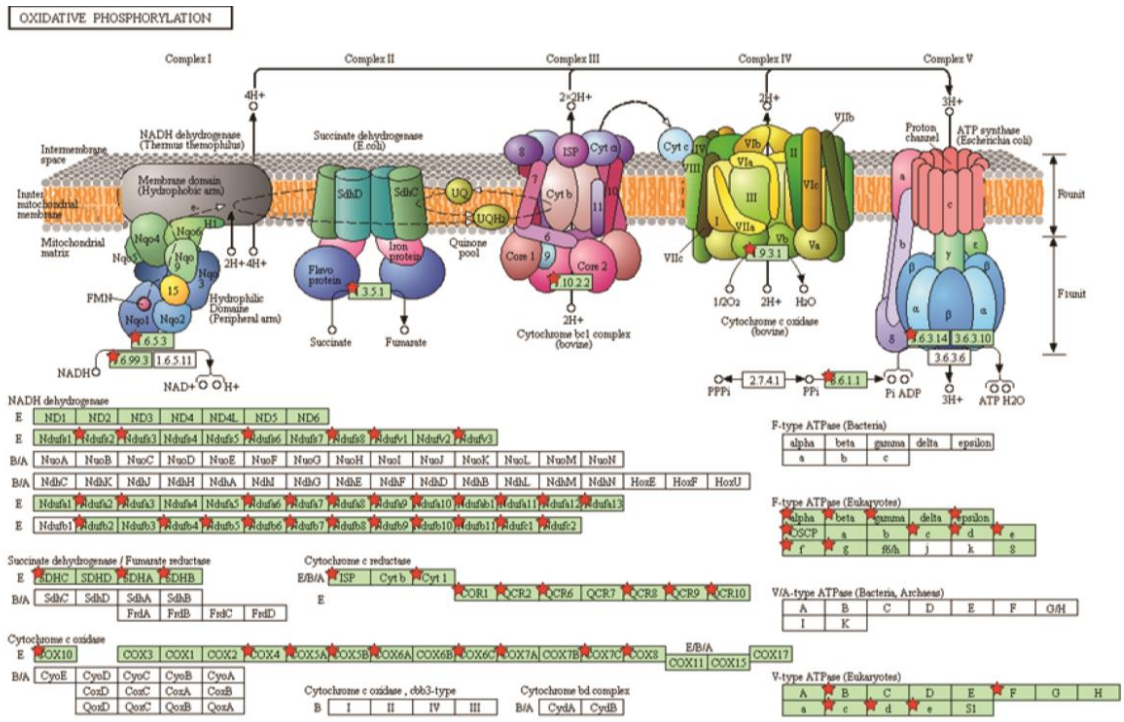

Genes	GENE NAME
Atp5b	ATP synthase, H+ transporting mitochondrial F1 complex, beta subunit(Atp5b)
Atp5g1	ATP synthase, H+ transporting, mitochondrial F0 complex, subunit C1 (subunit 9)(Atp5g1)
Atp5g2	ATP synthase, H+ transporting, mitochondrial F0 complex, subunit C2 (subunit 9)(Atp5g2)
Atp5g3	ATP synthase, H+ transporting, mitochondrial F0 complex, subunit C3 (subunit 9)(Atp5g3)
Atp5h	ATP synthase, H+ transporting, mitochondrial F0 complex, subunit D(Atp5h)
Atp5j2	ATP synthase, H+ transporting, mitochondrial F0 complex, subunit F2(Atp5j2)
Atp5l	ATP synthase, H+ transporting, mitochondrial F0 complex, subunit G(Atp5l)
Atp5o	ATP synthase, H+ transporting, mitochondrial F1 complex, O subunit(Atp5o)
Atp5a1	ATP synthase, H+ transporting, mitochondrial F1 complex, alpha subunit 1(Atp5a1)
Atp5e	ATP synthase, H+ transporting, mitochondrial F1 complex, epsilon subunit(Atp5e)
Atp5c1	ATP synthase, H+ transporting, mitochondrial F1 complex, gamma polypeptide 1(Atp5c1)
Atp5k	ATP synthase, H+ transporting, mitochondrial F1F0 complex, subunit E(Atp5k)
Atp6v0b	ATPase, H+ transporting, lysosomal V0 subunit B(Atp6v0b)
Atp6v0d1	ATPase, H+ transporting, lysosomal V0 subunit D1(Atp6v0d1)
Atp6v0e	ATPase, H+ transporting, lysosomal V0 subunit E(Atp6v0e)
Atp6v1b2	ATPase, H+ transporting, lysosomal V1 subunit B2(Atp6v1b2)
Atp6v1f	ATPase, H+ transporting, lysosomal V1 subunit F(Atp6v1f)
Ndufa10	NADH dehydrogenase (ubiquinone) 1 alpha subcomplex 10(Ndufa10)
Ndufa11	NADH dehydrogenase (ubiquinone) 1 alpha subcomplex 11(Ndufa11)
Ndufa12	NADH dehydrogenase (ubiquinone) 1 alpha subcomplex, 12(Ndufa12)
Ndufa13	NADH dehydrogenase (ubiquinone) 1 alpha subcomplex, 13(Ndufa13)
Ndufa2	NADH dehydrogenase (ubiquinone) 1 alpha subcomplex, 2(Ndufa2)
Ndufa3	NADH dehydrogenase (ubiquinone) 1 alpha subcomplex, 3(Ndufa3)
Ndufa6	NADH dehydrogenase (ubiquinone) 1 alpha subcomplex, 6 (B14)(Ndufa6)
Ndufa7	NADH dehydrogenase (ubiquinone) 1 alpha subcomplex, 7 (B14.5a)(Ndufa7)
Ndufa8	NADH dehydrogenase (ubiquinone) 1 alpha subcomplex, 8(Ndufa8)
Ndufa9	NADH dehydrogenase (ubiquinone) 1 alpha subcomplex, 9(Ndufa9)
Ndufb4	NADH dehydrogenase (ubiquinone) 1 beta subcomplex 4(Ndufb4)
Ndufb8	NADH dehydrogenase (ubiquinone) 1 beta subcomplex 8(Ndufb8)
Ndufb10	NADH dehydrogenase (ubiquinone) 1 beta subcomplex, 10(Ndufb10)
Ndufb11	NADH dehydrogenase (ubiquinone) 1 beta subcomplex, 11(Ndufb11)
Ndufb2	NADH dehydrogenase (ubiquinone) 1 beta subcomplex, 2(Ndufb2)
Ndufb5	NADH dehydrogenase (ubiquinone) 1 beta subcomplex, 5(Ndufb5)
Ndufb6	NADH dehydrogenase (ubiquinone) 1 beta subcomplex, 6(Ndufb6)
Ndufb7	NADH dehydrogenase (ubiquinone) 1 beta subcomplex, 7(Ndufb7)

Genes	GENE NAME
Ndufb9	NADH dehydrogenase (ubiquinone) 1 beta subcomplex, 9(Ndufb9)
Ndufab1	NADH dehydrogenase (ubiquinone) 1, alpha/beta subcomplex, 1(Ndufab1)
Ndufc1	NADH dehydrogenase (ubiquinone) 1, subcomplex unknown, 1(Ndufc1)
Ndufc2	NADH dehydrogenase (ubiquinone) 1, subcomplex unknown, 2(Ndufc2)
Ndufs2	NADH dehydrogenase (ubiquinone) Fe-S protein 2(Ndufs2)
Ndufs3	NADH dehydrogenase (ubiquinone) Fe-S protein 3(Ndufs3)
Ndufs6	NADH dehydrogenase (ubiquinone) Fe-S protein 6(Ndufs6)
Ndufs8	NADH dehydrogenase (ubiquinone) Fe-S protein 8(Ndufs8)
Ndufv1	NADH dehydrogenase (ubiquinone) flavoprotein 1(Ndufv1)
Ndufv3	NADH dehydrogenase (ubiquinone) flavoprotein 3(Ndufv3)
Cox10	cytochrome c oxidase assembly protein 10(Cox10)
Cox4i1	cytochrome c oxidase subunit IV isoform 1(Cox4i1)
Cox8a	cytochrome c oxidase subunit VIIIa(Cox8a)
Cox7a1	cytochrome c oxidase subunit VIIa 1(Cox7a1)
Cox7a2	cytochrome c oxidase subunit VIIa 2(Cox7a2)
Cox7c	cytochrome c oxidase subunit VIIc(Cox7c)
Cox6a1	cytochrome c oxidase subunit VIa polypeptide 1(Cox6a1)
Cox6c	cytochrome c oxidase subunit VIc(Cox6c)
Cox5a	cytochrome c oxidase subunit Va(Cox5a)
Cox5b	cytochrome c oxidase subunit Vb(Cox5b)
Cyc1	cytochrome c-1(Cyc1)
Lhpp	phospholysine phosphohistidine inorganic pyrophosphate phosphatase(Lhpp)
Ppa1	pyrophosphatase (inorganic) 1(Ppa1)
Ppa2	pyrophosphatase (inorganic) 2(Ppa2)
Sdha	succinate dehydrogenase complex, subunit A, flavoprotein (Fp)(Sdha)
Sdhb	succinate dehydrogenase complex, subunit B, iron sulfur (Ip)(Sdhb)
Sdhc	succinate dehydrogenase complex, subunit C, integral membrane protein(Sdhc)
Uqcrc2	ubiquinol cytochrome c reductase core protein 2(Uqcrc2)
Uqcrc1	ubiquinol-cytochrome c reductase core protein 1(Uqcrc1)
Uqcrh	ubiquinol-cytochrome c reductase hinge protein(Uqcrh)
Uqcrfs1	ubiquinol-cytochrome c reductase, Rieske iron-sulfur polypeptide 1(Uqcrfs1)
Uqcrq	ubiquinol-cytochrome c reductase, complex III subunit VII(Uqcrq)
Uqcr10	ubiquinol-cytochrome c reductase, complex III subunit X(Uqcr10)
Uqcr11	ubiquinol-cytochrome c reductase, complex III subunit XI(Uqcr11)

Appendix 7.2 – OXPHOS upregulated genes determined by KEGG pathway analysis

Upregulated genes involved in oxidative phosphorylation upon culture of ESC on soft substrates *vs.* ESC on stiff substrates.

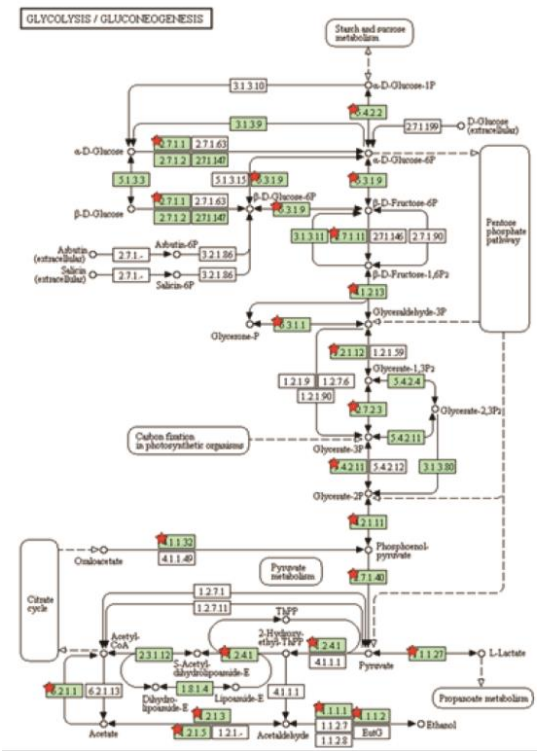

Genes	GENE NAME
Acss1	acyl-CoA synthetase short-chain family member 1(Acss1)
Acss2	acyl-CoA synthetase short-chain family member 2(Acss2)
Adh5	alcohol dehydrogenase 5 (class III), chi polypeptide(Adh5)
Aldh1b1	aldehyde dehydrogenase 1 family, member B1(Aldh1b1)
Aldh2	aldehyde dehydrogenase 2, mitochondrial(Aldh2)
Aldh3b1	aldehyde dehydrogenase 3 family, member B1(Aldh3b1)
Aldh9a1	aldehyde dehydrogenase 9, subfamily A1(Aldh9a1)
Aldh7a1	aldehyde dehydrogenase family 7, member A1(Aldh7a1)
Akr1a1	aldo-keto reductase family 1, member A1 (aldehyde reductase)(Akr1a1)
Aldoa	aldolase A, fructose-bisphosphate(Aldoa)
Eno1	enolase 1, alpha non-neuron(Eno1)
Eno1b	enolase 1B, retrotransposed(Eno1b)
Eno3	enolase 3, beta muscle(Eno3)
Gpi1	glucose phosphate isomerase 1(Gpi1)
Gapdh	glyceraldehyde-3-phosphate dehydrogenase(Gapdh)
Hk1	hexokinase 1(Hk1)
Ldha	lactate dehydrogenase A(Ldha)
Ldhb	lactate dehydrogenase B(Ldhb)
Pck2	phosphoenolpyruvate carboxykinase 2 (mitochondrial)(Pck2)
Pfkl	phosphofructokinase, liver, B-type(Pfkl)
Pfkm	phosphofructokinase, muscle(Pfkm)
Pfkp	phosphofructokinase, platelet(Pfkp)
Pgm2	phosphoglucomutase 2(Pgm2)
Pgk1	phosphoglycerate kinase 1(Pgk1)
Pgam1	phosphoglycerate mutase 1(Pgam1)
Pgam2	phosphoglycerate mutase 2(Pgam2)
Pdhb	pyruvate dehydrogenase (lipoamide) beta(Pdhb)
Pkm	pyruvate kinase, muscle(Pkm)
Tpi1	triosephosphate isomerase 1(Tpi1)

Appendix 7.3 –Glycolysis upregulated genes determined by KEGG pathway analysis

Upregulated genes involved in glycolysis pathway of ESC cultured on soft substrates *vs.* ESC on stiff substrates.